Title
Recruitment and Spread of Heterochromatin in the Budding Yeast Saccharomyces cerevisiae

Author
Brothers, Molly Elizabeth

Publication Date
2021

Peer reviewed|Thesis/dissertation

Recruitment and Spread of Heterochromatin in the Budding Yeast *Saccharomyces cerevisiae*

By

Molly Elizabeth Brothers

A dissertation submitted in partial satisfaction of the

requirements for the degree of

Doctor of Philosophy

in

Molecular and Cell Biology

in the

Graduate Division

of the

University of California, Berkeley

Committee in charge:

Professor Jasper Rine, Chair
Professor Kathleen Collins
Professor Donald Rio
Professor Anders Naar

Fall 2021

Abstract

Recruitment and Spread of Heterochromatin in the Budding Yeast *Saccharomyces cerevisiae*

by

Molly Elizabeth Brothers

Doctor of Philosophy in Molecular and Cell Biology

University of California, Berkeley

Professor Jasper Rine, Chair

Transcriptional silencing in the budding yeast *Saccharomyces cerevisiae* occurs at the cryptic mating-type loci *HML* and *HMR* on chromosome III and at all 32 telomeres. Transcriptional silencing occurs through the formation of a repressive chromatin structure, featuring nucleosome compaction and removal of active chromatin marks. These features are the result of the activity of the Silent Information Regulator (SIR) complex, made up of Sir2, Sir3, and Sir4. Sir2, founding member of the wide spread class of protein deacetylases known as sirtuins, deacetylates histone tails, whereas Sir3 and Sir4 serve structural roles, binding to histones and compacting chromatin.

The formation of silent chromatin by the SIR complex conceptually involves two steps: recruitment and spreading. Recruitment, also referred to as nucleation, occurs at DNA sequence elements called silencers that are present at telomeres and flank *HML* and *HMR*. The *E* and *I* silencers that flank both *HML* and *HMR* contain different combinations of binding sites for the Origin Recognition Complex (ORC) and the general transcription factors Rap1 and Abf1. Silencers at telomeres are less well characterized, but include an array of Rap1 binding sites in telomere repeats and possibly ORC/Abf1 sites further into the chromosome. Fully silent chromatin displays SIR complex binding beyond recruitment sites for multiple kilobases. The difference in SIR complex occupancy between nucleation and full silencing occurs through an ill-defined process referred to as ‘spreading’.

To date, most studies on spreading of the SIR complex have focused on telomeres, sometimes only one, and relied on low-resolution ChIP-PCR, inducible systems that resulted in massive overexpression of Sir3, or both. These studies defined to a limited resolution positions of SIR complex binding and occupancy, and provided a foundation for genome-wide studies with higher temporal and spatial resolution. My work further characterized and distinguished the two processes of recruitment and spread at telomeres as well as *HML* and *HMR*. I accomplished this by developing a new method for tracing the history and trajectory of SIR complex binding: measuring DNA methylation by long-read nanopore sequencing of DNA from cells expressing a fusion protein between Sir3 and an N6-methyladenosine methyltransferase, M.EcoGII.

The fusion protein Sir3-M.EcoGII strongly and specifically methylated *HML*, *HMR*, and telomeres and was able to detect transient or low-affinity Sir3-chromatin interactions better than ChIP-seq. This new method allowed me to characterize the occupancy of a *SIR3* allele encoding

a protein deficient in binding to nucleosomes, *sir3-bah*Δ. The sir3-bahΔ-M.EcoGII fusion protein methylated DNA only at recruitment sites, clearly providing evidence that recruitment and spread of Sir3 were separable processes and that the interaction between Sir3 and nucleosomes was not required for recruitment but was required for spread. I also tested prior claims that overexpression of *SIR3* results in binding of the protein at even longer distances from recruitment sites. The overexpression of *SIR3-M.ECOGII*, with few exceptions, did not extend regions of DNA methylation.

I also defined the dynamics of Sir3 spreading during silencing establishment and how its occupancy related to transcriptional silencing of *HML* and *HMR*. A fusion between *sir3-8*–a temperature sensitive allele of *SIR3*–and *M.ECOGII* allowed for regulated induction of DNA methylation without straying above the endogenous level of *SIR3* expression. Over the course of about one cell cycle, methylation appeared only at the *E* and *I* silencers and the promoters of *HML* and *HMR*, demonstrating recruitment. Despite a lack of Sir3 occupancy between these recruitment sites, repression of transcription occurred early in the time course, suggesting that the early stages of silencing did not require Sir3 occupancy across the entire locus.

Once silent chromatin is established, it must be faithfully inherited through the disruptive process of DNA replication. Certain point mutations in PCNA (*POL30*), the processivity clamp for DNA polymerase at replication forks, result in loss of transcriptional silencing at *HML* and *HMR*. I used classical genetics to study three of these alleles, *pol30-6*, *pol30-8*, and *pol30-79*, in more detail. All three alleles disrupted silencing only in actively-cycling cells, and the disruption in silencing was only transient, suggesting that the inheritance of silent chromatin through cell division was not as robust as in wild-type cells. All three alleles of *POL30* destabilized silencing through disrupting the function of histone chaperones, highlighting the importance of histone trafficking at the replication fork for the stability of transcriptional silencing.

Table of Contents

List of Figures

List of Tables

Acknowledgments

My time as a graduate student has been one of tremendous scientific and personal growth. There are so many people to thank and so many things to thank them for that I couldn't possibly fit all of the words into this tiny section, but I will try my best.

I owe hearty and deep thanks to Jasper Rine for his selfless and dedicated mentorship. I have found his common refrain 'I live to serve' to be no exaggeration. He has an unlimited supply of creative metaphors, optimism, and advice. In addition to being a fantastic scientific mentor, he truly cares about his lab members' well-being and happiness. I especially thank him for all of the delicious, home-cooked meals at lab parties and for inviting me to his family's Christmas dinner my second year when I was unable to make it home for the holidays.

Science is sometimes fickle, frustrating, and infuriating, but having a lab filled with people that know when to commiserate, when to encourage, or when to distract with a hot pot of coffee, has made the lows more bearable and the highs more exciting. Thanks to Marc Fouet, Jean Yan, Nick Marini, Ellie Bondra, Delaney Farris, and Katya Yamamoto for being great lab members and helping to create a fun and scientifically stimulating environment. Thanks to my rotation mentor Ryan Janke for showing me the awesome power of yeast genetics, which made for a fun first paper. Thanks to Gavin Schlissel for being my bay bae and pushing me to think critically and creatively about science. Thanks to Davis Goodnight for being my go-to, wise senior grad student. Sitting across from him and popping my head over from my desk to ask him questions has certainly helped my science. I can always count on him for help (and witty remarks). Finally, many thanks to Daniel Saxton, who has become a close and cherished friend. I will forever hold dear our lunches, early-morning coffees, 'sip-and-walks', bloop battles, and outdoor adventures.

I would like to thank other mentors who provided scientific support and encouragement during grad school. Thank you to my thesis committee members, Don Rio, Kathy Collins, and Anders Naar. Thanks also to Nick Ingolia and Elçin Ünal for providing enriching rotation experiences and continued scientific advice. Thanks to Koen Van den Berge and Sandrine Dudoit for stimulating discussions on the Nanopore sequencing project. Thanks to Brian Keith, Mia Levine, and Kushol Gupta for science and career support that continued past my undergraduate years at the University of Pennsylvania.

Thank you to all of my friends, new and old. I owe special thanks to a few of you. Thank you to my ride-or-die roommates, Natalie Dall, Sophia Friesen, and Danielle Spitzer, who have been by my side since day one of grad school. Natalie was my first friend at Berkeley. We met at recruitment, and I still have a typed a note in my phone reading "I like Natalie–walks fast". Natalie has often been the first person I look to for support. She is always ready with an empathetic and understanding ear, and has an uncanny sense for when you want advice and when you just want to vent. Sophia has a kind and thoughtful heart, and they are always unfazed and down to join in on my goofy antics around the house. As a bonus, Sophia is an amazing baker, and I especially thank them for all of the lemon bars (my favorite!). Danielle is a force of nature. Her endless energy and voracious appetite for learning means she is the first person I ask for help with almost everything–bike maintenance, practice talks, mounting photos on my wall, book recommendations. Thanks to Daisy, my sweet and soft princess of a cat, who has provided many comforting purrs over the last three years since I adopted her. Thanks also to my two new roommates, Fiona Callahan and Mari Brady, for bringing some fresh, first-year energy into our home. Thank you to my best friend Jackie Valeri, who, even from 3000 miles away, has been a

never-ending supply of emotional support through my undergraduate and graduate years. She is someone I can let my guard completely down around and talk to about literally anything. I have had some of my longest-lasting and hardest laughs swapping stories with Jackie.

Finally, thanks to my family for all of the love and support. Words are not enough to express my gratitude for my mom, Shelby Borgelt. As a single mother to me and my sister, a cancer survivor, and someone who went back to finish college while raising two kids, my mom has taught me the value of education and hard work, of advocating for myself, and of being brave in the face of adversity. There is no way I would have made it through grad school without her. I am confident that I have the best mom in the whole world. I love you to the moon and back infinity times. Thanks to Kelsea Brothers, my little sister, for being the emotional smarts to my book smarts. She is a fierce, loving mother as well, and I am proud to call her my sister. Our little family has been through some tough times, but I wouldn't have wanted to go through it with anyone else.

Chapter 1:

Principles of Recruitment and Spread of Large Chromatin Domains

1.1 Abstract

The maintenance of cell identity in eukaryotes requires coordinating the transcriptional state of multiple genes in large chromatin domains, such as heterochromatin. The formation of large chromatin domains involves the recruitment of chromatin-binding and chromatin-modifying complexes to specific sites, the 'spread' of these complexes and their chromatin modifications along chromatin, and the change in transcription of genes within the larger domain. We review the process of recruitment and spread in the contexts of mating-type transcriptional silencing in *Saccharomyces cerevisiae* and *Schizosaccharomyces pombe*. We discuss how the principles of recruitment and spread in these two contexts apply to mammalian X-chromosome inactivation, dosage compensation by the Male Specific Lethal (MSL) complex in *Drosophila*, and dosage compensation by the Dosage Compensation Complex (DCC) in *C. elegans*.

1.2 Introduction

DNA sequence dictates the transcription level of most genes in eukaryotic genomes through a combination of direct and indirect mechanisms. Local DNA sequence elements in promoters and enhancers determine a gene's regulation by targeted recruitment of transcription factors. But there are some genomic regions where a set of contiguous genes are regulated as a bloc. These coordinated, stable states of gene expression such as in heterochromatic silencing and sex-chromosome dosage compensation require changes in chromatin structure across large domains. Specialized chromatin-binding complexes make these changes through covalent modifications of chromatin and nucleosome remodeling. The establishment of these domains by chromatin-binding complexes involves two processes–**nucleation,** the process that initiates formation of the domain, and **spreading**, the process that enables extension of the domain to cover a larger region.

Nucleation is achieved by recruitment of chromatin-binding complexes to regulatory sites within the domain. Nucleation sites vary between and within organisms, but they are defined by their DNA sequence. In some cases, nucleation is achieved by the juxtaposition of DNA sequence-specific binding proteins that collectively recruit chromatin-modifying proteins. In other cases, transcription at the site of nucleation leads to RNA molecules that can recruit nucleation factors.

Nucleation is followed by DNA sequence-independent spreading of the chromatin-binding complex throughout an entire region of chromatin. The size of the region varies among contexts and organisms and ranges from a few genes to megabases of simple sequence repeats to entire chromosomes. Chromatin-binding complexes transition from binding at a nucleation site to covering an entire target region in a process commonly called spreading. So far, in yeast and other eukaryotes, spreading is an inferred process invoked to explain the differences in chromatin between the 'before' state and the state after an impact on gene expression has been achieved. In no case has a clear definition or characterization of intermediate steps been achieved.

Mechanistic models for spreading fall into four broad classes: (1) Starting at a nucleation site, complexes iteratively bind one nucleosome after another and, through cooperative interactions and local modification of nucleosomes, spread in a sequential fashion. (2) Nucleation sites serve as a high-affinity 'anchors' to increase the concentration of the chromatin-binding complex in a genomic region, thereby allowing the complexes to stochastically bind throughout that region until cooperative interactions stabilize them. (3) Long-range 3D contacts, or loops, between nucleation sites and other locations along the chromatin facilitate cooperative recruitment and stabilize binding of chromatin-binding complexes. (4) Complexes bind first at a nucleation site and then actively move or slide along the chromatin. Looping or sliding of the chromatin-binding complex alone would not result in large region of contiguous occupancy, so models (3) and (4) invoke a combination of looping with another mechanism. There is no requirement that these models be mutually exclusive, and spreading likely involves a combination of these mechanisms.

In this review, we explore how the collective behavior of chromatin-binding complexes creates domains of coordinated gene expression, focusing on the molecular basis of nucleation and spread of these complexes. We also discuss the various elements and mechanisms that exist to define the boundaries, or barriers, to spreading. These barriers exist to restrict the spread of chromatin-binding complexes and ensure the proper regulation of genes flanking the targeted domain. In the first section, we concentrate on heterochromatin complexes in *S. cerevisiae* and *S. pombe*. In the second section, we use the case studies of sex-chromosome dosage compensation in mammals, *Drosophila*, and *C. elegans* and discuss the extent to which characteristics of nucleation and spread are shared in other contexts that result in different transcriptional effects.

1.3 Spreading of heterochromatin in *S. cerevisiae* and *S. pombe*

Compared to plants and animals, *S. cerevisiae* and *S. pombe* have several features that allow a detailed consideration of the core processes needed for the spread of heterochromatic gene silencing. First, both encode a smaller number of chromatin modifiers and remodelers and a smaller number of histone genes and histone variants than plants and animals. Additionally, mutation of histones and chromatin modifiers are rarely lethal, making molecular dissection of their contribution to gene regulation easier. Although the specific chromatin modifications and proteins required for heterochromatin complex recruitment and spreading differ between organisms, even between *S. pombe* and *S. cerevisiae,* the basic principles are conserved from yeast to humans.

1.3.1 Building blocks of heterochromatin

Transcriptional silencing in *S. cerevisiae* is one of the best-studied heterochromatic phenomena. Silencing, which occurs at the mating-type loci *HML* and *HMR* and at telomeres, depends on the binding and enzymatic activity of a complex consisting of the Silencing Information Regulator (Sir) proteins (Rine and Herskowitz 1987; reviewed in Gartenberg and Smith 2016). The current model involves the recruitment of Sir proteins to nucleation sites at silenced regions (dubbed "silencers") followed by the binding of Sir2/Sir3/Sir4 (the SIR complex) across the silenced locus through a process called spreading. This spreading results in changes to the chromatin structure that include histone hypoacetylation (Braunstein et al. 1993, 1996; de Bruin et al. 2000; Suka et al. 2001; Thurtle and Rine 2014; Ellahi et al. 2015) and

physical compaction (Gottschling 1992; Singh and Klar 1992; Loo and Rine 1994; Onishi et al. 2007; Johnson et al. 2009; Swygert et al. 2018). Notably, the most conserved difference between heterochromatin and euchromatin across all eukaryotes is heterochromatin's hypoacetylation.

S. pombe combines histone deacetylation with RNA interference (RNAi) and the heterochromatin-specific methylation of H3K9 to establish and maintain heterochromatin (reviewed in Allshire and Ekwall 2015). Transcription of repetitive regions produces double-stranded RNA that is processed by RNAi machinery to yield short, single-stranded RNAs that recruit silencing machinery to complementary sequences through a series of direct interactions with histone deacetylases, histone methyltransferases, and Swi6, the *S. pombe* ortholog of the *Drosophila* heterochromatin protein 1 (HP1) (Bannister et al. 2001; Nakayama et al. 2001; Hall et al. 2002). Following nucleation, these complexes spread over tens of kilobases, modifying histones and compacting chromatin, to create a transcriptionally silent domain (Ekwall et al. 1995; Hall et al. 2002; Noma et al. 2004; Cam et al. 2005).

1.3.2 Nucleation

Heterochromatin's structural components do not have DNA sequence-binding specificity and thus require other factors for targeting specific regions of the genome. Specificity comes in some cases from protein-protein interactions and in other cases from short RNAs that guide the heterochromatin complexes to specific sites. This process is called nucleation. In each context, no single factor is enough to establish stable transcriptional silencing. Instead, specific combinations of factors that define nucleation sites enable subsequent recruitment of chromatin-modifying heterochromatin complexes.

DNA sequence-specific recruiting proteins

In *S. cerevisiae*, nucleation occurs at silencers, which flank the mating type loci *HML* and *HMR,* and at less-well described elements at telomeres (Abraham et al. 1984; Feldman et al. 1984; Brand et al. 1985; Mahoney and Broach 1989; Stavenhagen and Zakian 1994). Silencers at *HML* and *HMR* contain a combination of binding sites for the Origin Recognition Complex (ORC) and the transcription factors Abf1 and Rap1 (Figure 1.1A) (Shore and Nasmyth 1987; Shore et al. 1987; Buchman et al. 1988). Telomeres contain an array of Rap1 binding sites (Longtine et al. 1989; Stavenhagen and Zakian 1994; Buchman et al. 1988), but arrays of Rap1 binding sites alone silence poorly, implying a contribution of other factors to nucleate telomeric silencing (Stavenhagen and Zakian 1994). The DNA binding of each of these proteins has specificity and interacts with a member of the SIR complex. ORC binds to Sir1, which recruits Sir2/4, Rap1 binds to Sir3 and Sir4, and Abf1 binds to Sir3 (Figure 1.1A) (Cockell et al. 1995; Triolo and Sternglanz 1996; Moretti and Shore 2001). ORC, Abf1, and Rap1 have many binding sites throughout the yeast genome, yet heterochromatin is formed only at designated regions. Interestingly, there are a subset of replication origins that the SIR complex binds to (Hoggard et al. 2018, 2020), but there is little binding of Sir proteins beyond a few hundred base pairs from the origins, suggesting that formation of a large domain requires more than one nucleation factor. The combination of protein-protein interactions between these factors, Sir1, and members of the SIR complex reinforce or stabilize Sir protein binding specifically at silencers, whereas an ORC, Abf1, or Rap1 site alone is not sufficient for transcriptional silencing.

In *S. pombe,* DNA binding sites within a region called *REIII* near the cryptic mating-type locus *mat3* mirror silencers in *S. cerevisiae.* Rather than the recruitment of Abf1 and Rap1, *REIII*

recruits the transcription factors Atf1 and Pcr1 (Figure 1.1B) (Thon et al. 1999; Kim et al. 2004; Jia et al. 2004; Yamada et al. 2005). These two factors directly interact with the H3K9 deacetylase Clr6 and with Swi6 (Kim et al. 2004). Swi6 then directly recruits the histone deacetylase complex SHREC (Yamada et al. 2005). A deletion of *ATF1* or *PCR1* affects transcriptional silencing of *mat2* and *mat3* only if components of the RNAi machinery, discussed below, are also missing (Jia et al. 2004), supporting the notion that nucleation requires a combination of inputs for successful silencing. At telomere ends, the *S. pombe* Rap1 homolog Taz1 nucleates heterochromatin alongside RNAi-based nucleation described in the next section (Kanoh et al. 2005).

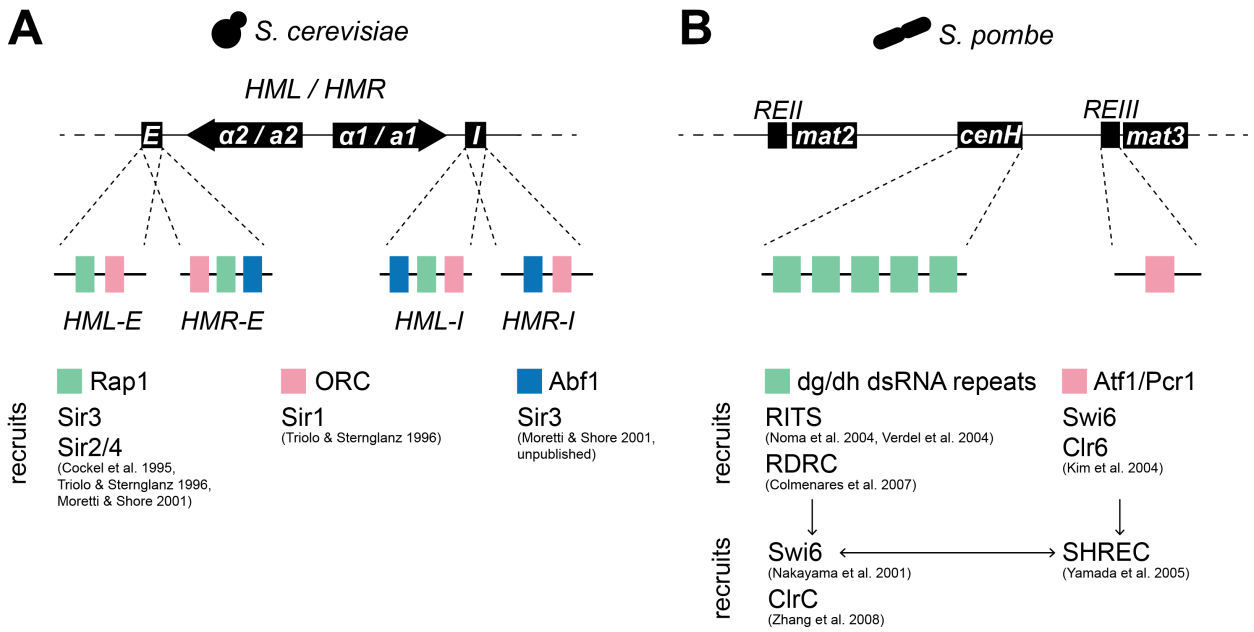

Figure 1.1. Nucleation of heterochromatin at the mating-type loci of budding and fission yeast.
A) Nucleation in *S. cerevisiae* relies on sequence-specific recruitment of the transcription factors Rap1 and Abf1 and the Origin Recognition Complex (ORC). These binding sites are found in different combinations at the *E* and *I* silencers of *HML* (*α1* and *α2*) and *HMR* (*a1* and *a2*). Rap1, Abf1, and ORC then recruit the Sir1, Sir2, Sir3, and Sir4 to *HML* and *HMR*. **B)** Nucleation in *S. pombe* occurs at the *cenH dg* and *dh* repeats and at the *REIII* element near *mat3*. The *dg* and *dh* repeats are transcribed to create double-strand RNAs that are processed by RNAi machinery into short single-strand RNAs. The single-strand RNAs make a complex, RITS (RNA-Induced Transcriptional Silencing), that is recruited to *cenH* through complementary base pairing. RDRC (RNA-Dependent RNA polymerase Complex) creates more double-strand *dg* and *dh* RNAs using the single-strand RNA as template. RITS and RDRC recruit Swi6 (HP1), the histone methyltransferase CLRC (Clr4 methyltransferase Complex), and the histone deacetylase SHREC (Snf2/HDAC-containing Repressor Complex) through various protein-protein interactions.

RNA interference

Almost paradoxically, transcription of RNA within a silenced domain is another mode of heterochromatin nucleation in *S. pombe* as well as metazoans (reviewed in Martienssen and Moazed 2015). In each case, non-coding RNAs are required only for nucleation of heterochromatin factors; once silencing is established, non-coding RNAs are not required to maintain silencing, even through DNA replication and cell division (Hall et al. 2002; Noma et al. 2004).

At *S. pombe* centromeres, telomeres, and between *mat2* and *mat3*, sense and anti-sense transcription of centromere-like repeats called *dg* and *dh* yields double-stranded RNA (dsRNA) (Figure 1.1B) (Volpe et al. 2002; Cam et al. 2005; Djupedal et al. 2005; Kato et al. 2005). This dsRNA is processed by Dicer into smaller fragments and then assembled as a single-stranded RNA in the RITS complex. The RITS (RNA-induced transcriptional silencing) and RDRC (RNA-directed RNA polymerase complex) complexes nucleate heterochromatin at the *dg* and *dh* repeats through complementary base-pairing (Hall et al. 2002; Noma et al. 2004; Verdel et al. 2004; Colmenares et al. 2007; Zhang et al. 2008). Nucleation of RITS and RDRC is followed by recruitment of the histone deacetylase complex SHREC, the H3K9 methyltransferase complex CLRC, and Swi6 (HP1) (Nakayama et al. 2001; Zhang et al. 2008). Tethering of a single RITS subunit is sufficient to nucleate heterochromatin at an ectopic locus, but spreading and silencing depend on the presence of CLRC and Swi6 (Bühler et al. 2006).

1.3.3 Spread

The size of heterochromatin domains varies widely across and within eukaryotes. Domains range from the few kilobases of *HML* and *HMR* in *S. cerevisiae* to 150 megabases of the mammalian X chromosome. Transcriptional silencing of such extensive regions requires that spreading of heterochromatin proteins be largely independent of DNA sequence. Consistent with this view, genes ectopically placed within heterochromatin domains are usually repressed, and ectopic recruitment of heterochromatin factors can result in transcriptional silencing. Therefore, although nucleation depends on underlying DNA sequence, spreading of heterochromatin proteins, and the associated chromatin modifications and transcriptional silencing, does not.

Spreading requires histone modifications

In all known cases, spreading requires histone modification. *S. cerevisiae* and *S. pombe* mutants harboring a catalytically dead mutation in Sir2 or Clr3, respectively, retain binding of the heterochromatin factors at nucleation sites but have little to no binding within the target region (Hoppe et al. 2002; Rusche et al. 2002; Noma et al. 2004; Yamada et al. 2005; Zhang et al. 2008). The complexes that create heterochromatin marks also recognize the chromatin modification they make (Johnson et al. 1990; Hecht et al. 1995; Ivanova et al. 1998; Onishi et al. 2007; Zhang et al. 2008; Johnson et al. 2009; Al-Sady et al. 2013; Swygert et al. 2018; Akoury et al. 2019). The SIR complex in *S. cerevisiae* deacetylates specific positions on the N-terminal tails of histones H3 and H4—most importantly H4K16—through the catalytic activity of Sir2 (Landry et al. 2000; Imai et al. 2000; Hoppe et al. 2002; Borra et al. 2004), and Sir3 binds more strongly to deacetylated chromatin than acetylated chromatin. Likewise, in *S. pombe*, CLRC contains an H3K9 methyltransferase domain as well as a chromodomain that recognizes methylated histones. This duality inspires an intuitive model for spreading: after recruitment to nucleation sites, complexes iteratively modify and bind nucleosomes one after the other until they reach some barrier to their spread.

A positive feedback loop involving complexes iteratively creating and binding chromatin marks as support for a sequential spreading model would require (1) a sufficiently large difference in affinity between modified and unmodified chromatin, (2) cooperative binding of silencing complexes to particular histone marks, (3) a difference in rate of catalysis when bound to modified and unmodified chromatin, or a combination of the three. Multiple components of *S. pombe* heterochromatin meet this requirement. Multiple heterochromatin proteins, including Clr4

and Swi6, contain a chromodomain, which binds to K9-methylated H3 with high specificity (Bannister et al. 2001; Lachner et al. 2001; Fischle et al. 2003; Yamada et al. 2005; Canzio et al. 2013; Akoury et al. 2019). There is also one study that found cooperative binding of Swi6/HP1 dimers to histone peptides *in vitro* (Mendez et al. 2011). Further, Clr4 catalysis is stimulated by binding methylated H3K9 (Al-Sady et al. 2013; Akoury et al. 2019). The combination of affinity and catalysis differences between modified and unmodified chromatin and possible cooperativity of silencing complexes lends support for a sequential spreading model, but does not exclude the possibility of other spreading mechanisms.

In contrast to *S. pombe* heterochromatin proteins, *S. cerevisiae* Sir proteins do not display a large difference in affinity between acetylated or unacetylated chromatin. Two subunits of the complex, Sir2/Sir4, have no preference for acetylated vs. deacetylated chromatin *in vitro*, and although Sir3 displays a preference for deacetylated chromatin, it still associates strongly with acetylated chromatin (Onishi et al. 2007; Armache et al. 2011; Oppikofer et al. 2011; Swygert et al. 2018). There is, however, one *in vitro* study and two computational modeling studies that support cooperative binding of Sir proteins (Mendez et al. 2011; Sneppen and Dodd 2015; Behrouzi et al. 2016), and Sir2 in complex with Sir4 has a higher rate of catalysis than Sir2 alone (Tanny et al. 2004; Hsu et al. 2013). These results suggest that Sir2/4 could bind to any nucleosome and deacetylate it, followed by Sir3 recruitment or stabilization of the complex, perhaps through cooperative interactions. In principle, the SIR complex could bind stochastically within silenced regions after recruitment to silencers. Experiments to date have lacked sufficient temporal and spatial resolution to clarify the mechanism (Radman-Livaja et al. 2011; Lynch and Rusche 2009).

Spreading results in discontinuous 'islands' of binding

Telomeric silencing in *S. cerevisiae* has been thought to spread inward from telomere ends (Renauld et al. 1993; Hecht et al. 1996; Strahl-Bolsinger et al. 1997; Kimura et al. 2002; Suka et al. 2002). While a minority of telomere-adjacent regions (subtelomeres) display a decreasing gradient of Sir protein binding away from telomere ends, most show 'islands' of SIR binding as far as 15 kilobases away from telomeres, which suggests spreading may not be strictly sequential (Fourel et al. 1999; Pryde and Louis 1999; Radman-Livaja et al. 2011; Ellahi et al. 2015). Discontinuous SIR binding distribution in subtelomeric regions argues against a simple sequential-spread model. Perhaps Sir proteins have the ability to 'hop' over some genomic features. Alternatively, sequential spreading of SIR may initially occur, but the islands of Sir-protein binding revealed in ChIP-seq data may represent regions that stabilize otherwise dynamic SIR binding. We note that two studies found small islands of SIR binding in euchromatic regions of the genome (Radman-Livaja et al. 2011; Li et al. 2013), but these sites are due to a ChIP artifact that led interpretations astray (Fan and Struhl 2009; Park et al. 2013; Teytelman et al. 2013).

A sequential spread model also does not consider genome organization; 3D contacts, or 'looping' with a nucleation site are conceivably an avenue for spread of heterochromatin factors that could result in discontinuous SIR complex binding. *S. cerevisiae* displays 3D contacts within and between *HML* and *HMR* (Hofmann et al. 1989; Valenzuela et al. 2008; Miele et al. 2009; Kirkland and Kamakaka 2013), and telomeres cluster in the nucleus (Gotta et al. 1996; Taddei et al. 2004). Telomeres and centromeres cluster in *S. pombe* as well, but only transiently during mitosis and meiosis (Funabiki et al. 1993; Scherthan et al. 1994). At least in *S. cerevisiae*, this clustering is not required to maintain silencing of *HML* or *HMR* (Gartenberg et al. 2004; Miele et

al. 2009). We do not know, however, the contribution of telomere and mating-type loci clustering on the process of heterochromatin establishment.

Spreading as a dynamic process

Transcriptional silencing is stable through major challenges to chromatin structure such as DNA replication and chromosome condensation and segregation during cell division, yet the factors that confer that silencing have dynamic associations with chromatin. This phenomenon is most well-studied for Swi6/HP1, for which high-resolution, single-molecule microscopy has shown short residence times on chromatin *in vivo* and *in vitro* (Cheutin et al. 2003; Festenstein et al. 2003; Cheutin et al. 2004; Müller et al. 2009; Kilic et al. 2015; Stunnenberg et al. 2015; Strom et al. 2017). The dynamics of Swi6 are also accompanied by dynamic spreading of transcriptional silencing at the mating-type loci (Greenstein et al. 2018). This transient binding may also be true for Sir proteins in *S. cerevisiae*, but the evidence is limited to observations that Sir proteins must be continually expressed for silencing maintenance (Miller and Nasmyth 1984) and one experiment that shows exchange of Sir3 molecules over time *in vivo* (Cheng and Gartenberg 2000).

The highly dynamic nature of heterochromatin proteins adds another dimension to spreading models. Perhaps these factors, after nucleation, quickly sample a region around that nucleation site but bind more strongly or stably only when they can interact cooperatively with themselves and other factors. Testing such models is difficult but becoming more accessible with advances in microscopy and improved ChIP-seq-type experiments that can capture more transient interactions. Application of combinations of these new methods to heterochromatin will bring important quantitative understanding to the mechanism of heterochromatin spreading.

1.3.4 Barriers

Because heterochromatin factors can spread independently of DNA sequence, there must exist ways to protect euchromatic genes from the stifling influence of heterochromatic neighbors. The unifying theme within and between organisms is that there is not a single barrier determinant but rather a multiplicity of barrier determinants. Evidence for barriers comes from characterization of chromatin at the boundaries of euchromatin and heterochromatin and from mutants that cause spread beyond wild-type boundaries or ectopic binding of heterochromatin factors. Identifying and characterizing spreading barriers informs spreading mechanisms by highlighting the components crucial to spread.

Conceptually, barriers could arise from a number of chromatin features: (1) A break in the nucleosome array due to nucleosome-poor DNA sequences or histone eviction by chromatin remodelers, (2) regions in which the rate of acetylation exceeds the rate of deacetylation, (3) the presence of histone variants or other histone modifications that could change the affinity of heterochromatin proteins for nucleosomes, or (4) 3D nuclear organization that defines or restricts the location of heterochromatin factors.

Nucleosome-depleted regions

The presence of nucleosome-depleted regions (NDRs) at transitions between heterochromatin and euchromatin is conserved among eukaryotes. These NDRs are commonly associated with the promoters of RNA Polymerase II and III-transcribed genes (Yuan et al. 2005;

Lee et al. 2007b; Ozsolak et al. 2007; Kirkland et al. 2013; Struhl and Segal 2013; Zhang et al. 2015; Helbo et al. 2017).

In *S. cerevisiae,* the silencers flanking *HML* and *HMR* are nucleosome-depleted (Weiss and Simpson 1998; Ravindra et al. 1999; Thurtle and Rine 2014). The binding of Sir proteins decreases distal to silencers, but there is still detectable binding, suggesting that these NDRs do not strictly limit the spread of Sir proteins (Thurtle and Rine 2014). DNA tracts of dA:dT or dG:dC can prevent nucleosome binding and act as barriers to heterochromatin spread (Iyer and Struhl 1995; Bi et al. 2004). Targeting the bacterial DNA binding protein LexA also creates a barrier to heterochromatin spread in *S. cerevisiae* by disrupting nucleosomes (Bi et al. 2004). In *S. pombe,* the inverted repeats that flank the silent 20-kilobase mating-type region (IR-R and IR-L) are also nucleosome-depleted and are correlated with a sharp decrease in binding of heterochromatin factors and associated modifications (Noma K et al. 2001; Thon et al. 2002; Garcia et al. 2015). Work in *S. pombe* shows that heterochromatin factors eliminate NDRs within heterochromatin, but the NDRs in IR-R and IR-L (as well as other NDRs at boundaries in centromeric heterochromatin) are somehow resistant to this activity (Garcia et al. 2010).

Outside of the telomere-proximal silencer at *HMR* lies a nucleosome-depleted tRNA gene, distal to which Sir protein binding to nucleosomes drops off dramatically (Oki and Kamakaka 2005; Dhillon et al. 2009). Deletion of this tRNA gene allows more extensive Sir protein binding beyond that site. (Donze et al. 1999; Donze and Kamakaka 2001). Interestingly, recruitment of RNA polymerase III is not required for the tRNA gene to serve a barrier function, but recruitment of TFIIIC and TFIIIB, which bind before RNA polymerase III at tRNA promoters, is. (Donze and Kamakaka 2001; Simms et al. 2008; Valenzuela et al. 2009). tRNA genes are found at the boundaries of pericentromeric heterochromatin of *S. pombe*, and DNA sequences that contain a tRNA gene can block heterochromatin proteins (Partridge et al. 2000; Scott et al. 2006). The nucleosome-depleted inverted repeats that flank the silent mating-type loci in *S. pombe* also have binding sites for the basal transcription factor, TFIIIC, but RNA Polymerase III is not recruited (Noma et al. 2006; Charlton et al. 2020). Therefore, it is not the transcription of the tRNA or IR elements, but possibly an NDR, that blocks the spread of heterochromatin. We cannot exclude the possibility, however, that some other aspect of tRNA promoters or TFIIIC binding sites, such as the recruitment of a histone acetyltransferase among the subunits of the RNA polymerase III holoenzyme or the recruitment of a Mediator-like complex, is responsible for barrier function.

The histone variant H2A.Z is enriched near nucleosome-depleted regions and active genes in most eukaryotes (Raisner et al. 2005; Zhang et al. 2005; Mavrich et al. 2008; Lantermann et al. 2010; Ranjan et al. 2013; reviewed in Altaf et al. 2009), and there is evidence that it plays a role at heterochromatin barriers. H2A.Z is enriched at telomere boundaries in *S. cerevisiae*, and its deletion results in spread of SIR beyond those boundaries (Meneghini et al. 2003; Venkatasubrahmanyam et al. 2007). More specifically, acetylation of H2A.Z is required for its barrier function because unacetylatable H2A.Z mutants have impaired barrier function (Babiarz et al. 2006). In *S. pombe*, H2A.Z is depleted within heterochromatin domains (Buchanan et al. 2009; Zofall et al. 2009). Further, deletion of certain subunits in the H2A.Z chaperone, Swr1C, causes H2A.Z to mislocalize to heterochromatin in centromeres and subtelomeres, resulting in a loss of silencing in those regions (Buchanan et al. 2009; Hou et al. 2010). H2A.Z is also acetylated in *S. pombe*, but we do not know how acetylation affects heterochromatin function (Buchanan et al. 2009; Kim et al. 2009).

Opposing chromatin-binding proteins and histone modifiers

The most conserved feature of heterochromatin is deacetylation of histone H3 and H4 tails. Studies using reconstituted chromatin *in vitro* demonstrate that histone acetylation prevents tight nucleosome packaging (Shogren-Knaak et al. 2006; Wang and Hayes 2008). This evidence in combination with sharp changes in histone acetylation at the boundaries of heterochromatin and euchromatin *in vivo* suggests that there are opposing acetyltransferases and deacetylases that balance heterochromatin spread and chromatin compaction.

With few exceptions, the action of a chromatin modifier can be reversed by a competing enzyme. Achieving balance between active and repressive marks is important for determining the extent of heterochromatin spreading. Competition for binding to particular histone marks also exists between heterochromatin proteins and other heterochromatin factors. Balancing the expression of competing chromatin modifiers prevents the spread of heterochromatin into regions containing essential genes: The combination of mutations in *SAS2* and *RPD3* that oppose H4K16 deacetylation by Sir2 in *S. cerevisiae* (Ehrentraut et al. 2010) and *MST1* and *EPE1* that oppose H3K9 methylation by Clr4 in *S. pombe* (Wang et al. 2015) are lethal, likely due to unconstrained heterochromatin silencing essential genes. In addition to directly opposing chromatin modifications, other modifications can weaken or strengthen the ability of heterochromatin factors to bind, such as H3K79 methylation, which precludes Sir3 association with the nucleosome (Park et al. 2002a; Ng et al. 2002; van Leeuwen et al. 2002; Ng et al. 2003; Xu et al. 2005; Altaf et al. 2007; Martino et al. 2009; Armache et al. 2011; Ehrentraut et al. 2011; Oppikofer et al. 2011; Stulemeijer et al. 2011; Hocher et al. 2018; Goodnight and Rine 2020).

In *S. cerevisiae*, Sir2 deacetylates, whereas Sas2 acetylates, H4K16 (Osada et al. 2001; Kimura et al. 2002; Suka et al. 2002; Imai et al. 2000; Borra et al. 2004). Somewhat paradoxically, Sas2-deficient cells experience a mild loss of silencing despite the loss of a heterochromatin-opposing mark (Dodson and Rine 2016; Thurtle-Schmidt et al. 2016). This decreased silencing may be an indirect effect if the global reduction of H4K16 acetylation permits the SIR complex to associate ectopically throughout the genome, titrating Sir proteins away from the mating-type loci and telomeres. Consistent with this hypothesis, Sir proteins spread past wild-type boundaries in Sas2-deficient cells (Kimura et al. 2002; Suka et al. 2002). Although ectopic binding to other regions of the genome in Sas2-deficient cells has not been confirmed in *S. cerevisiae*, there is evidence of genome-wide binding of the H3K9 methyltransferase SU(VAR)3-9 in *Drosophila* when specificity for heterochromatin has been lost or dampened (Schotta et al. 2002).

Histone acetylation and deacetylation also oppose one another in *S. pombe* heterochromatin. Clr3, the catalytic deacetylase subunit in SHREC, is opposed by Mst2, a histone acetyltransferase (Wang et al. 2015). Furthermore, in a mutant that results in ectopic heterochromatin spreading, tethering a different histone acetyltransferase, Mst1, to boundary regions suppresses that spread (Verrier et al. 2015).

In *S. pombe* and metazoans, another striking difference between heterochromatin and euchromatin is the enrichment of H3K9 methylation in heterochromatin. In *S. pombe*, H3K9 methylation by CLRC is opposed by the demethylase Epe1 (Ayoub et al. 2003; Trewick et al. 2007; Zofall et al. 2012; Audergon et al. 2015; Garcia et al. 2015; Ragunathan et al. 2015; Sorida et al. 2019). Epe1 is enriched at the inverted repeats flanking the silenced region between *mat2* and *mat3* and at centromere and telomere boundaries (Zofall and Grewal 2006). Epe1 also recruits the structural protein Bdf2 to compete with deacetylases to bind acetylated H3 and H4 (Wang et al. 2013), paralleling the barrier function of the *S. cerevisiae* homolog Bdf1 (Ladurner

et al. 2003). Similar to Sas2-deficient cells in *S. cerevisiae*, a loss of Epe1 also paradoxically results in a loss of silencing due to titration of CLRC and other factors that recognize H3K9 methylation away from target regions (Trewick et al. 2007).

Dosage of heterochromatin factors

The dosage of silencing proteins has been a strong hypothesis for delimiting heterochromatin since position effect variegation was discovered in *Drosophila* (Locke et al. 1988; Henikoff 1996), and was strengthened by later discoveries of variegation in *S. cerevisiae* and *S. pombe* (Allshire and Ekwall 2015; Gartenberg and Smith 2016). Many enhancers and suppressors of heterochromatin variegation are dosage sensitive: Overexpression results in a stronger phenotype, and reduced expression results in a weaker phenotype. These dosage-sensitive enhancers and suppressors are enriched for the structural components of heterochromatin rather than the catalytic components. By finely tuning the expression of heterochromatin factors, organisms could impose a physical limit on the size of heterochromatin.

Consistent with dosage determining heterochromatin boundaries, overexpression of Sir3 in *S. cerevisiae* and Swi6 in *S. pombe* results in the spread of each protein beyond some, but not all, boundaries, accompanied by repression or silencing of genes in those extended regions (Renauld et al. 1993; Hecht et al. 1996; Strahl-Bolsinger et al. 1997; Ng et al. 2003; Hocher et al. 2018). Accordingly, abnormally long telomeres cause silencing loss at *HMR*, probably due to titration of Sir proteins away from *HMR* (Buck and Shore 1995). There is also Sir2 and Sir4 dosage-sensitive transcriptional silencing at rDNA, the major region of the genome that Sir2 associates with other than heterochromatin (Smith et al. 1998). Recent work in *S. cerevisiae* even suggests that there is a feedback loop on Sir2 expression in response to varying levels of rDNA (Iida and Kobayashi 2019). Although there is no evidence that a loss of silencing changes the expression of Sir proteins, it is reasonable to imagine that this rDNA-Sir2 feedback loop would influence Sir protein distribution and thus have indirect effects on transcriptional silencing at *HML, HMR*, and telomeres in the absence of compensating mechanisms.

3D genome organization

The 3D organization that may contribute to spreading of heterochromatin factors may also be important to barrier function. Telomeres, *HML*, and *HMR* cluster at the nuclear periphery in *S. cerevisiae*. Mutations that disrupt that clustering do not cause a loss of silencing, but do result in repression of a few euchromatic genes containing Abf1 binding sites, suggesting that clustering may limit SIR diffusion (Taddei et al. 2009). There is also some evidence IR-R and IR-L in *S. pombe* exert their barrier function by tethering heterochromatin to the nuclear periphery (Noma et al. 2006; Charlton et al. 2020).

Phase separation

Swi6 in *S. pombe* and its homolog in *Drosophila* and mammals, HP1, show evidence of phase separation *in vitro* and *in vivo* (Larson et al. 2017; Strom et al. 2017; Sanulli et al. 2019). In principle, phase separation could form a barrier between heterochromatin and euchromatin, but experiments to test this *in vivo* are difficult; chemogenetic approaches to disrupt these phase-separated compartments, such as treatment with 6-hexanediol, are highly pleiotropic and we do not know their effect on transcriptional silencing. Mutations in Swi6/HP1 that could separate silencing and phase separation functions have yet to be discovered but would be pivotal in evaluating the potential contribution of phase separation to heterochromatin.

1.4 Case studies in spreading: Dosage compensation in mammals, *C. elegans,* and *Drosophila*

The biological sex of *C. elegans, Drosophila,* and mammals is determined by sex chromosomes. Female *Drosophila* and mammals have two X chromosomes whereas males have one X and one Y. *C. elegans* hermaphrodites have two X chromosomes whereas males have only one X chromosome. The difference in X chromosome number requires that the animal modify the transcription from one or both X chromosomes in one sex to equalize gene expression between the two sexes, a process called dosage compensation. Inability to compensate for dosage is often lethal or results in infertility. Each of these organisms has a different mechanism to achieve dosage compensation, but each involves the nucleation and DNA sequence-independent spread of specific dosage-compensation factors. We present short descriptions of the nucleation and spread of dosage compensation complexes, as well as their barriers, to highlight general features of chromatin-based spreading of gene expression states.

1.4.1 X-chromosome inactivation in female mammals

To accomplish dosage compensation in the expression of X-linked genes between males (XY) and females (XX) mammals, the females heterochromatinize one of their two X chromosomes, forming a highly condensed chromosome first described cytologically as a Barr body (Barr and Bertram 1949; reviewed in Galupa and Heard 2018). Whereas *S. cerevisiae* and *S. pombe* silence transcription within multi-kilobase domains, female mammals silence transcription of nearly an entire ~150 Mb X chromosome, a mighty task, with only a few genes escaping inactivation. In particular the gene *Xist* initiates the very compensation it avoids! The inactive X chromosome has a wealth of features: transcription of the long non-coding RNA *Xist*, extensive DNA methylation, major changes in 3D organization, incorporation of the histone variant macroH2A, and enrichment of various heterochromatin factors including histone deacetylases, H3K9 methyltransferases, Swi6/HP1 homologs, and Polycomb complexes (reviewed in Galupa and Heard 2018).

<u>*Nucleation*</u>

In mammals, transcription of the long non-coding RNA called Xist initiates silencing during X chromosome inactivation (Figure 1.2A). The *Xist* locus itself is the nucleation site for X chromosome inactivation, much like sites of non-coding RNA transcription in *S. pombe* serve as nucleation sites. It is contained within a cluster of non-coding RNA genes on the X chromosome known as the X-Inactivation Center. The *Xist* locus within the X-Inactivation Center is required to form heterochromatin along the entire X chromosome (Augui et al. 2011), and its ectopic insertion or translocation into an autosome triggers heterochromatin formation *in cis* along that autosome (Minks et al. 2013; Kelsey et al. 2015; Loda et al. 2017).

Xist is a multi-kilobase-long transcript with multiple domains, each of which binds to and recruits different silencing factors. The transcript localizes to nearly the entire X chromosome and recruits histone deacetylases and methyltransferases (including polycomb group complexes) to confer transcriptional silencing (Brockdorff et al. 2020).

Much like the DNA sequence-specific factors in *S. cerevisiae* and *S. pombe* serve as a bridge between DNA and silencing factors, the transcription factor YY1 may serve to tether Xist

to the X-Inactivation Center of the inactive X chromosome (Figure 1.2A). Loss of YY1 results in a loss of Xist localization on the X chromosome (Donohoe et al. 2007; Jeon and Lee 2011; Syrett et al. 2017), but conflicting results on whether YY1 regulates the expression of Xist itself muddies YY1's physical role as a nucleation factor (Donohoe et al. 2007; Jeon and Lee 2011; Makhlouf et al. 2014).

Spread

Characteristic of the contexts described in this review, spreading of the heterochromatin factors involved in mammalian X chromosome inactivation is DNA-sequence independent. Famous mouse studies from the late 1950s and early 1960s found that translocation of an autosome carrying a coat-color gene onto the female X chromosome results in a mosaic, rather than solid, coat color due to X chromosome inactivation (Cattanach 1961; Russell and Bangham 1961).

Some of the strongest evidence for 3D structure influencing the spread of heterochromatin factors comes from two studies on the spread of Xist during X chromosome inactivation (Engreitz et al. 2013; Simon et al. 2013). In contrast to the other contexts described in this review, the first sites of *Xist* localization along the X chromosome lack a shared DNA sequence motif. Instead, these early binding sites correlate with points of frequent 3D-contact with the *Xist* locus. During X chromosome inactivation, Xist and Polycomb complexes first localize to regions of the X chromosome that contact the *Xist* locus at 'early-entry' sites before they cover the entire chromosome. This proposed two-step mechanism, however, does not address the mechanism of spread in *cis* to those early-entry sites. Studies to address this issue require higher temporal and spatial resolution.

Although the large majority of the inactive X is transcriptionally silent, there are a few 'escaper' genes that are not repressed and not bound by heterochromatin factors (Brown and Willard 1989; Carrel and Willard 2005; Balaton and Brown 2016). The escapers in this context are consistent with a conserved characteristic of spreading factors discussed throughout this review: discontinuous binding within a larger region of repression. This is consistent with a spreading mechanism that cannot be purely sequential from nearby nucleation sites.

Barriers

The barriers that allow some genes to remain active on the inactive X chromosome has been the subject of intense study with few clear answers, but there are correlations between these escaper genes and various DNA sequences and 3D organization (reviewed in Peeters et al. 2014; Galupa and Heard 2018). Escaper genes tend to be present within the same Topologically Associated Domain (TAD) prior to X chromosome inactivation (Marks et al. 2015; Giorgetti et al. 2016). The transcription factor CTCF, which binds at TAD boundaries, may enforce a barrier between heterochromatin and euchromatin (Horvath et al. 2013; Loda et al. 2017). However, the importance of 3D structure for X chromosome inactivation has recently been called into question: Abolishing the formation of the inactive X-specific 3D structure called a "megadomain" by deletion of its coordinating noncoding locus Dxz4 has no impact on transcriptional silencing or the expression of escaper genes, and the ectopic expression of Xist on an autosome does not affect the 3D structure of that chromosome (Froberg et al. 2018).

Once the choice of which X to inactivate is made, the physical distance between the active and inactive X may provide another type of barrier that helps ensure that Xist does not act in *trans* to compromise the expression of the active X (Brockdorff 2019). Indeed, the discovery

of the Barr body noted that it was always seen near the outer periphery of the nucleolus (Barr and Bertram 1949), away from other chromosomes. Other influences restricting the potential of Xist to act in *trans* may be the attachment of Xist to the nuclear matrix (Ridings-Figueroa et al. 2017; Sunwoo et al. 2017) and tethering of nascent Xist to the inactive X chromosome by transcription factors like YY1 to prevent its diffusion within the nucleus (Syrett et al. 2017).

1.4.2 Upregulation of the X chromosome in male *Drosophila*

Drosophila upregulate the transcription of genes on the X chromosome in males (XY) by approximately two-fold to match transcription from the two X chromosomes in females (reviewed in Samata and Akhtar 2018). Despite achieving the opposite transcriptional output compared to *S. cerevisiae* and *S. pombe* heterochromatin and mammalian X chromosome inactivation, many of the features of repressive complex spreading are conserved in *Drosophila* dosage compensation. As opposed to hypoacetylation of chromatin in heterochromatin context, the male X chromosome in *Drosophila* is marked by hyperacetylation, particularly of H4K16 (Bone et al. 1994; Smith et al. 2001; Gelbart et al. 2009). The spreading complex in this context is known as the Male Specific Lethal (MSL) complex, so named for the male-specific lethality associated with mutations affecting the complex. MSL is made up of five protein subunits (MSL1, MSL2, MSL3, MLE, and MOF) and one of two non-coding RNAs (*roX1* or *roX2*) (Samata and Akhtar 2018).

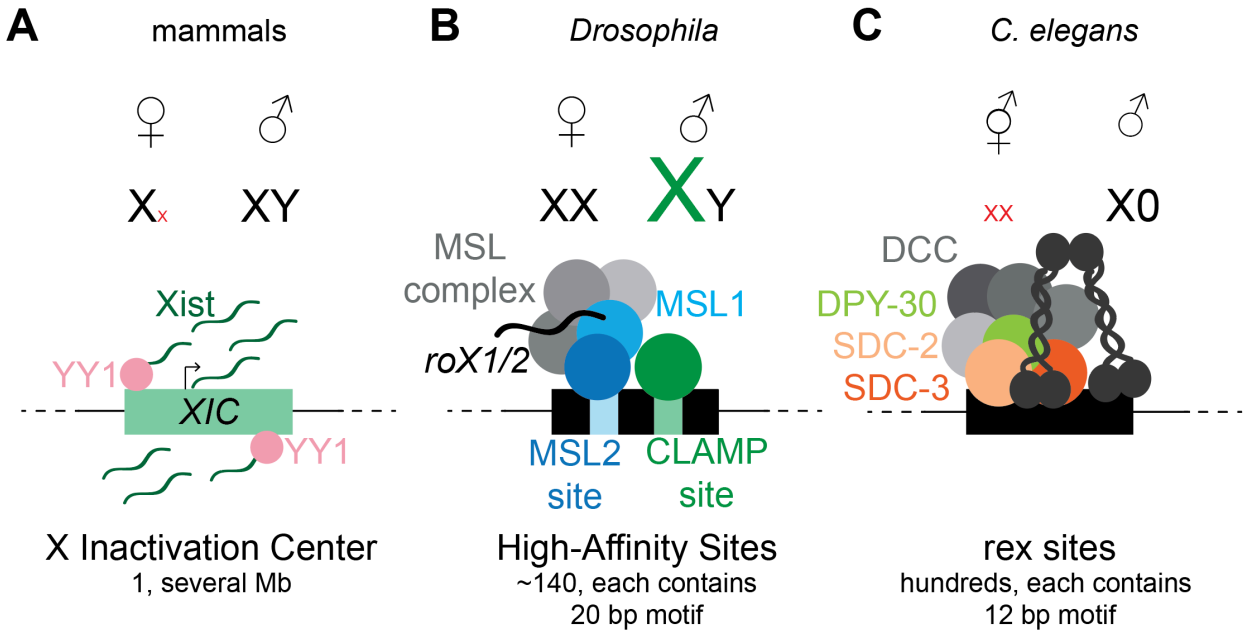

Figure 1.2. Nucleation of X-chromosome dosage compensation in mammals, *Drosophila*, and *C. elegans*
A) Female mammals transcriptionally silence one X chromosome to match expression of the single X chromosome in males. Nucleation of heterochromatin on the silent X chromosome begins with the transcription of the non-coding RNA Xist from the X Inactivation Center (XIC). YY1 may help to tether Xist to the X inactivation center. Xist then recruits heterochromatin proteins to the X inactivation center and along the entire X chromosome as it spreads. **B)** Male *Drosophila* upregulate transcription of genes on their single X chromosome by two-fold to match expression of the two X chromosomes in females. Transcriptional upregulation is mediated by the MSL (Male Specific Lethal) complex, which is composed of both proteins and a non-coding RNA (*roX1* or *roX2*). MSL1 in the MSL complex
(continued on next page)

and CLAMP (Chromatin-Linked Adaptor for MSL Proteins), a zinc-finger protein, bind to DNA sequences in hundreds of High-Affinity Sites on the male X chromosomes. These two proteins recruit the rest of the MSL complex to upregulate genes on the X chromosomes. **C)** Hermaphrodite *C. elegans* repress transcription by half on each X chromosome to match expression of the single X in males *C. elegans*. Transcriptional downregulation is mediated by the DCC (Dosage Compensation Complex), a condensin-like protein complex. SDC-2 is first recruited to hundreds of *rex* (Recruitment Elements on the X) sites on the X chromosomes. SDC-2 then recruits DPY-30, followed by SDC-3. All three of these DCC members are sufficient to recruit the remainder of the DCC to the X chromosomes.

Nucleation

The X chromosome in *Drosophila* has approximately 130-150 sites where MSL binds before spreading to cover genes on the 24 Mb X chromosome of males (Dahlsveen et al. 2006; Alekseyenko et al. 2008; Straub et al. 2008). These initial binding sites, called High-Affinity Sites or Chromatin Entry Sites, contain DNA motifs bound by MSL2 and the zinc-finger protein CLAMP (Figure 1.2B) (Soruco et al. 2013; Villa et al. 2016; Albig et al. 2019; Rieder et al. 2019; Tikhonova et al. 2019). Like Abf1 and Rap1 in *S. cerevisiae* and Atf1 and Pcr1 in *S. pombe*, CLAMP serves as a DNA sequence-specific adaptor protein that helps recruit the MSL complex. However, the CLAMP DNA motif alone is not sufficient to nucleate MSL; other factors such as DNA structure or nearby satellite repeats may also play a role in recruiting MSL (Menon et al. 2014; Villa et al. 2016; Joshi and Meller 2017).

MSL1 and MSL2 together are sufficient to target the entire MSL complex to High-Affinity Sites (Gu et al. 1998). The other subunits of MSL are not necessary to localize MSL1 and MSL2 to these nucleation sites (Lyman et al. 1997; Gu et al. 1998). Like Xist in mammals and RNAi in *S. pombe* heterochromatin, the non-coding RNAs *roX1* and *roX2* are required for nucleation of MSL, and the *roX1* and *roX2* genes themselves serve as High-Affinity Sites (Kelley et al. 1999; Meller and Rattner 2002; Park et al. 2002b; Oh et al. 2003; Kelley and Kuroda 2003; Kelley et al. 2008; Ramírez et al. 2015).

Spread

The enzymatic activity of MOF, a histone acetyltransferase subunit of MSL, is required for spreading of MSL from nucleation sites (Gu et al. 2000; Conrad et al. 2012). However, no binding module for acetylation of H4 on lysine 16 (H4K16ac) has been described. Trimethylation of lysine 36 on histone H3 (H3K36me3) and methylation of lysine 20 on histone H4 (H4K20me1) may contribute to the spread of MSL from High-Affinity Sites to gene bodies on the male X chromosome. MSL and H3K36me3 colocalize on the X chromosome (Larschan et al. 2007; Bell et al. 2008; Sural et al. 2008; Straub et al. 2013), and *set2* mutants that cannot methylate H3K36 show reduced occupancy of MSL on the X chromosome (Larschan et al. 2007). A crystal structure of MSL3 bound to an H4K20me1 peptide fragment suggests this histone modification could play a role *in vivo* (Kim et al. 2010; Moore et al. 2010). How each of these histone modifications contribute mechanistically to spread is unclear and requires further investigation.

As in each spreading context discussed in this review, MSL binding along the male X is discontinuous (Gu et al. 1998; Alekseyenko et al. 2006; Gilfillan et al. 2006; Bell et al. 2008). It is enriched over gene bodies, especially toward the 3' end of the gene, suggesting that transcription itself might drive the spread of MSL (Alekseyenko et al. 2006; Gilfillan et al. 2006). But not every gene is near a High-Affinity Site, so there must be some mechanism of spreading from those High-Affinity Sites to distant gene bodies. Interestingly, histone acetylation on the X has a wider distribution than MSL binding by ChIP (Gelbart et al. 2009). MSL might

have transient interactions with the entire X chromosome and is only stabilized over gene bodies, perhaps due to interactions between H3K36me3 and/or H4K20me1 and MSL3 (Sural et al. 2008; Kim et al. 2010; Moore et al. 2010). Experiments to address this difference between MSL and histone acetylation distribution would bring clarity to the mechanism of MSL spreading and inform models of spreading in other contexts.

High-Affinity MSL binding sites are enriched at TAD boundaries and are in frequent 3D contact with one another (Grimaud and Becker 2009; Ramírez et al. 2015), which could help concentrate MSL and aid in spreading outward from High-Affinity Sites. Higher time-resolved ChIP-seq experiments are needed to address this hypothesis.

Barriers

The pericentromeric regions and telomeres of the X chromosome are heterochromatic in both males and females. Therefore, something limits the spread of MSL on the male X chromosome at these regions. Dosage of MSL subunits and the balance of heterochromatin and euchromatin factors may play a role in restricting MSL to euchromatin on the X chromosome (Henikoff 1996; Demakova et al. 2003). Upon *roX1* and *roX2* deletion, or upon overexpression of MSL components, MSL mislocalizes to heterochromatin (Meller and Rattner 2002; Demakova et al. 2003). Further, overexpression of at least one heterochromatin factor, Su(var)3-7, also causes mislocalization of MSL to heterochromatin (Spierer et al. 2008). In seeming contradiction, expression of genes within heterochromatin decreases in *roX* mutants compared to wild-type (Koya and Meller 2015), but position effect variegation is suppressed (Deng et al. 2009; Koya and Meller 2015). Thus, the expression and distribution of MSL balances that of heterochromatin factors in male flies, but the molecular details are unsolved.

DNA sequences may also play a barrier role, through reducing MSL affinity or recruiting MSL-antagonizing factors. Repetitive elements specific to the X chromosome are found at the euchromatin/heterochromatin boundaries, but whether they have a barrier function is unknown (Tudor et al. 1996; O'Hare et al. 2002). Whether the boundary between heterochromatin and MSL binding on the *Drosophila* male X chromosome is enforced by a physical barrier, by the relative level of components, or by some dynamic equilibrium between the two spreading mechanisms awaits determination with new tools that provide time-resolved, single-molecule resolution at the single-cell level.

1.4.3 Repression of the X chromosomes in hermaphrodite *C. elegans*

Dosage compensation in *C. elegans* is the conceptual inverse of the outcome in *Drosophila.* Hermaphrodite *C. elegans* (XX) repress transcription of genes on both X chromosomes by half to equal the dosage of transcripts from the single X chromosome in males (X0) (Meyer and Casson 1986). Dosage compensation in *C. elegans* is conferred by the nucleation and spread of the Dosage Compensation Complex (DCC). DCC is homologous to condensin, a conserved, multi-subunit complex that condenses chromosomes during mitosis. The DCC is bound along the X chromosome only in hermaphrodites and is thought to cause two-fold transcriptional repression by compacting the X chromosome, limiting the accessibility of transcription factors and RNA polymerase (reviewed in Ercan and Lieb 2009; Strome et al. 2014; Albritton and Ercan 2018; Meyer In press).

Nucleation

Mirroring the nucleation of MSL at High-Affinity Sites in *Drosophila* dosage compensation, the *C. elegans* DCC is recruited to hundreds of nucleation sites along the 17 Mb X chromosome called recruitment elements on the X (*rex*) (Figure 1.2C) (Csankovszki et al. 2004; McDonel et al. 2006; Ercan et al. 2007; Jans et al. 2009). These sites share a 12 bp DNA sequence that is required to recruit DCC (McDonel et al. 2006; Jans et al. 2009; Albritton et al. 2017). In contrast to the other nucleation sites discussed in this review, *rex* is not sufficient to recruit DCC. Ectopic insertion of a *rex* site on an autosome does not result in DCC recruitment (Csankovszki et al. 2004; Anderson et al. 2019). Additionally, this 12 bp sequence is found throughout autosomes without any DCC recruitment (McDonel et al. 2006; Jans et al. 2009). The context and density of *rex* sites within the X chromosome or within the nucleus is important, but the determinants of DCC recruitment beyond *rex* sites are not clear.

A subunit of the DCC, SDC-2, is the first subunit on the scene and is required to recruit the rest of the DCC to *rex* sites (Chuang et al. 1996; Dawes et al. 1999). SDC-2 recruits DPY-30, followed by SDC-3 (Figure 1.2C) (Pferdehirt et al. 2011). All three of these DCC members are required to recruit the remainder of the DCC (Davis and Meyer 1997; Pferdehirt et al. 2011). There is no evidence that any member of the DCC, including SDC-2, directly recognizes the *rex* sequence. But as SDC-2 binds independently of all other DCC subunits, it is the top candidate.

Spread

DCC is found along both X chromosomes in hermaphrodites, enriched in gene promoters. DCC localization shares the characteristic with other examples in this review in that it is discontinuous. Low levels of binding are punctuated by high enrichment of the DCC at gene promoters (Ercan et al. 2007, 2009; Jans et al. 2009; Pferdehirt et al. 2011). As with the other examples in this review, where the DCC nucleates and where it ends up are well characterized, but the mechanism(s) connecting the start and end points remains elusive. Perhaps 3D contact sites help; *rex* sites cluster together and the establishment of dosage compensation is accompanied by large-scale 3D-contact changes (Crane et al. 2015; Anderson et al. 2019; Bian et al. 2020). However, these topology changes are not required for dosage compensation, so their role in dosage compensation may be a consequence of compensation or some unrelated process (Anderson et al. 2019).

H4K20me1 is found along the hermaphrodite X chromosome but not on the X chromosome of males (Kramer et al. 2015; Liu et al. 2011). A DCC subunit, DPY-21, is a histone demethylase that converts H4K20me2 into H4K20me1 (Brejc et al. 2017). Because demethylation occurs temporally after transcriptional downregulation, any role it plays is likely to be in the maintenance of dosage compensation. So far, no other chromatin modifications have been linked to spreading of the DCC from recruitment sites.

Barriers

A 12 bp *rex* site is not sufficient for recruitment of DCC on autosomes, so there must be contexts on the X chromosome that achieve DCC specificity. One possibility consistent with results in *S. cerevisiae* is that H2A.Z serves as a barrier to DCC binding or spreading. H2A.Z is depleted on the X chromosomes in hermaphrodites but not males, and the loss of H2A.Z in hermaphrodites results in a modest loss of dosage compensation and some mislocalization of DCC outside of the X chromosome territory in the nucleus (Petty et al. 2009). However, the

disruption of dosage compensation and DCC localization is minor, so there are likely other factors at play.

There is also evidence of a balance between levels of DCC and levels of transcriptional activators in the nucleus. When DCC fails to assemble and turn down transcription on the X chromosome, transcription of many genes throughout the genome is reduced, while expression from the X chromosome slightly increases, probably due to titration of activators away from autosomes (Jans et al. 2009). It is possible that the DCC directly competes with transcriptional activators to achieve the appropriate level of transcription, but the transcriptional effects of overexpression of DCC components has not been assessed.

1.5 Concluding Remarks

The molecules and mechanisms of nucleation are well-established in contexts described here. Although the specific molecules differ among organisms, nucleation generally depends on some feature of the DNA sequence combined with other proteins or RNA molecules that recruit and/or tether spreading complexes to chromatin. Barriers lack a single mechanism, but there are several reasonable ways that spreading can be limited, whether it be the positioning of nucleosomes at a locus or the broader mechanism of balanced expression between transcriptional activation machinery and transcriptional silencing machinery. What is completely lacking is a detailed mechanism for spreading; we know where spreading complexes nucleate and we know (across a population) where those complexes exist at equilibrium, but how they get from state A to state B is unknown. To address these issues, we need single-molecule resolution at single-cell level. We need ways of capturing not just where these spreading complexes reside but a historical record of where they have been during the creation of the new state of expression. As these higher-resolution tools and methods are developed across disciplines–biochemistry, genomics, molecular, and cellular biology–those fascinating details are sure to come closer into focus.

Chapter 2:

Distinguishing between recruitment and spread of silent chromatin structures in *Saccharomyces cerevisiae*

2.1 Abstract

The formation of heterochromatin at *HML*, *HMR*, and telomeres in *Saccharomyces cerevisiae* involves two main steps: Recruitment of Sir proteins to silencers and their spread throughout the silenced domain. We developed a method to study these two processes at single base-pair resolution. Using a fusion protein between the heterochromatin protein Sir3 and the non-site-specific bacterial adenine methyltransferase M.EcoGII, we mapped sites of Sir3-chromatin interactions genome-wide using long-read Nanopore sequencing to detect adenines methylated by the fusion protein. A silencing-deficient mutant of Sir3 lacking its Bromo-Adjacent Homology (BAH) domain, *sir3-bah*Δ, was still recruited to *HML*, *HMR*, and telomeres. However, in the absence of the BAH domain, it was unable to spread away from those recruitment sites. Overexpression of Sir3 did not lead to further spreading at *HML*, *HMR*, and most telomeres. A few exceptional telomeres, like 6R, exhibited a small amount of Sir3 spreading, suggesting that boundaries at telomeres responded variably to Sir3 overexpression. Finally, by using a temperature-sensitive allele of *SIR3* fused to *M.ECOGII*, we tracked the positions first methylated after induction and found that repression of genes at *HML* and *HMR* began before Sir3 occupied the entire locus.

2.2 Introduction

Cells have an interest in coordinating the expression of genes: It allows them to turn sets of genes on and off in response to various stimuli or ensure certain genes are always expressed or always repressed to create and maintain cell identity. There are multiple ways to coordinate transcription, including shared binding sites for activators or repressors in promoters, nuclear compartmentalization, and creation of large domains like heterochromatin. The establishment of coordinated, stable blocs of gene expression, such as heterochromatin, can be broken down into two main steps: Nucleation, which involves the recruitment of chromatin-modifying factors, followed by the expansion of these chromatin-modifying factors beyond recruitment sites in an ill-defined process known as spreading.

An impressive example of the concepts of nucleation and spread is inactivation of the X chromosome in female mammals (reviewed in Galupa and Heard 2018). Nucleation begins with the transcription of the non-coding RNA Xist from one of the two X chromosomes, which recruits heterochromatin factors in *cis* that eventually coat and transcriptionally silence nearly the entire 167-megabase X chromosome. Two studies have characterized early steps in nucleation at the *Xist* locus and at recruitment sites throughout the X chromosome (Engreitz et al. 2013; Simon et al. 2013), but the mechanics of how the Xist transcript and associated heterochromatin proteins spread remains unclear even for this well-studied phenomenon. Furthermore, 'spreading' itself is an inferred process that connects known recruitment sites to the final binding profile of heterochromatin proteins. A clear mechanistic distinction between nucleation and spread, with a characterization of intermediate steps, has not been achieved for any organism.

Transcriptional silencing in the budding yeast *Saccharomyces cerevisiae* is one of the best-studied heterochromatic phenomena (reviewed in Gartenberg and Smith 2016). Heterochromatin is created by the Silent Information Regulator (SIR) complex that silences the transcription of genes at *HML* and *HMR* and the 32 telomeres. Recruitment of the SIR complex to *HML*, *HMR*, and telomeres is sequence specific, whereas its spreading is sequence nonspecific. More specifically, different combinations of Rap1, Abf1, and Origin Recognition Complex (ORC) binding sites are present at the *E* and *I* silencers that flank *HML* and *HMR* (Shore and Nasmyth 1987; Shore et al. 1987; Buchman et al. 1988; Kimmerly et al. 1988) and at the TG repeats and X elements of telomeres (Longtine et al. 1989; Stavenhagen and Zakian 1994; Buchman et al. 1988). These proteins in turn interact with and recruit the SIR complex (Cockell et al. 1995; Triolo and Sternglanz 1996; Moretti and Shore 2001). The SIR complex then deacetylates chromatin (Braunstein et al. 1993; Suka et al. 2001; Thurtle and Rine 2014; Ellahi et al. 2015), resulting in chromatin compaction (Gottschling 1992; Singh and Klar 1992; Loo and Rine 1994; Georgel et al. 2001; Johnson et al. 2009; Swygert et al. 2018). As a result, transcription is blocked at least in part by steric occlusion, though details remain unknown (Sekinger and Gross 2001; Chen and Widom 2005; Gao and Gross 2008; Lynch and Rusche 2009; Johnson et al. 2013; Steakley and Rine 2015). Almost any gene placed within the defined domain can be transcriptionally silenced, establishing the locus-specific, gene non-specific nature of heterochromatic silencing (Schnell and Rine 1986; Gottschling et al. 1990; Sussel et al. 1993; Dodson and Rine 2015; Saxton and Rine 2019). This difference in sequence dependence between recruitment and spread implies they are separable processes that rely on different factors and interactions.

Of the three SIR complex members (Sir2, Sir3, and Sir4), Sir3 is thought to be the major structural driver of heterochromatin spread and compaction. Sir3 interacts with the silencer-binding proteins Abf1 and Rap1 (Moretti et al. 1994; Moretti and Shore 2001), with the other members of the SIR complex, Sir2 and Sir4 (Strahl-Bolsinger et al. 1997; Chang et al. 2003; Rudner et al. 2005; Ehrentraut et al. 2011; Samel et al. 2017), with nucleosomes (Johnson et al. 1990; Hecht et al. 1995; Onishi et al. 2007; Norris et al. 2008; Armache et al. 2011), and with itself (King et al. 2006; Oppikofer et al. 2013; Liaw and Lustig 2006). All of these Sir3 interactions are required for transcriptional silencing. *In vitro*, Sir3 dimers can bridge neighboring nucleosomes and compact chromatin (Behrouzi et al. 2016). Among the SIR complex members, Sir3 has the largest difference in affinity for acetylated and deacetylated histone tails (Carmen et al. 2002; Onishi et al. 2007; Armache et al. 2011; Oppikofer et al. 2011; Swygert et al. 2018). By binding deacetylated histone tails more strongly than acetylated ones, Sir3 helps create a positive feedback loop wherein Sir2 deacetylates histone tails (Landry et al. 2000; Imai et al. 2000; Smith et al. 2000; Ghidelli et al. 2001) and Sir3 reinforces and further recruits Sir2/4 to silent regions.

Characterization of SIR complex nucleation and spread is limited by techniques like ChIP-seq that measure processes on populations of molecules and at a resolution limited by sequencing-read length. We developed a new method that allowed us to characterize the binding of heterochromatin proteins at base-pair resolution. Using long-read sequencing, we used this new method to resolve the distinction between the recruitment and spread of Sir3 and to track the establishment of heterochromatin over time. These data pinpointed when the process of transcriptional silencing begins.

2.3 Results

2.3.1 The Sir3-M.EcoGII fusion protein strongly and specifically methylated *HML* and *HMR*

To achieve a higher-resolution method for assessing SIR complex binding, we made a fusion protein between Sir3 and M.EcoGII (Figure 2.1A), a non-site-specific bacterial N6-methyladenosine methyltransferase (Murray et al. 2018; Woodcock et al. 2020). In principle, wherever Sir3 binds chromatin, even transiently, M.EcoGII should methylate nearby accessible adenines to make m^6A. *S. cerevisiae* has no endogenous DNA methylation and no demethylases, allowing us to attribute m^6A only to the activity of the fusion protein, reflecting where it resides as well as where it has been. M. EcoGII has no specific recognition sequencing, which should provide more resolution than methyltransferases like *E. coli* Dam, which has a four base-pair recognition site. The positions of Sir3-M.EcoGII can be determined conventionally by immunoprecipitation with an antibody against m^6A followed by sequencing the precipitated DNA using Illumina sequencing. The more powerful implementation would come from distinguishing between individual m^6A bases and unmodified A bases using long-read Nanopore sequencing. (Xu and Seki 2020).

To test this concept, we first assessed the silencing ability of Sir3-M.EcoGII by growing colonies with GFP integrated at *HMRα2* and RFP integrated at *HMLα2*. Colonies expressing Sir3-M.EcoGII produced colonies with no fluorescence (Figure 2.1B). Thus, the fusion protein retained full function of Sir3.

To compare the binding profile of Sir3-M.EcoGII to the distribution of methylation it produced, we performed DNA immunoprecipitation and Illumina sequencing (DIP-seq) using an antibody that specifically recognizes m^6A alongside ChIP-seq for a V5 epitope-tagged Sir3-M.EcoGII. ChIP-seq revealed strong Sir3-M.EcoGII occupancy over the *E* and *I* silencers at *HML* and over the *E* silencer at *HMR* with weaker but consistent signal above background between the two silencers (Figure 2.1C, top row). Compared to ChIP-seq, methylation measured by DIP-seq had a stronger signal over the entirety of *HML* and *HMR* and a broader signal that extended beyond the silencers (Figure 2.1C, Figure 2.1–figure supplement 1). The methylation over *HML* and *HMR* was from the fusion protein Sir3-M.EcoGII, as neither a strain without M.EcoGII nor a strain expressing unfused M.EcoGII from the *SIR3* promoter showed appreciable DIP-seq signal (Figure 2.1C, Figure 2.1–figure supplement 1).

Methylation by Sir3-M.EcoGII measured by Nanopore sequencing agreed well with DIP-seq, showing strong methylation over *HML* and *HMR* with little background methylation outside of these regions (Figure 2.1D, Figure 2.1–figure supplement 2A). Fusions of Sir2 and Sir4 with M.EcoGII were also fully silencing competent (Figure 2.1B) and produced methylation signals that matched Sir3-M.EcoGII at *HML* and *HMR* (Figure 2.1D), suggesting that all three members of the SIR complex were equally distributed, as expected. In addition to the aggregate methylation signal (% of reads methylated at each position), we analyzed methylation of single adenines on single reads across *HML* and *HMR* (Figure 2.1E, Figure 2.1–figure supplement 2B). Sir3-M.EcoGII methylated most strongly near the *E* and *I* silencers and at the *HMLα1/α2* promoter, with lower, but significant, methylation between these sites (Figure 2.1E, Figure 2.1–figure supplement 2B). Analysis of single reads revealed a periodicity of methylation across *HML* and *HMR* (Figure 2.1E, Figure 2.1–figure supplement 2B). These small regions of higher methylation corresponded to linker regions between nucleosomes (Figure 2.1–figure supplement 3). Sir3-M.EcoGII did methylate within nucleosome-occupied regions at *HML* and *HMR* but at a

lower frequency (Figure 2.1–figure supplement 3), consistent with *in vitro* studies that use methylation by M.EcoGII or another non-specific adenine methyltransferase, Hia5, as a measurement of chromatin accessibility (Abdulhay et al. 2020; Shipony et al. 2020; Stergachis et al. 2020; Altemose et al. 2021).

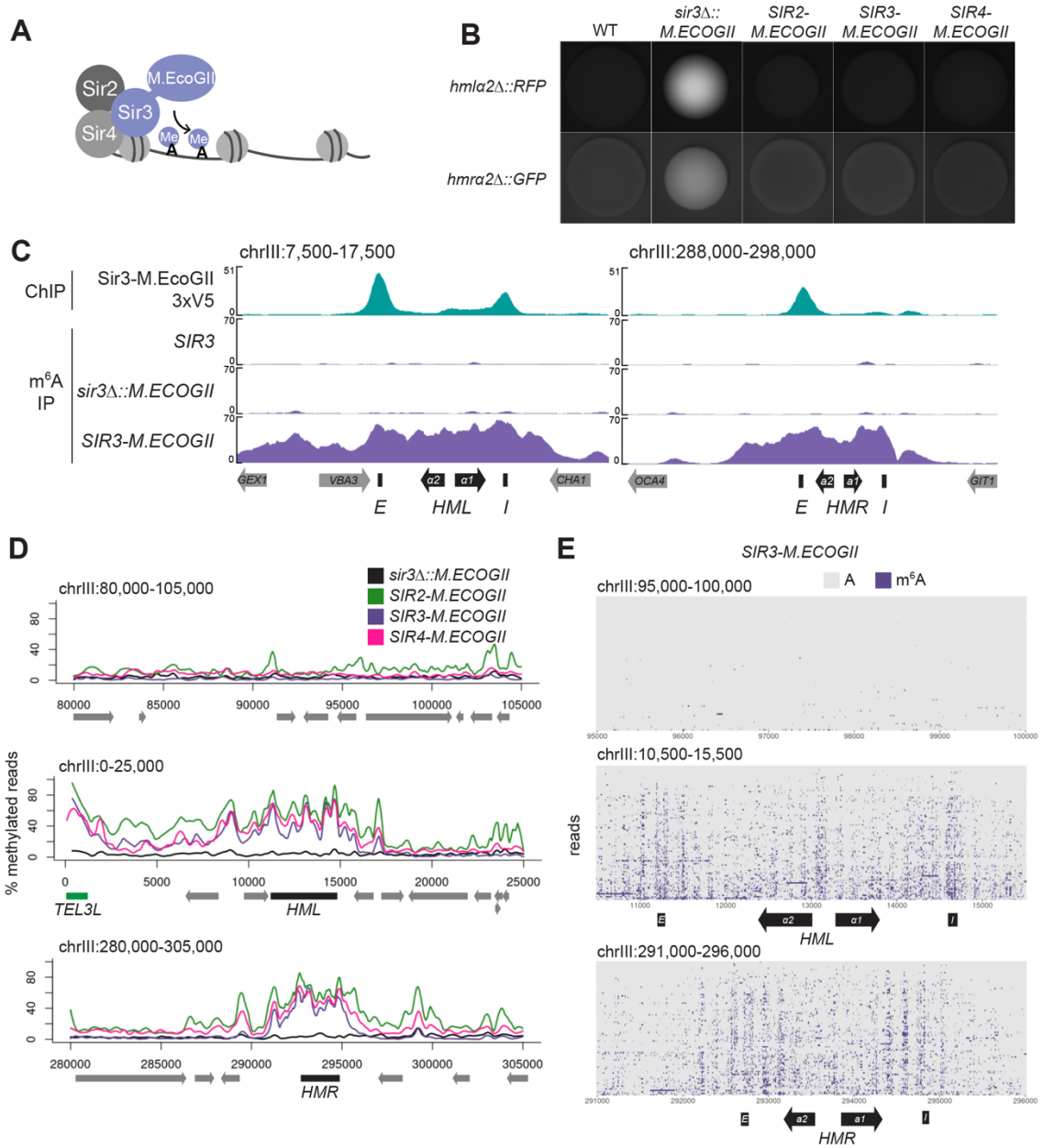

Figure 2.1. The Sir3-M.EcoGII fusion protein strongly and specifically methylated *HML* and *HMR*
A) Sir3-M.EcoGII is a fusion protein that non-specifically methylates adenines in regions that Sir3 binds. **B)** Genes encoding fluorescence reporters were placed at *HMLα2* (*RFP*) and *HMRα2* (*GFP*) to report on transcription from the two loci. Shown are representative images of colonies from each strain: no M.EcoGII (WT, JRY12731), unfused M.EcoGII (*sir3Δ::M.EcoGII*, JRY12842), *SIR2-M.ECOGII* (JRY13660), *SIR3-M.ECOGII* (JRY12844), and *SIR4-M.ECOGII* (JRY13019). **C)** ChIP-seq of Sir3-M.EcoGII-3xV5 (top row, JRY12839) and DNA m6A immunoprecipitation and sequencing (DIP-seq) of no EcoGII (row two, JRY11699), *sir3Δ::M.ECOGII* (row three, JRY12838), and *SIR3-M.ECOGII* (row four, JRY12840). Shown are 10 kb regions centered at *HML* (left) and *HMR* (right). Input results are plotted but not visible due to the strong ChIP-seq and DIP-seq signals. **D)** Aggregate results
(continued on next page)

from long-read Nanopore sequencing of *sir3*Δ*::M.ECOGII* (black line, JRY12838), *SIR2-M.ECOGII* (green line, JRY13625), *SIR3-M.ECOGII* (purple line, JRY13027), and *SIR4-M.ECOGII* (pink line, JRY13021). The y-axis represents the percentage of reads in each position called as methylated by the modified-base calling software Megalodon (see Materials & Methods). Shown are 25 kb windows at a control region on chromosome III to show background methylation (top row), at *HML* (middle row), and at *HMR* (bottom row). **E)** Single-read plots from long-read Nanopore sequencing of *SIR3-M.ECOGII* (JRY13027). Each row of the plots is a single read the spans the entire query region, ordered by lowest average methylation on the top to highest average methylation on the bottom. Methylated adenines are colored purple, and unmethylated adenines are colored gray. Shown are 5 kb windows at a control region on chromosome III to show background methylation (top row), at *HML* (middle row), and at *HMR* (bottom row)

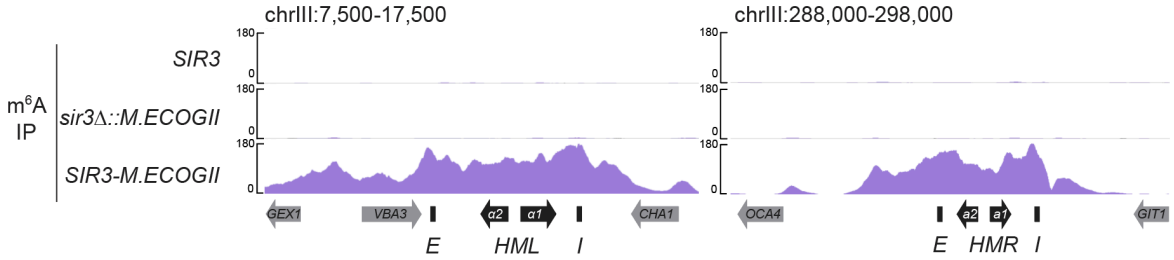

Figure 2.1–Figure Supplement 1. *Sir3-M.EcoGII* strongly and specifically methylated *HML* and *HMR*
Biological replicates of DIP-seq of no EcoGII (top row, JRY09316), *sir3*Δ*::M.ECOGII* (middle row, JRY12838), and *SIR3-M.ECOGII* (bottom row, JRY13027)

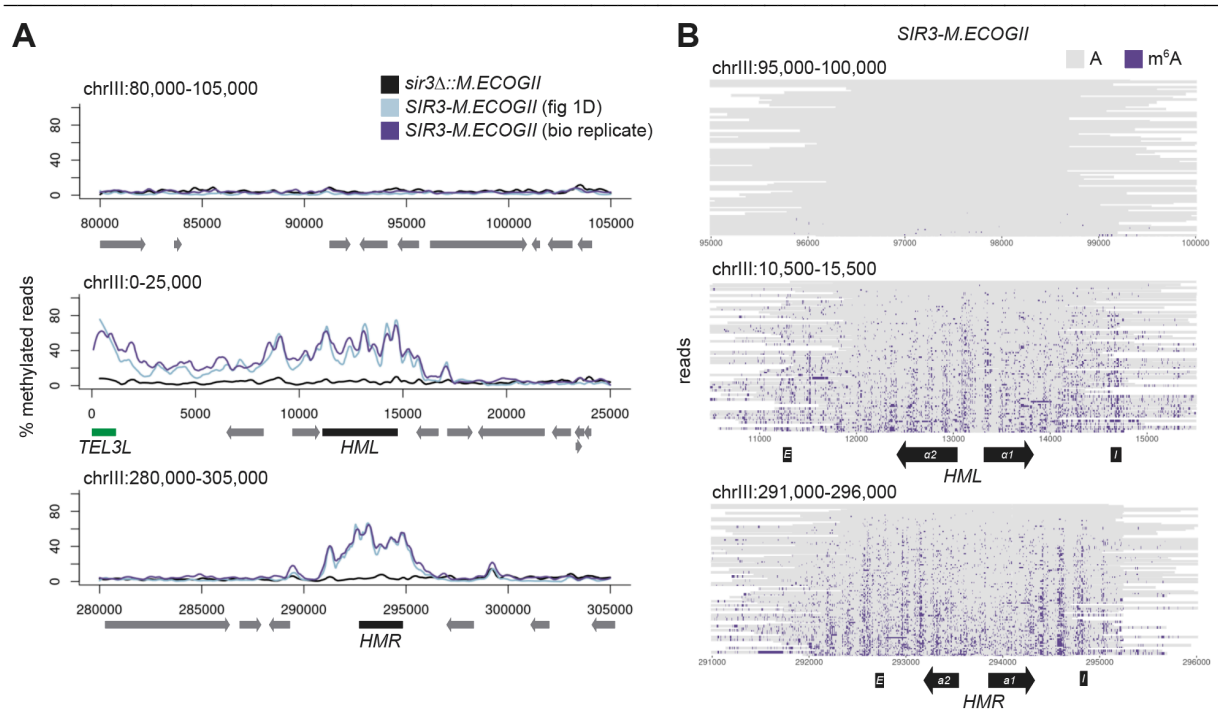

Figure 2.1–Figure Supplement 2. *Sir3-M.EcoGII* strongly and specifically methylated *HML* and *HMR*
A) Aggregate results from long-read Nanopore sequencing of *sir3*Δ*::M.ECOGII* (black line, JRY12838, same as figure 2.1D), *SIR3-M.ECOGII* (blue line, JRY13027, same as figure 2.1D), and a biological replicate of *SIR3-M.ECOGII* (purple line, JRY12840). Plots are as described in Fig 1D. **B)** Single-read plots from a biological replicate of long-read Nanopore sequencing of *SIR3-M.ECOGII* (JRY13027). Plots are as described in Fig 1E.

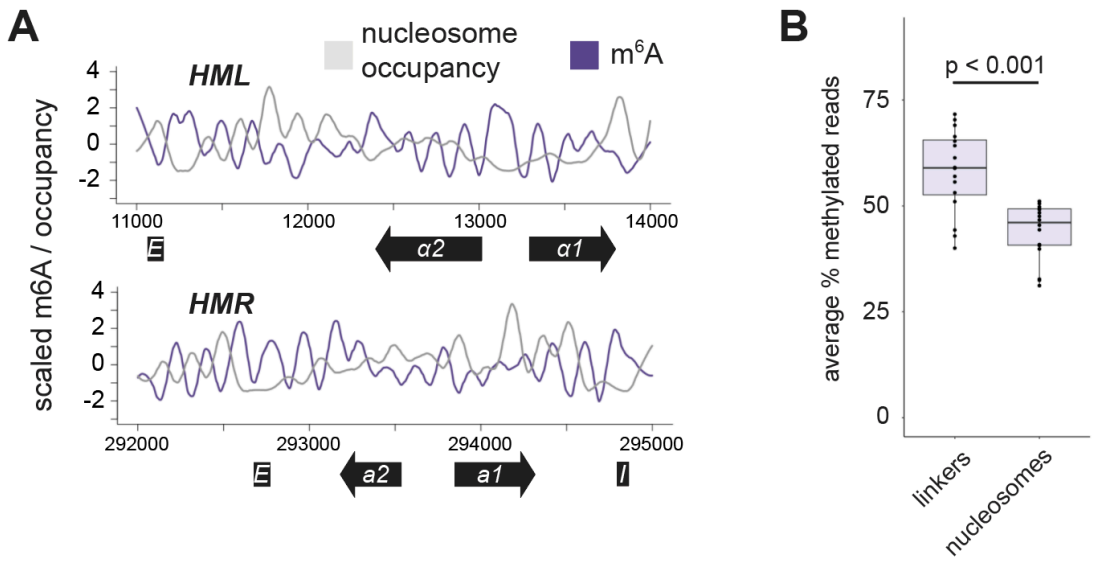

Figure 2.1–Figure Supplement 3. Sir3-M.EcoGII preferentially methylated linker regions
A) Aggregate methylation signal by Nanopore sequencing (purple line) of *SIR3-M.ECOGII* (JRY13027) plotted against nucleosome occupancy (gray line, Chereji et al. 2018) over a 3 kb window at *HML* (top) and *HMR* (bottom). The y-axis represents the signal of both % of reads methylated and nucleosome occupancy scaled to fit in the same plot. Data were smoothed using a loess function. **B)** The average % of methylated reads from *SIR3-M.ECOGII* (JRY13027) in linker regions at *HML* and *HMR* (nucleosome occupancy below a threshold of 0.4 from Chereji et al. 2018) compared to nucleosomal regions at *HML* and *HMR* (nucleosome occupancy above a threshold of 0.4 from Chereji et al. 2018). The center line of each box plot represents the median. The boxes represent the 25th and 75th percentiles. Whiskers represent the range of values within 1.5× the interquartile range. P-value was calculated using a quasibinomial general linear model (glm).

2.3.2 Nucleosome binding was required for spreading, but not recruitment, of Sir3

Recruitment of the SIR complex to silencers is sequence specific. Rap1, Abf1, and ORC bind at these recruitment sites and recruit the Sir proteins directly through protein-protein interactions. In contrast, SIR complex binding away from recruitment sites is sequence independent and instead relies on interactions with nucleosomes and among the Sir proteins themselves.

We therefore hypothesized that the interaction between Sir3 and nucleosomes would not be required for nucleation at recruitment sites but would be required for binding outside of those recruitment sites. Sir3 has multiple recognized domains (Figure 2.2A): The BAH domain, which interacts with nucleosomes (Rudner et al. 2005; Onishi et al. 2007; Buchberger et al. 2008; Norris et al. 2008; Sampath et al. 2009; Armache et al. 2011), the AAA^+ domain, which interacts with Sir4 (King et al. 2006; Ehrentraut et al. 2011; Samel et al. 2017), and the winged helix (wH) domain, which allows for homodimerization (King et al. 2006; Oppikofer et al. 2013; Liaw and Lustig 2006). We deleted the BAH domain of Sir3-M.EcoGII (*bah*Δ), which largely abrogates Sir3-nucleosome interactions *in vitro* (Onishi et al. 2007; Buchberger et al. 2008; Sampath et al. 2009). Previous studies established that deletion of the BAH domain causes a phenotypic loss of silencing, likely due to a loss of interaction with nucleosomes (Gotta et al. 1998; Onishi et al. 2007; Buchberger et al. 2008), but did not characterize its binding at regions of heterochromatin. Importantly for what follows, deletion of the BAH domain did not destabilize Sir3 (Figure 2.2B). We also confirmed that *sir3-bah*Δ*-M.ECOGII* strains displayed a loss of silencing, but found that the loss was more severe at *HML* than at *HMR* (Figure 2.2C).

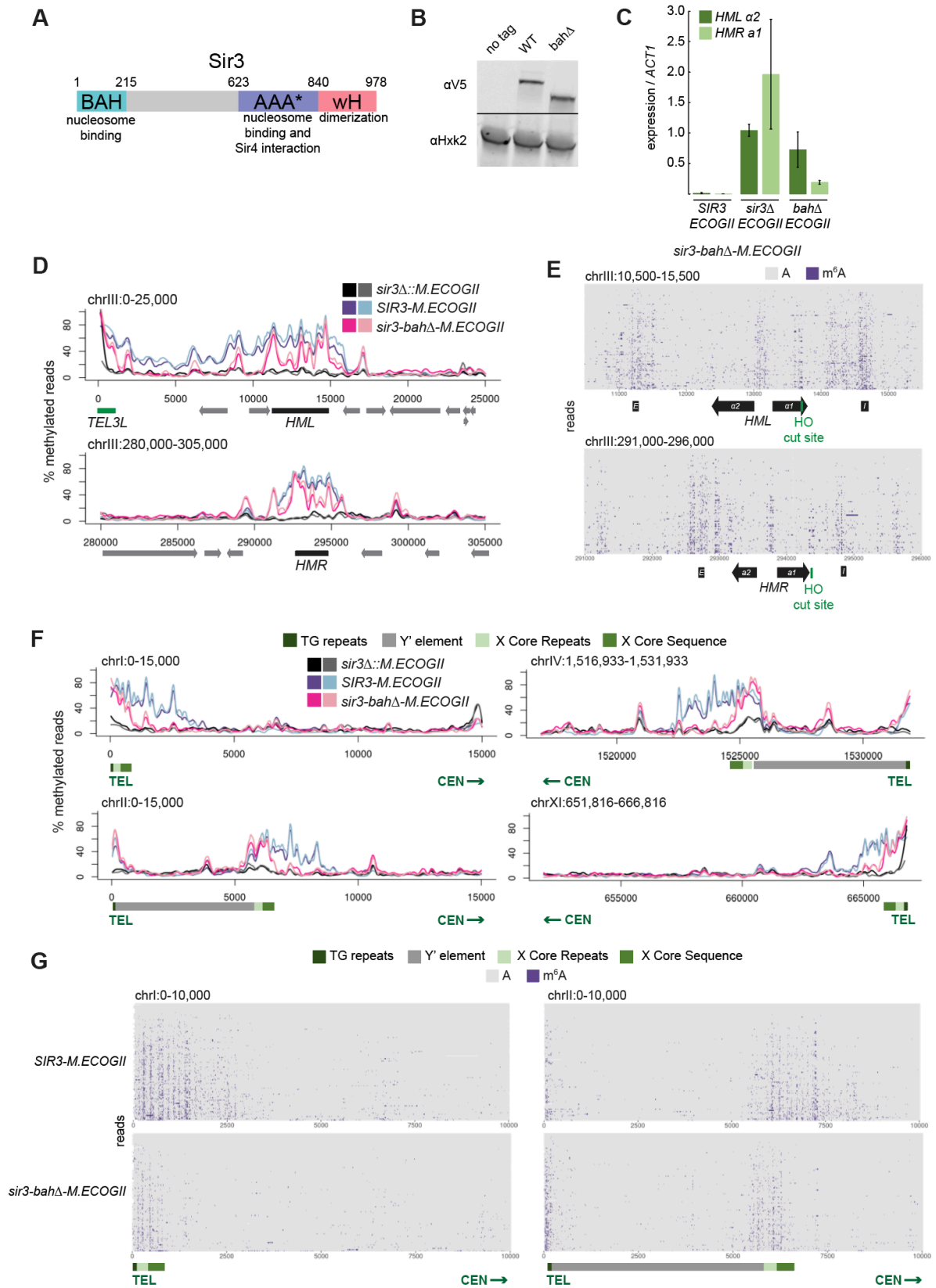

Figure 2.2. Nucleosome binding was required for spread, but not recruitment, of Sir3 to regions of heterochromatin *(continued on next page)*

A) Schematic of Sir3 protein domains. **B)** Protein immunoblotting in strains expressing Sir3 (no tag, JRY11699), Sir3-3xV5 (JRY12601), and sir3-bahΔ-3xV5 (JRY13621). Top row are 3xV5-tagged Sir3 proteins, and bottom row is the loading control Hxk2. **C)** RT-qPCR of *HMLα2* and *HMRa1* mRNA, normalized to *ACT1* mRNA, in strains expressing *SIR3-M.ECOGII* (JRY12840, JRY13027), *sir3Δ::M.ECOGII* (JRY13029, JRY13030), and *sir3-bahΔ-M.ECOGII* (JRY13438, JRY13439). Bars are the average of three biological replicates, and bars mark one standard deviation. **D)** Aggregate methylation results at *HML* (top) and *HMR* (bottom) from long-read Nanopore sequencing of *sir3Δ::M.ECOGII* (JRY13029, JRY13030), *SIR3-M.ECOGII* (JRY12840, JRY13027), and *sir3-bahΔ-M.ECOGII* (JRY13438). Plots are as described in Fig 1D. **E)** Single-read plots from long-read nanopore sequencing of *sir3-bahΔ-M.ECOGII* (JRY13438) at *HML* (top) and *HMR* (bottom). Plots are as described in Fig 1E. **F)** Aggregate methylation results at four representative telomeres (1L, 2L, 4R, and 11R) from long-read Nanopore sequencing of the same strains as Fig 2D. Shown are 15 kb windows of each telomere. Plots are as described in Fig 1D. **G)** Single-read plots from long-read nanopore sequencing of *SIR3-M.ECOGII* (JRY13027) and *sir3-bahΔ-M.ECOGII* (JRY13438) at two representative telomeres (1L and 2L). Shown are 10 kb windows of each telomere.

Despite the loss of silencing at *HML* and *HMR* in the *sir3-bahΔ-M.ECOGII* strain, there was still detectable methylation across the two loci (Figure 2.2D, 2.2E, Figure 2.2–figure supplement 1A). At the aggregate level, sir3-bahΔ-M.EcoGII methylated silencers at *HML* and *HMR* at the same level as Sir3-M.EcoGII but showed decreased methylation between them (Figure 2.2D). Analysis of single reads spanning *HML* and *HMR* in the *bahΔ* mutant showed similarly strong levels of methylation at silencers, and revealed strong methylation both at the promoters of *HML* and *HMR* and the recognition site for the HO endonuclease (Figure 2.2E). In contrast, little methylation was seen over gene bodies between these sites (Figure 2.2E).

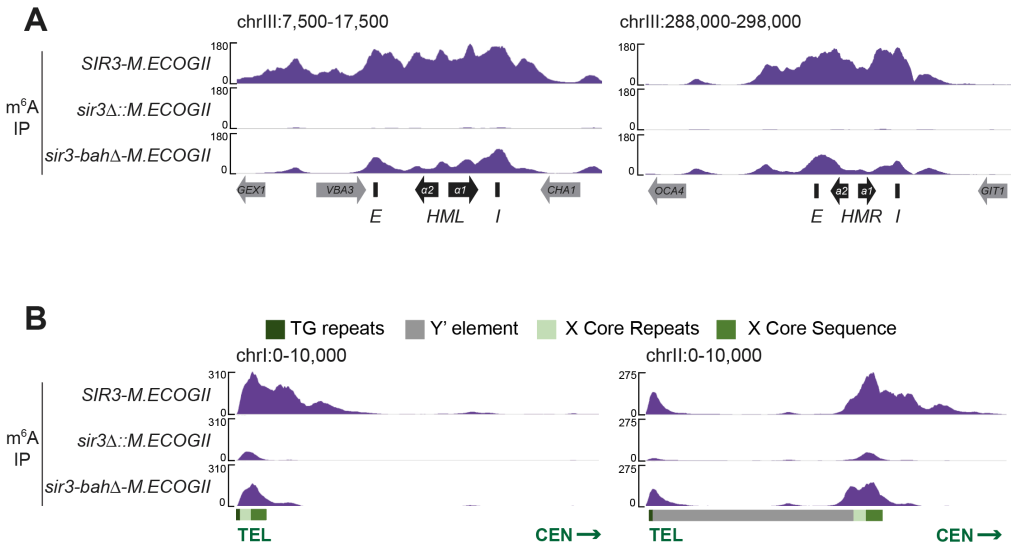

Figure 2.2–Figure Supplement 1. DIP-seq of *SIR3-M.ECOGII* (top row, JRY13027), *sir3Δ::M.ECOGII* (middle row, JRY13030), and *sir3-bahΔ-M.ECOGII* (bottom row, JRY13438)
Input results are plotted but not visible due to the strong DIP-seq signals.
A) Shown are 10 kb regions centered at *HML* (left) and *HMR* (right). **B)** Shown are 10 kb regions at two representative telomeres (1L and 2L)

The technology's long-read capacity also allowed analysis of the repetitive and highly homologous telomeres. In addition to methylating *HML* and *HMR* (Figure 2.1), Sir3-M.EcoGII strongly methylated telomeres at TG repeats and X elements (Figure 2.2F, Figure 2.2–figure supplement 1B, Figure 2.2–figure supplement 2), and the periodicity of methylation was apparent on single reads as well (Figure 2.2G), likely corresponding to more-accessible linker

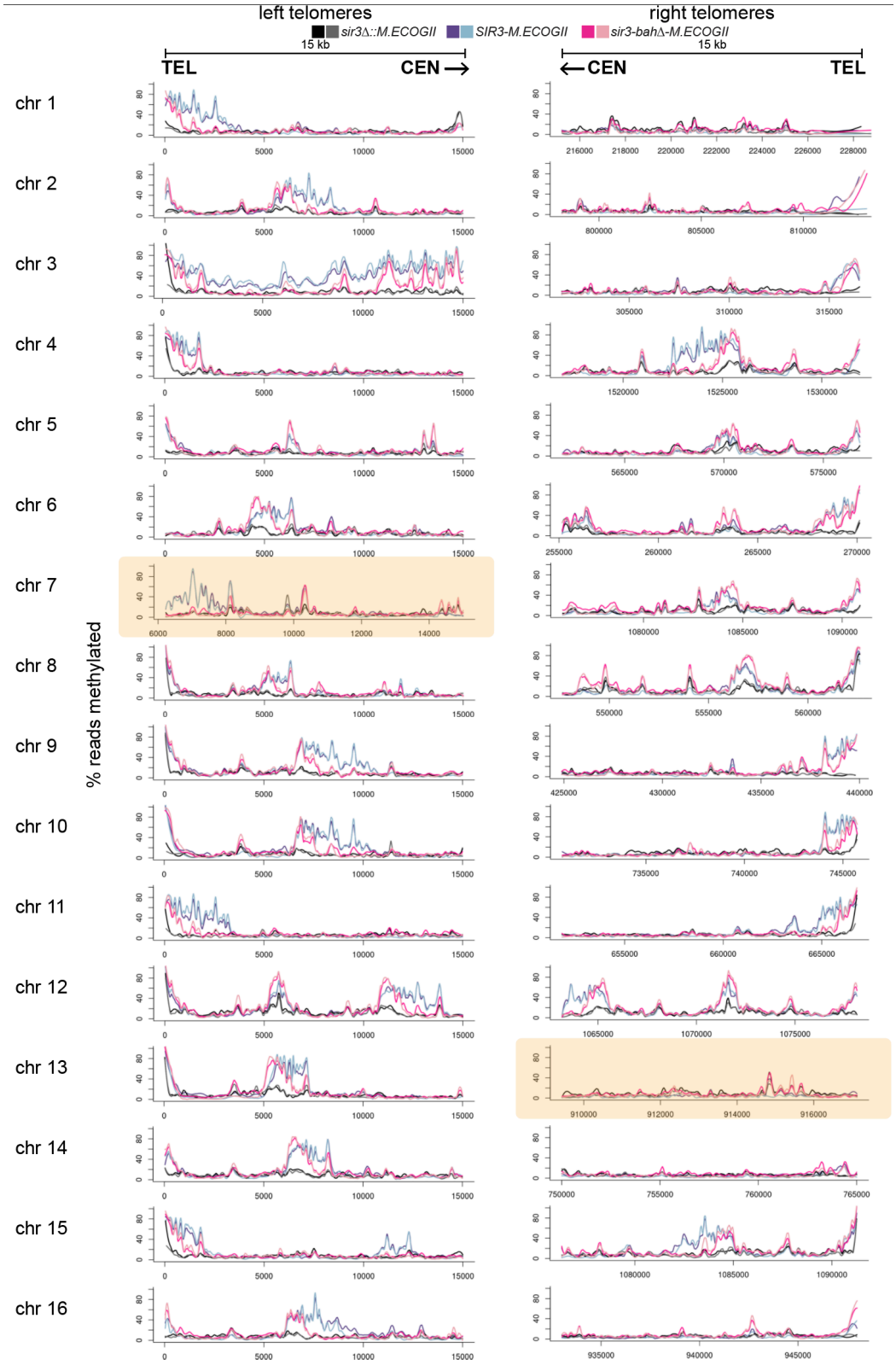

Figure 2.2–Figure Supplement 2. Methylation by Sir3-M.EcoGII and sir3-bahΔ-M.EcoGII at all 32 telomeres
Aggregate methylation results from long-read Nanopore sequencing of the same strains as Fig 2D. Shown are 15 kb windows of each telomere. Plots are as described in Fig 1D. Highlighted in yellow are windows shorter than 15kb due to discrepancies between the S288C and W303 genomes (see Ellahi et al. 2015)

regions. The loss of binding outside of recruitment sites of sir3-bahΔ-M.EcoGII was more striking at telomeres than *HML* and *HMR*, where methylation by the *bah*Δ mutant matched wild-type levels at TG and X repeats but dropped off steeply centromere-proximal to the X elements (Figure 2.2F, 2.2G, Figure 2.2–figure supplement 1B, Figure 2.2–figure supplement 2). The results at telomeres, supported by the data at *HML* and *HMR*, suggested that the nucleosome binding activity of Sir3 was required for Sir3 to spread away from recruitment sites, but not for its initial recruitment.

2.3.3 *SIR3* expression level did not limit its spread from recruitment sites

In addition to understanding what enables Sir3 spreading, we were also interested in what limits its spread. One common feature of heterochromatin proteins is that their activity is dose-dependent: lowered expression causes loss of heterochromatin whereas elevated expression can cause silencing of genes near heterochromatin (Locke et al. 1988; Henikoff 1996). Indeed, it was previously reported that overexpression of Sir3 results in its spread beyond wild-type boundaries, accompanied by repression of genes in those extended regions (Renauld et al. 1993; Hecht et al. 1996; Strahl-Bolsinger et al. 1997; Ng et al. 2003; Hocher et al. 2018). To provide an independent test of those conclusions, we tested whether the expression level of Sir3 limited how far it could spread beyond recruitment sites at *HML*, *HMR*, and telomeres.

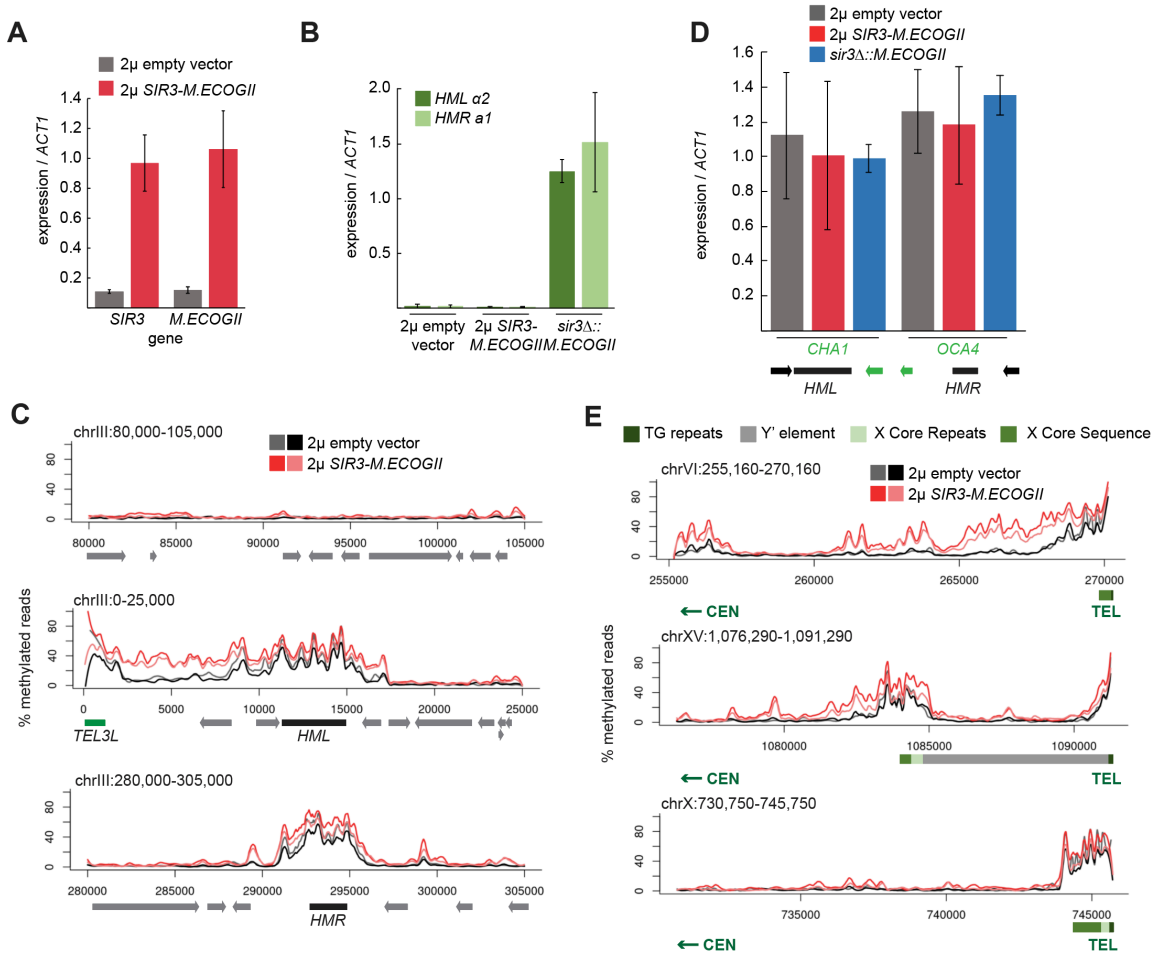

Figure 2.3. Sir3 expression was not limiting for its spread from recruitment sites *(continued on next page)*

A) RT-qPCR of *SIR3* and *M.ECOGII* mRNA normalized to *ACT1* mRNA in strains carrying an empty multi-copy 2μ vector (JRY13670, JRY13671) and strains carrying a multi-copy 2μ *SIR3-M.ECOGII* plasmid (JRY13672, JRY13673). Data are the average of four biological replicates, and bars mark one standard deviation. **B)** RT-qPCR of *HMLα2* and *HMRa1* mRNA normalized to *ACT1* mRNA in the same strains as Fig 3A as well as *sir3Δ::M.ECOGII* (JRY13029, JRY13030). Data are the average of four biological replicates, and bars mark one standard deviation. **C)** Aggregate methylation results at a control region on chromosome III to show background levels of methylation (top row), at *HML* (middle row) and *HMR* (bottom row) from long-read Nanopore sequencing of the same strains in Fig 3A. The two colors for each genotype correspond to two biological replicates. Plots are as described in Fig 1D. **D)** RT-qPCR of CHA1 and OCA4 mRNA normalized to ACT1 mRNA in the same strains as Fig 3B. **E)** Aggregate methylation results at three representative telomeres (6R, 15R, and 10R) from long-read Nanopore sequencing of the same strains as Fig 3A. The two colors for each genotype correspond to two biological replicates Shown are 15 kb windows of each telomere. Plots are as described in Fig 1D.

Expression of both *SIR3-M.ECOGII* from a multi-copy 2μ plasmid was 10-fold higher than the endogenous level of *SIR3-M.ECOGII* in a strain carrying an empty 2μ plasmid (Figure 2.3A). Overexpression of *SIR3-M.ECOGII* had no effect on silencing at *HML* and *HMR* (Figure 2.3B).

Overexpression of *SIR3-M.ECOGII* had little effect on the boundaries of methylation at *HML* and *HMR*. Strains overexpressing *SIR3-M.ECOGII* had increased methylation over both loci but no new methylation outside the bounds of strains expressing only one copy of *SIR3-M.ECOGII* (Figure 2.3C). There was some increase in methylation over the promoters of two genes closest to *HML* and *HMR* (*CHA1* and *OCA4*, respectively), but it did not result in any change in the level of their expression (Figure 2.3D).

Surprisingly, the results at telomeres were qualitatively similar but revealed three categories of effects. Some telomeres showed a large increase in the amount of methylation upon overexpression of *SIR3-M.ECOGII* with a small extension of binding farther into the chromosome (Figure 2.3E, top row, Figure 2.3–figure supplement 1). Some telomeres showed a modest increase in the amount methylation upon overexpression of *SIR3-M.ECOGII* with little, if any, extension of range (Figure 2.3E, middle row, Figure 2.3–figure supplement 1). Finally, some telomeres showed no appreciable change in methylation (Figure 2.3E, bottom row, Figure 2.3–figure supplement 1). Only three of the 32 telomeres, including the paradigmatic telomere 6R from earlier studies, showed convincing spread of methylation to new sites compared to telomeres in strains expressing one copy of *SIR3-M.ECOGII* (Figure 2.3E, Figure 2.3–figure supplement 1). Therefore, the expression level of *SIR3* was not a universal limiting factor in heterochromatin spread. These results imply the existence of other chromatin features that create boundaries for Sir3 spreading.

2.3.4 Repression of *HML* and *HMR* preceded heterochromatin maturation

To evaluate the dynamics of Sir3 recruitment and spreading during the establishment of heterochromatin over time, we used a temperature-sensitive allele of *SIR3*, *sir3-8,* fused to *M.ECOGII* and took samples at various time points for Nanopore sequencing after switching from the restrictive (37°C) to the permissive (25°C) temperature (Figure 2.4A). In agreement with previous studies (Stone et al. 2000), growth at 37°C caused lower protein levels of *sir3-8* (Figure 2.4B). Over the course of 150 minutes, the protein levels of *sir3-8* slowly increased to match levels in constitutive 25°C growth conditions (Figure 2.4B). In cells grown at 37°C, *sir3-8-M.ECOGII* did not methylate *HML* and *HMR*, but when grown constitutively at 25°C, there was strong methylation over both loci (Figure 2.4C, Figure 2.4–figure supplement 1).

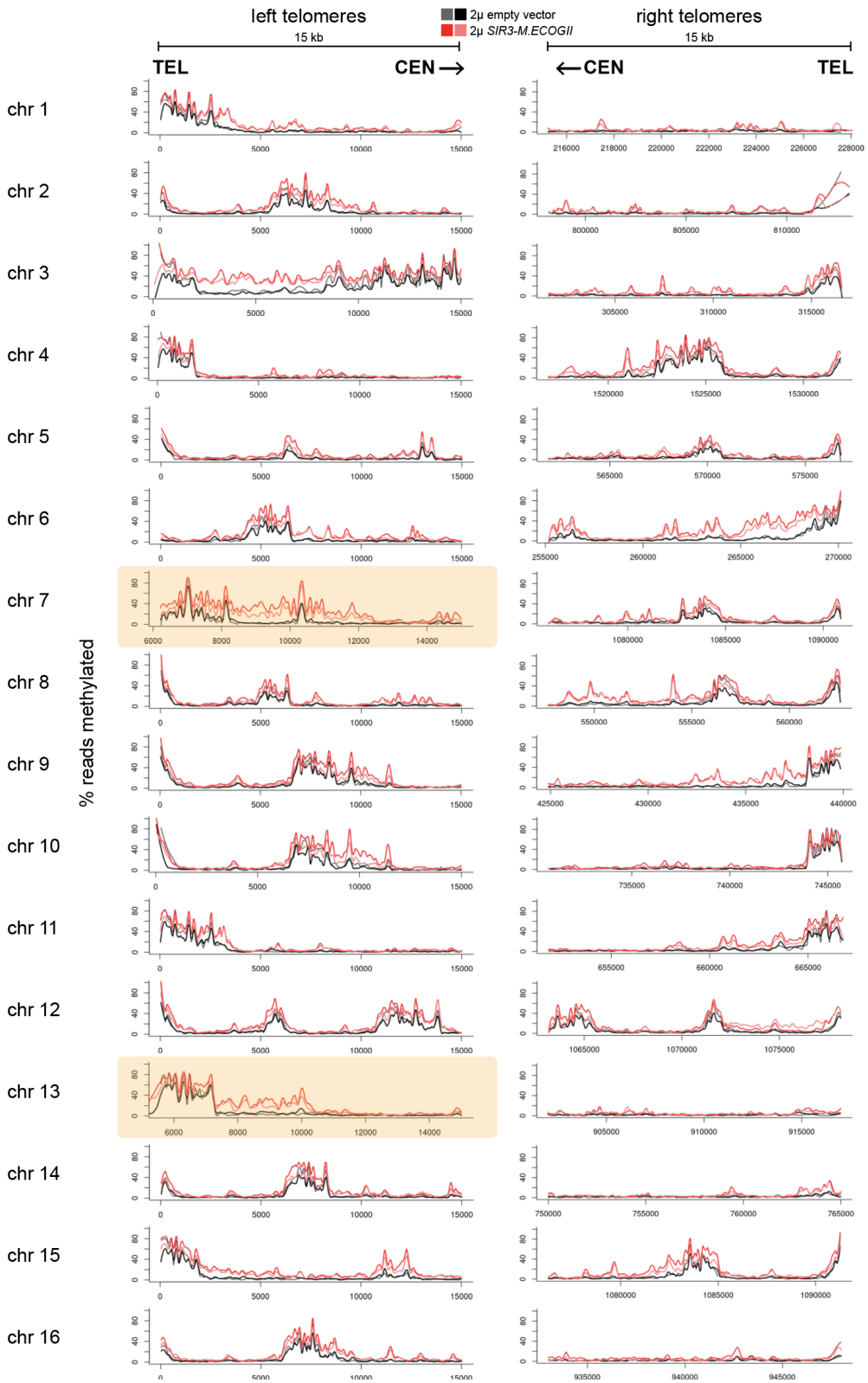

Figure 2.3–Figure Supplement 1. Methylation upon overexpression of *SIR3-M.ECOGII* at all 32 telomeres
Aggregate methylation results from long-read Nanopore sequencing of the same strains as Fig 3B. Shown are 15 kb windows of each telomere. Plots are as described in Fig 1D. Highlighted in yellow are windows shorter than 15kb due to discrepancies between the S288C and W303 genomes (see Ellahi et al. 2015)

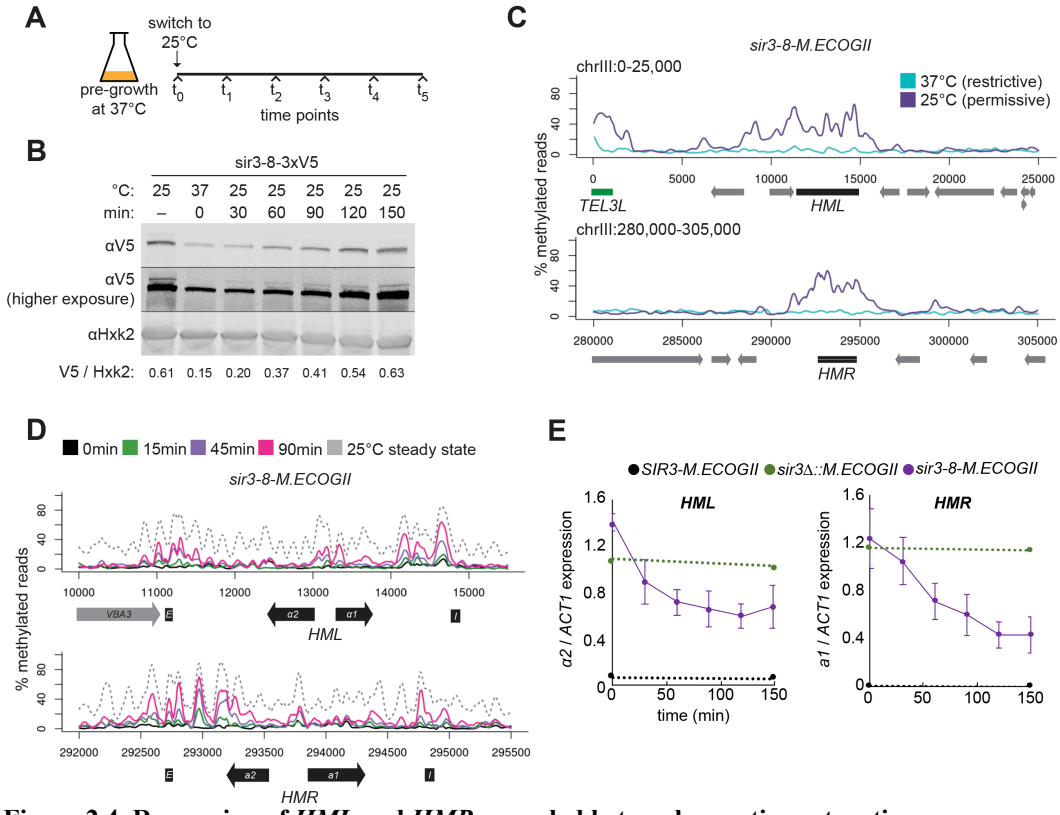

Figure 2.4. Repression of *HML* and *HMR* preceded heterochromatin maturation
A) Schematic of temperature-shift time course with *sir3-8-M.ECOGII*. **B)** Protein immunoblotting in a strain expressing sir3-8-3xV5 (JRY13467) constitutively at 25°C (first lane), constitutively at 37°C (second lane), and at 30 min, 60 min, 90 min, 120 min, and 150 min after a shift to 25°C. Top row is 3xV5-tagged sir3-8 protein, the middle row is the same as the top row but at a higher exposure, and the bottom row is the loading control Hxk2. **C)** Aggregate methylation results at *HML* (top) and *HMR* (bottom) from long-read Nanopore sequencing of strains expressing *sir3-8-M.ECOGII* (JRY13114) grown constitutively at 25°C or 37°C. Plots are as described in Fig 1D. **D)** Aggregate methylation results at *HML* (top) and *HMR* (bottom) from long-read Nanopore sequencing of a strain expressing *sir3-8-M.ECOGII* (JRY13134) grown constitutively at 25°C (dotted gray line) and collected at 0 min, 15 min, 45 min, and 90 min after a temperature switch from 37°C to 25°C. **E)** RT-qPCR of *HMLα2* (left) and *HMRa1* (right) mRNA in strains expressing *SIR3-M.ECOGII* (black, JRY13027, JRY12840), *sir3Δ::M.ECOGII* (green, JRY13029, JRY13030) or *sir3-8-M.ECOGII* (purple, JRY13114, JRY13134) collected at 0 min, 30 min, 60 min, 90 min, 120 min, and 150 min after a temperature switch from 37°C to 25°C. Points are the average of three biological replicates and bars mark one standard deviation.

Over a 90-minute time course, methylation increased only over the silencers and promoters of *HML* and *HMR* (Figure 2.4D, Figure 2.4–figure supplement 2, solid lines). Methylation at the promoter of *HML* during the time course and in the *sir3-bahΔ* mutant was expected, as it contains a Rap1 binding site, and Rap1 interacts directly with Sir3 and Sir4. However, methylation at the promoter of *HMR* at these early time points and in the *sir3-bahΔ* mutant was a surprise, as there is not a known SIR complex-interacting protein that binds at the promoter. In the absence of Sir3, Sir4 is still bound at silencers (Rusche et al. 2002; Hoppe et al. 2002; Goodnight and Rine 2020), so the faster recruitment at these sites, and perhaps the promoters as well, might be due to the interaction of Sir3 with Sir4 and Rap1.

By 90 minutes (~1 cell division), methylation at no position reached the level found in cells constitutively grown at 25°C–the level of methylation of mature, stable heterochromatin (Figure 2.4D, Figure 2.4–figure supplement 2, dotted line). Strikingly, even by 30 minutes after the temperature shift, when methylation was just rising above background at silencers, partial repression of *HML* and *HMR* was apparent (Figure 2.4E). This result suggested that binding of Sir3 at silencers and promoters was sufficient for partial repression and preceded its spread over the entirety of both loci.

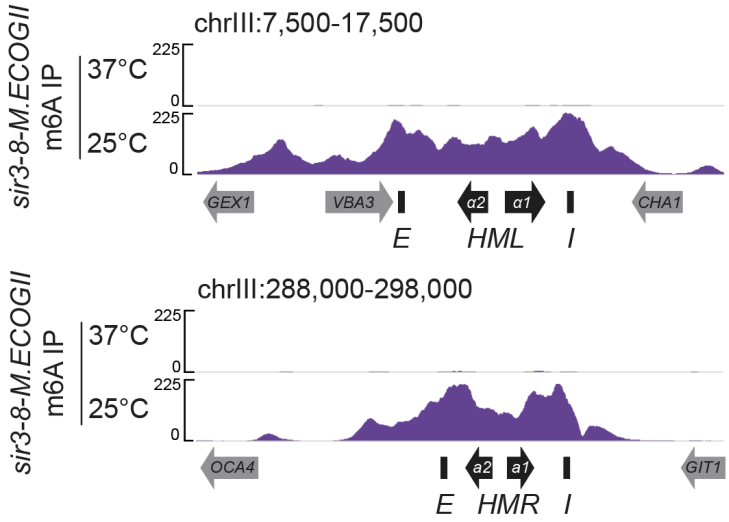

Figure 2.4–Figure Supplement 1. DIP-seq of *sir3-8-M.ECOGII* (JRY13114)
Shown are 10 kb regions centered at *HML* (left) and *HMR* (right). Cells were grown constitutively at either 25°C or 37°C. Input results are plotted but not visible due to the strong DIP-seq signals.

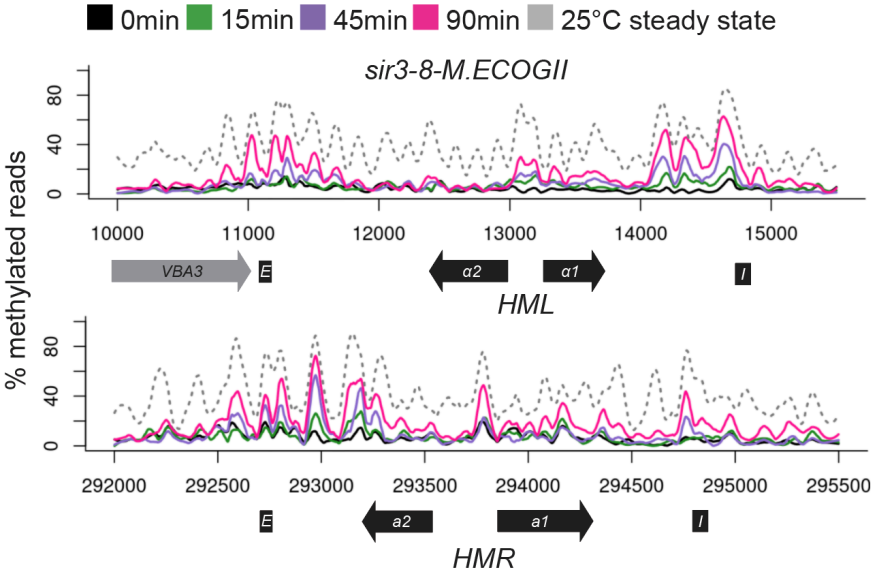

Figure 2.4–Figure Supplement 2. Nanopore sequencing over temperature switch time course (biological replicate)
Aggregate methylation results at *HML* (top) and *HMR* (bottom) from long-read Nanopore sequencing of a strain expressing *sir3-8-M.ECOGII* (JRY13114) grown constitutively at 25°C (dotted gray line) and collected at 0 min, 15 min, 45 min, and 90 min after a temperature switch from 37°C to 25°C.

2.4 Discussion

In this study, we developed a new method to study the process of recruitment and spread of the *S. cerevisiae* heterochromatin protein Sir3 in living cells with a resolution approximating the frequency of single A-T base pairs. We created a fusion protein between a key structural protein of heterochromatin, Sir3, and the bacterial adenine methyltransferase M.EcoGII that retained function and activity of each. We used DNA methylation as a read-out for Sir3 occupancy on chromatin. Long-read Nanopore sequencing allowed us to distinguish directly between methylated and unmethylated adenine and transcended the limitations of earlier studies imposed by repetitive regions common at telomeres.

The methylation by Sir3-M.EcoGII at *HML* and *HMR* was stronger and had a larger footprint than its occupancy as judged by ChIP-seq, suggesting that our method captured transient contacts of Sir3 with chromatin that ChIP-seq could not. This result reinforced the idea that protein-chromatin interactions are dynamic, even for a feature like heterochromatin, commonly thought of as 'stable'. We also harnessed the power of single base-pair resolution afforded by Nanopore sequencing to distinguish between recruitment and spread of Sir3 by studying a mutant of Sir3 whose distribution and binding profile had not yet been characterized, *sir3-bah*Δ. This mutant cannot bind to nucleosomes and loses transcriptional silencing at *HML* and *HMR* (Gotta et al. 1998; Onishi et al. 2007; Buchberger et al. 2008). The mutant sir3-bahΔ-M.EcoGII was still recruited to silencers at *HML, HMR,* and to telomeres where it methylated local adenines. However, the mutant did not spread beyond those recruitment sites, unlike wild-type Sir3-M.EcoGII. Our findings supported that recruitment and spread were separate processes that involved different interactions between Sir3 and other proteins at silenced loci and telomeres.

The ability to unambiguously map long reads to telomeres allowed us to challenge historic conclusions about Sir3 dosage-driven heterochromatin spreading. Overexpressing Sir3-M.EcoGII increased the methylation signal where there already was methylation at endogenous levels of expression, but the boundaries where methylation dropped off at *HML*, *HMR,* and telomeres mainly remained fixed in the two conditions. This result suggested that overexpression of Sir3 was not sufficient for spreading past most wild-type boundaries. The original idea that overexpression of Sir3 results in its further spread relied on low-resolution RT-PCR at two telomeres, 5R and 6R (Renauld et al. 1993; Hecht et al. 1996; Strahl-Bolsinger et al. 1997). In our genome-wide analysis, telomere 6R was an exception, not the rule, as most telomeres did not show spreading of Sir3 upon its overexpression. We were not able to reproduce the result at telomere 5R (Hecht et al. 1996).

Our data suggested that binding of Sir3 outside of *HML*, *HMR*, X elements, and telomere TG repeats was probabilistic: When Sir3 was overexpressed, its interactions outside of recruitment sites became more frequent, thus increasing the methylation signal produced by Sir3-M.EcoGII. However, most boundaries were left largely unchanged under overexpression conditions, in agreement with more recent Sir3 ChIP-seq results (Radman-Livaja et al. 2011). Perhaps other features, such as transcription, tRNA genes (Donze and Kamakaka 2001; Simms et al. 2008; Valenzuela et al. 2009), the presence of histone variants like H2A.Z (Meneghini et al. 2003; Babiarz et al. 2006; Venkatasubrahmanyam et al. 2007; Giaimo et al. 2019), or the presence of Sir3-inhibiting chromatin marks like methylation of H3 on lysine 79 (Park et al. 2002a; Ng et al. 2002, 2003; Oki et al. 2004; Altaf et al. 2007; Stulemeijer et al. 2011), enforce a boundary that overexpression of Sir3 itself cannot overcome.

Two results suggested that repression of *HML* and *HMR* did not require that Sir3 occupy the entire locus to the level seen in wild-type cells. During the temperature-switch time course, methylation by sir3-8-M.EcoGII appeared first and most strongly at promoters and silencers of *HML* and *HMR*, with little or no detectable methylation between these sites. Yet, partial transcriptional repression was already evident at both loci within 30 minutes. The gradual repression that appeared during the time course was consistent with single-cell studies that show gradual tuning down of transcription during silencing establishment (Goodnight and Rine 2020). The level of repression achieved during the time course was commensurate with that expected within the first cell cycle following restoration of Sir3 function (Goodnight and Rine 2020). We also found that *sir3-bah*Δ, a nucleosome-binding mutant that was recruited to silencers and promoters but could not bind outside of them, achieved some repression at both *HML* and *HMR*. Repression was stronger at *HMR* than at *HML* in the *bah*Δ mutant, perhaps because *HMR* is smaller and less dependent on spreading. The time course and *bah*Δ results together suggested a difference between repression of transcription per se and the stability of silencing ultimately achieved by the SIR complex binding over the entirety of *HML* and *HMR*.

We focused our efforts on the heterochromatin protein Sir3 in *S. cerevisiae,* but this method may have broad utility. By relaxing the requirement for stable binding to detect interaction of a protein with DNA or chromatin, the method could find binding sites of transcription factors and/or chromatin-binding proteins that elude detection by ChIP-seq. Further, with an inducible M.EcoGII fusion protein, one could track processes over time like the spread of heterochromatin proteins during X-chromosome inactivation, the movement of cohesin and condensin along chromosomes during chromosome pairing and condensation, and the homology search during homologous recombination. Improvements in Nanopore technology and modified base-calling software will likely extend the method's utility to other processes that have directional movement along chromosomes.

2.5 Materials and Methods

Strains

All strains in this study were derived from W303 (Table 2.1). *M.ECOGII* integrations were created by one-step integration of a PCR-amplified *M.ECOGII-natMX* cassette from pJR3525 using the primers listed in Table 2.3. Deletion of the BAH domain of *SIR3* was done using CRISPR-Cas9 gene editing using the guide RNA and repair template listed in Table 2.3. The guide RNA target and nontarget strands were integrated into a single guide RNA dropout-Cas9 expression plasmid (pJR3428, (Brothers and Rine 2019) by Golden Gate cloning, using the restriction enzyme *Bsm*BI as described in (Lee et al. 2015). The repair template was made by annealing oligos described in Table 2.3 and extending the 3' ends using Phusion Polymerase (New England Biolabs, Beverly, MA). *SIR3* overexpression strain and its control strain was created by transformation and maintenance of 2-micron plasmids pJR3526 and YEp24, respectively.

Plasmids

Plasmids used in this study are listed in Table 2.2. The *M.ECOGII-NatMX6* tagging plasmid (pJR3525) was made using standard Gibson cloning into pFA6a-natMX6 (Hentges et al. 2005). The codon-optimized *M.ECOGII* ORF with homology to the vector backbone was on a gene block (Table 2.3) from Integrated DNA Technologies (IDT, Coralville, IA) and was inserted into

pFA6a-natMX6 linearized by PCR. The *SIR3p-SIR3-M.ECOGII* overexpression plasmid (pJR3526) was made using standard Gibson cloning into YEp24, a 2μ yeast expression plasmid carrying a *URA3* selectable marker.

Growth and fluorescence imaging of colonies

Strains were grown in a patch on YPD overnight at 30°C. Cells were then resuspended in water and plated for single colonies on a YPD plate. Colonies were imaged after 3 days of growth at 30°C. At least 10 colonies per genotype were imaged using a Leica M205FA fluorescence stereomicroscope, a Leica DFC3000G CCD camera, and a Plan Apo x0.63 objective. All colonies were imaged at a magnification of 10X. Image analysis and assembly was performed using Fiji software (Schindelin et al. 2012).

ChIP-seq

Sample Collection

Strains were grown to mid-log phase in YPD at 30°C. Approximately 10^9 cells were collected, washed, and fixed for 15 minutes at 30°C in a final concentration of 1% formaldehyde. Fixation was quenched with a final concentration of 300mM glycine for 10 minutes at 30°C. Cells were washed 1X with PBS and 2X with FA lysis buffer (50mM HEPES pH7.5, 150 mM NaCl, 1 mM EDTA, 1% v/v Triton X-100, 0.1% w/v sodium deoxycholate, 0.1% SDS) before flash freezing pellets in a 2 mL screw-cap tube. Pellets were resuspended in 1 mL FA lysis buffer and 500 μL of 0.5 mm zirconium ceramic beads (BioSpec Products, Bartlesville, OK, Cat # 11079105z) were added. Resuspended cells were bead beat with in a FastPrep-24 (MP Biomedicals, Burlingame, CA) at 5.5 amplitude, 4 cycles of 40 sec ON/2 min on ice. Each tube was punctured at the bottom with a hot 20G needle and placed into a new 1.5 mL tube, and sample was spun out of the tube into the new tube by spinning at 150 xg for 1 min. The sample was moved into a 15 mL Bioruptor sonication conical tube with 100 μL of Bioruptor sonication beads (Diagenode, Denville, NJ, Cat # C01020031) and sonicated using the Bioruptor Pico (Diagenode) for 10 cycles of 30 sec ON / 30 sec OFF.

Immunoprecipitation

The sonicated extract was moved into a new 1.5 mL tube and spun at 16,000 xg for 15 min at 4°C. The supernatant was moved into a new 1.5mL tube and adjusted to 1 mL volume with FA lysis buffer. 50 μL of sample was taken aside as input, and then 25 μL of 20 mg/mL BSA and 5 μL of anti-V5 antibody (Invitrogen, Waltham, MA, Cat # R960-25) was added to the rest of the sample and rotated overnight at 4°C. 50 μL of Protein A magnetic Dynabeads (Thermo-Fisher, Waltham, MA, Cat # 10002D) were added to the sample and rotated at 4°C for 1 hr. Magnetic beads were immobilized using a magnetic rack and washed by resuspension in 1mL of various buffers in the following order: FA lysis buffer + 0.05% Tween-20, FA lysis buffer + 0.05% Tween-20 + 0.25 mM NaCl, ChIP wash buffer (10 mM Tris pH 8.0, 0.25 M LiCl, 1mM EDTA, 0.5% Nonidet P-40, 0.5% sodium deoxycholate, 0.05% Tween-20), and TE (10 mM Tris pH 8.0, 1 mM EDTA) + 0.05% Tween-20. The washed beads were resuspended in 130 μL of ChIP elution buffer (10 mM Tris pH 7.5, 1 mM EDTA, 1% SDS) and incubated at 65°C shaking at 900rpm overnight. The next day, 2.5 μL of 10 mg/mL Proteinase K (New England Biolabs, Ipswich, MA, Cat # P8107S) and 2.5 μL of 10 mg/mL RNase A (Thermo-Fisher, Cat # EN0531) were added to the elution and incubated at 42°C for 2 hr. Beads were immobilized on a magnetic rack and the supernatant containing the desired DNA to be sequenced was taken and purified

using 1X v/v SPRI Select magnetic beads (Beckman Coulter, Brea, CA, Cat # B23317) according to the manufacturer's instructions.

Library Preparation and Sequencing
Samples were prepared for sequencing using NEBNext Ultra II DNA Library Prep Kit for Illumina (New England Biolabs, Cat # E7645) according to the manufacturer's instructions. Samples were multiplexed using NEBNext Multiplex Oligos for Illumina (New England Biolabs, Cat # E7335/E7500). Library-prepped samples were sequenced on a MiniSeq System (Illumina, San Diego, CA)

Analysis
Sequencing reads were aligned to the S288C sacCer3 reference genome (release R64-2-1_20150113, yeastgenome.org), modified to include *mat*Δ using Bowtie2 with the options "--local --soft-clipped-unmapped-tlen --no-unal --no-mixed --no-discordant" (Langmead and Salzberg 2012). Reads were normalized to the genome-wide median, excluding rDNA, chromosome III, and subtelomeric regions (the first and last 10 kb of each chromosome). Analysis was performed using custom Python scripts modified from (Goodnight and Rine 2020) and displayed using IGV (Thorvaldsdóttir et al. 2013).

DIP-seq
DNA extraction
Cells were grown to mid-log phase in YPD, Complete Supplement Mixture (CSM) or CSM without Uracil (Sunrise Science Products, Knoxville, TN) at 30°C. Approximately 10^9 cells were pelleted by centrifugation at 3200 xg for 2 min, washed with 1 mL of water, moved to a 2 mL screw-cap tube, and flash frozen. Cells were resuspended in 400 µL of Triton SDS Lysis Buffer (10 mM Tris pH 8.0, 100 mM NaCl, 1 mM EDTA, 2% Triton X-100, 1% SDS), and 400 µL of phenol:chloroform:isoamyl alcohol 25:24:1 and 300 µL of 0.5 mm zirconium ceramic beads (BioSpec Products, Cat # 11079105z) were added to the resuspension. Cells were lysed by bead beating with in a FastPrep-24 (MP Biomedicals) at 5.5 amplitude, 4 cycles of 40 sec ON/2 min on ice. The aqueous and organic phases were separated by centrifugation at 21,000 xg for 5 min, and the aqueous phase was moved to a new 1.5 mL tube. 400 µL of chloroform was added, vortexed at top speed for ~ 10 sec, and spun down at 21,000 xg for 5 min to separate the aqueous and organic phases. The aqueous phase was moved to a new 1.5 mL tube, and 1 mL of 100% ethanol was added to precipitate nucleic acids. The sample was incubated at 4°C for 10-15 min and then spun down at 21,000 xg for 2 min to pellet the precipitated nucleic acids. Supernatant was discarded, the pellet was air-dried, and then the pellet was resuspended in 400 µL of TE (10mM Tris-HCl pH 8.0, 1 mM EDTA) + 4 µL of 10 mg/mL RNase A (Thermo-Fisher, Cat # EN0531) and incubated at 37°C for 1 hour. 1 mL of 100% ethanol + 10 µL of 4M ammonium acetate was added to the RNase solution and incubated at 4°C for 10-15 min to precipitate DNA. The precipitate was pelleted by centrifugation at 21,000 xg for 2 min, washed 1X with 70% ethanol, air-dried, and resuspended in 150-300 µL of water.

Sonication
DNA concentration was measured using Qubit dsDNA HS reagents (Invitrogen, Cat #Q32854), and 6 µg of DNA was diluted to 20 ng/uL in 300 µL of water in 1.5 mL Bioruptor Pico Microtubes for sonication (Diagenode, Cat # C30010016). DNA was sonicated using a Bioruptor

Pico (Diagenode) for 18 cycles of 15 sec ON/90 sec OFF. The sonicated DNA was moved to a new 1.5 mL tube.

m^6A IP
DNA was denatured by incubating at 95°C for 10 min and then immediately placed on ice for 5 min. 200 µL of cold water and 500 µL of cold 5X DIP buffer (50 mM $NaPO_4$ pH 7.0, 700 mM NaCl, 0.25% Triton X-100) were added to bring the volume up to 1 mL. 50 µL were taken aside as input. 25 µL of 20 mg/mL BSA and 1.8 µg of antibody (Synaptic Systems rabbit anti-m^6A, Cat 202-003) were added to the rest of the sample and rotated overnight at 4°C. 50 µL of Protein A magnetic Dynabeads (Thermo-Fisher, Cat # 10002D) were added to the sample and rotated at 4°C for 1 hr. Magnetic beads were immobilized using a magnetic rack and washed by resuspension and rotation for 5 min at 4°C in 1mL of various cold buffers in the following order: 2X with 1X DIP buffer + 0.05% Tween-20, 1X with 1X DIP buffer. For elution, beads were resuspended in 190 µL of DIP Digestion Buffer (50 mM Tris-HCl pH 8.0, 10 mM EDTA, 0.5% SDS) + 10 µL of 10 mg/mL Proteinase K (New England Biolabs, Cat # P8107S). DIP digestion buffer was added to input samples up to 200 µL. Both the input and IP samples were incubated at 50°C for 2 hr and then cleaned up using the Qiaquick PCR Purification Kit (Qiagen, Hilden, Germany, Cat # 28104) and eluted in 35 µL of water.

Library Preparation and Sequencing
Samples were prepared for sequencing using Accel-NGS 1S Plus DNA Library Kit (Swift Biosciences, Ann Arbor, MI, Cat # 10024) according to the manufacturer's instructions. Samples were multiplexed using Swift Single Indexing Primers Set A (Swift Biosciences, Cat # X6024). Library prepped samples were sequenced on a MiniSeq System (Illumina).

Analysis
Analysis was done as described in the section on ChIP-seq above.

Nanopore sequencing
DNA extraction
Cells were grown to mid-log phase in YPD, CSM (Sunrise Science Products), or CSM without Uracil at 30°C. Approximately 10^8 cells were pelleted, washed with 1 mL of water, and pellets were flash frozen. gDNA was extracted using the YeaStar Genomic DNA Kit (Genesee Scientific, San Diego, CA, Cat #11-323) according to the manufacturer's "Protocol 1". Specifically, thawed cell pellets were resuspended in 240 µL of YD Digestion Buffer + 10 µL R-Zymolyase and incubated at 30°C for 1 hr. 240 µL of YD Lysis buffer was added to the solution and vortexed at top speed for 15 sec. 500 µL of chloroform was added to the solution and vortexed at top speed for 10 sec and then inverted 10 times. The aqueous and organic phases were separated by centrifugation at 10,000 xg for 2 min, and the aqueous phase was equally separated into two ZymoSpin columns. ZymoSpin columns were spun at 10,000 xg, washed 2X with 300 µL of DNA Wash Buffer, and DNA was eluted from each column with 75 µL of water. Eluates were combined. DNA was sheared to ~15-20kb by spinning through a Covaris g-TUBE (Covaris Inc., Woburn, MA, Cat #520079) at 4200 rpm for 1 min, and repeating 1X with the tube flipped the other way in an Eppendorf Centrifuge 5424, according to the Covaris protocol. DNA was purified and concentrated using 1X v/v SPRI Select beads (Beckman Coulter, Cat #

B23317) and eluted in 50 µL of water according to the manufacturer's instructions. DNA concentration was measured using Qubit dsDNA HS reagents (Invitrogen, Cat # Q32854).

Library Preparation and Sequencing
Approximately 1-3 µg of purified, sheared genomic DNA was library prepped using the following reagents: NEB Oxford Nanopore Companion (New England Biolabs, Cat # E7180S), NEB Blunt/TA Ligase Master Mix (New England Biolabs, Cat # M0367), NEBNext Quick Ligation Reaction Master Mix (New England Biolabs, Cat # B6058), Oxford Ligation Sequencing Kit (Oxford Nanopore Technologies, Oxford, United Kingdom, Cat # SQK-LSK109), and the Oxford Native Barcoding Expansion 1-12 (Oxford Nanopore Technologies, Cat # EXP-NBD104). The library was prepared and sequenced according to Oxford Nanopore's protocol for Ligation Sequencing Kit + Native Barcoding Expansion 1-12. Sequencing was done on a MinION sequencer with v9.4 flow cells (Oxford Nanopore Technolgies, Cat # FLO-MIN106).

Analysis
Basecalling was first done using Guppy v5.0.11 using the high-accuracy model (dna_r9.4.1_450bps_hac.cfg), and reads were demultiplexed using guppy_barcoder. Read IDs corresponding to each barcode were extracted and written to a .txt file using a custom Python script. Reads corresponding to each barcode were aligned to the S288C reference genome (release R64-2-1_20150113, yeastgenome.org, modified to include *mat*Δ) and modifications called with Megalodon (https://github.com/nanoporetech/megalodon, v2.3.3) using the all-context rerio model (https://github.com/nanoporetech/rerio, res_dna_r941_min_modbases-all-context_v001.cfg) and the flags --mod-motif "Y A 0", --files_out "basecalls mod_mappings per_read_mods" and --read-ids-filename "barcodeXX_readIDs.txt" (the file that contained the extracted list of readIDs for a given barcode).

Results were aggregated into .bed files using "megalodon_extras aggregate run", and these files were used for aggregate nanopore plots. Before plotting, aggregated data was filtered to include only adenines with at least 10X coverage, and lines were smoothed using base R loess() function with enp.target = 100 and weighted by the coverage at each position.

Assessment of linker-region preference of Sir3-M.EcoGII used nucleosome-occupancy data from GEO Accession GSE97290 (Chereji et al. 2018).

The per-read database from Megalodon was converted into a .txt file using "megalodon_extras per_read_text modified_bases". For ease of use in RStudio, the data for each chromosome was extracted into its own .txt file using custom bash and awk scripts and these files were used for single-read nanopore plots. The probabilities output by Megalodon were made binary by calling adenines with a >0.8 probability of being methylated as "m6A" and all others "A".

Limitations
This method showed possible limitations for some contexts: 1) The expression level of the fusion protein could increase the levels of background methylation. We found this to be true with the Sir2-M.EcoGII fusion protein, which is likely expressed at a higher level than Sir3-M.EcoGII due to the higher level of endogenous Sir2 expression. The level of methylation by Sir2-

M.EcoGII in heterochromatin regions was higher than by Sir3-M.EcoGII, and background levels of methylation outside of heterochromatin regions was also higher than by Sir3-M.EcoGII. Importantly, the signal at heterochromatin was evident above even this raised background methylation. 2) Methylation at the level of single reads was variable and spotty, possibly due to at least two contributors. There may be occupancies that are too transient to allow methylation. Secondly, computational limitations for calling modified adenines without a guiding sequence motif meant that lower-confidence (probably < 0.8) m^6A calls were not considered methylated. At present, qualitative conclusions based on single-read data can be made with confidence, but as nanopore technology improves, single-read data will become more amenable to statistical and spatial analysis. 3) Because this method can capture transient interactions better than methods like ChIP-seq it may overestimate degrees of occupancy unless combined with DIP-seq or ChIP-seq.

RT-qPCR

RNA extraction

Cells were grown to mid-log phase in YPD, CSM (Sunrise Science Products), or CSM–Uracil at 30°C, and RNA was extracted using the Qiagen RNeasy kit (Qiagen, Cat # 74104) according to the manufacturer's instructions for Purification of Total RNA from Yeast. Briefly, ~6 x 10^7 cells were resuspended in 600 µL of buffer RLT, 500 µL of 0.5 mm zirconium ceramic beads (BioSpec Products, Cat # 11079105z) were added, and cells were lysed by bead beating with in a FastPrep-24 (MP Biomedicals) at 5.5 amplitude, 3 cycles of 40 sec ON/2 min on ice. Cells were pelleted by spinning at 21,000 xg for 2 min, and the supernatant was moved to a new tube. One volume of 70% ethanol was added to the supernatant and the sample was spun through an RNeasy spin column. The column was washed with 350 µL of buffer RW1, then 10 µL of DNase + 70 µL of buffer RDD (Qiagen, Cat # 79256) were added to the column and incubated for 15 min at room temperature. 500 µL of buffer RW1 was added and spun through the column. The column was then washed with 500 µL of buffer RPE 2X, and RNA was eluted with 80-150 µL of RNase-free water.

RT-qPCR

Complementary DNA was synthesized using the SuperScript III First-Strand Synthesis System (Invitrogen, Cat # 18080051) and oligo(dT) primers according to the manufacturer's protocols. Quantitative PCR of complementary DNA was performed using the DyNAmo HS SYBR Green kit (Thermo-Fisher, Cat # F410L) on an Mx3000P machine (Stratagene, La Jolla, CA) using the primers listed in Table 2.3. Standard curves were generated using a 10-fold dilution series of one of the prepared samples.

Protein Immunoblotting

Each strain was grown to saturation overnight in 5mL YPD. Overnight cultures were diluted to ~2 x 10^5 cells/mL in fresh YPD, grown to mid-log phase, and ~10^8 cells were harvested and pelleted. Pellets were resuspended in 1 mL of 5% trichloroacetic acid and incubated at 4°C for 10-30 min. The precipitates were pelleted, washed once with 1mL of 100% acetone, and air-dried. Dried pellets were resuspended in 100 µL of protein breakage buffer (50mM Tris-HCl, pH 7.5, 1mM EDTA, 3mM DTT) and an equal volume of 0.5 mm zirconium ceramic beads (BioSpec Products, Cat # 11079105z) followed by four cycles of 40 sec bead beating / 2 min on ice in a FastPrep-24 (MP Biomedicals). 100 µL of 2X Laemmli buffer (120mM Tris-HCl pH 7.5,

20% glycerol, 4% SDS, 0.02% bromophenol blue, 10% beta-mercaptoethanol) was added to each sample and incubated at 95°C for 5 min. Insoluble material was pelleted by centrifugation and an equal volume of the soluble fraction from each sample was run on an SDS-polyacrylamide gel (Mini-PROTEAN TGS Any kD precast gel; Bio-Rad, Hercules, CA Cat # 4569033) and transferred to a nitrocellulose membrane using a TransBlot Turbo Mini 0.2 μm Nitrocellulose Transfer Pack (Bio-Rad, Cat # 1704158) on the High MW setting of a TransBlot Turbo machine (Bio-Rad). The membrane was blocked in Intercept Blocking Buffer (LI-COR Biosciences, Lincoln, NE, Cat # 927-70001), and the following primary antibodies and dilutions were used for detection: V5 (R960-25, 1:5000; Invitrogen), Hxk2 (#100-4159, 1:20,000; Rockland Immunochemicals Inc., Pottstown, PA). The secondary antibodies used were IRDye 800CW (926-32210) and 680RD (926-68071) (1:20,000; LI-COR Biosciences), and the membrane was imaged on a LI-COR Odyssey Imager. All washing steps were performed with PBS + 0.1% Tween-20.

Data Availability

All strains and plasmids are available upon request. Sequencing data is available in GEO under the SuperSeries GSE190137. ChIP-seq and DIP-seq data are under accession code GSE189038 in the SuperSeries. Nanopore are under accession code GSE190136 in the SuperSeries.

Table 2.1. Strains used in this study.
All strains listed were derived from the W303 background. Unless otherwise noted, all strains are *can1-100, his3-11,15, leu2-3,112, lys2, trp1-1, ura3-1*. Genotypes with [ ] denote a strain that carries the plasmid designated within the brackets. *K.l.* stands for *Kluyveromyces lactis*.

Strain Number	*MAT*	Genotype
JRY09316	Δ	*matΔ::HphMX,*
JRY11699	Δ	*matΔ::K.l.LEU2*
JRY12601	Δ	*matΔ::K.l.LEU2, SIR3-3xV5-NatMX*
JRY12731	Δ	*matΔ::K.l.LEU2, hmlα2Δ::yEmRFP, hmrα2Δ::yEGFP*
JRY12838	Δ	*matΔ::K.l.LEU2, sir3Δ::M.ECOGII-NatMX*
JRY12839	Δ	*matΔ::K.l.LEU2, SIR3-M.ECOGII-3xV5-NatMX*
JRY12840	Δ	*matΔ::K.l.LEU2, SIR3-M.ECOGII-NatMX*
JRY12842	Δ	*matΔ::K.l.LEU2, hmlα2Δ::yEmRFP, hmrα2Δ::yEGFP, sir3Δ::M.ECOGII-NatMX*
JRY12844	Δ	*matΔ::K.l.LEU2, hmlα2Δ::yEmRFP, hmrα2Δ::yEGFP, SIR3-M.ECOGII-NatMX*
JRY13019	Δ	*matΔ::K.l.LEU2, hmlα2Δ::yEmRFP, hmrα2Δ::yEGFP, SIR4-M.ECOGII-NatMX*
JRY13021	Δ	*matΔ::HphMX, SIR4-M.ECOGII-NatMX*
JRY13027	Δ	*matΔ::HphMX, SIR3-M.ECOGII-NatMX*
JRY13029	Δ	*matΔ::HphMX, sir3Δ::M.ECOGII-NatMX*
JRY13030	Δ	*matΔ::HphMX, sir3Δ::M.ECOGII-NatMX*
JRY13114	Δ	*matΔ::KanMX, sir3-8-M.ECOGII-NatMX*
JRY13134	Δ	*matΔ::KanMX, sir3-8-M.ECOGII-NatMX*
JRY13438	Δ	*matΔ::KanMX, sir3-bahΔ-M.ECOGII-NatMX*
JRY13439	Δ	*matΔ::KanMX, sir3-bahΔ-M.ECOGII-NatMX*
JRY13467	α	*sir3-8-3xV5*
JRY13621	Δ	*matΔ::K.l.LEU2, sir3-bahΔ-3xV5-NatMX*
JRY13625	Δ	*matΔ::HphMX, SIR2-M.ECOGII-NatMX*
JRY13660	α	*hmlα2Δ::yEmRFP, hmrα2Δ::yEGFP, SIR2-M.ECOGII-NatMX,*
JRY13670	Δ	*matΔ::K.l.LEU2, SIR3-M.ECOGII-NatMX, [YEp24: URA3 2micron]*
JRY13671	Δ	*matΔ::K.l.LEU2, SIR3-M.ECOGII-NatMX, [YEp24: URA3 2micron]*
JRY13672	Δ	*matΔ::K.l.LEU2, SIR3-M.ECOGII-NatMX, [pJR3526: SIR3-M.ECOGII URA3 2micron]*
JRY13673	Δ	*matΔ::K.l.LEU2, SIR3-M.ECOGII-NatMX, [pJR3526: SIR3-M.ECOGII URA3 2micron]*

Table 2.2. Plasmids used in this study.

Plasmid	Description	Published Source
pJR42 (YEp24)	*2μ ori, URA3, AmpR*	
pJR3428	*cas9, URA3, ARS4, KanR*	Brothers & Rine 2019, Lee *et al.* 2015
pJR3525	*M.ECOGII, NatMX, AmpR*	This study
pJR3526	*SIR3p-SIR3-M.ECOGII-natMX, 2μ ori, URA3, AmpR*	This study

Table 2.3. Oligonucleotides used in this study.

Name	Sequence (5' -> 3')
Oligonucleotides used for genome insertions	
SIR2-M.ECOGII-NatMX fwd	GGGCGTGTATGTCGTTACATCAGATGAACATCCCAAAACCCTCGGTG GATCTGGTGGATC
SIR2-M.ECOGII-NatMX rev	TATTAATTTGGCACTTTTAAATTATTAAATTGCCTTCTACGAATTCGA GCTCGTTTAAAC
SIR3-M.ECOGII-NatMX fwd	CGCCTTTTCGATGGATGAAGAATTCAAAAATATGGACTGCATTGGTG GATCTGGTGGATC
SIR3-M.ECOGII-NatMX rev	TAGGCATATCTATGGCGGAAGTGAAAATGAATGTTGGTGGGAATTC GAGCTCGTTTAAAC
SIR4-M.ECOGII-NatMX fwd	GATGGAAAAAGATTTTCAAGTGAATAAGGAGATAAAACCGTATGGT GGATCTGGTGGATC
SIR4-M.ECOGII-NatMX rev	ACACTTCGTTACTGGTCTTTTGTAGAATGATAAAAAGTCAGAATTCG AGCTCGTTTAAAC
*sir3*Δ*::M.ECOGII-NatMX* fwd	TTAAGAAAGTTGTTTTGTTCTAACAATTGGATTAGCTAAAATGGGTG GATCTGGTGGATC
*sir3*Δ*::M.ECOGII-NatMX* rev	TAGGCATATCTATGGCGGAAGTGAAAATGAATGTTGGTGGGAATTC GAGCTCGTTTAAAC
guide RNA sequences used for CRISPR-Cas9 gene editing	
*sir3-bah*Δ top	gactttAAGTATTCATCAGATTGTTT
*sir3-bah*Δ bottom	aaacAAACAATCTGATGAATACTTaa
CRISPR repair templates	
*sir3-bah*Δ fwd	ACAGGGGTTTAAGAAAGTTGTTTTGTTCTAACAATTGGATTAGCTAA AATGGTGAGTGGG
*sir3-bah*Δ rev	AACTCCCATCTTATGCATCACCTGTCTATTTGTCTTCTGCCCACTCAC CATTTTAGCTAA
primers used for quantitative PCR	
ACT1 fwd	TTTTGTCCTTGTACTCTTCCGGTAGAAC
ACT1 rev	CCAAATCGATTCTCAAAATGGCGTGAG
HMLα2 fwd	TCCACAAATCACAGATGAGT
HMLα2 rev	GTTGGCCCTAGATAAGAATCC
HMRa1 fwd	GGCGGAAAACATAAACAGAAC
HMRa1 rev	GGGTGATATTGATGATTTTCCC
CHA1 fwd	GGAAACGAATGGATGTCATG
CHA1 rev	GTTGTATTTGCGAGCGTATTC
OCA4 fwd	CATTGAGATAGAACAGGAGAAGG
OCA4 rev	GCAAAGGTCATCTTCATTTACTC
SIR3 fwd	ATTGGTAGTGTCACAGGAG
SIR3 rev	CAAGCGTATGACGATTCGT
M.ECOGII fwd	CAACAGGGAAGAAGAACATGG
M.ECOGII rev	ATGATGGGGTTTCTCTAACTCC
M.ECOGII gene block for pJR3525 construction	

M.ECOGII	aaccttatgtatcatacacatacgatttaggtgacactatagaacgcggccgccagctgaagcttcgtacgctgcag gggtggatctggtggatctATGTTGAACACGGTGAAAATAAGCTCCTGTGAGCT TATTAATGCTGACTGCCTAGAATTTATCCGTTCTTTACCCGAAAACTC CGTAGATTTAATTGTCACCGACCCGCCGTACTTCAAAGTAAAACCGG AGGGGTGGGACAACCAGTGGAAGGGTGACGATGATTATCTGAAATG GCTGGATCAGTGTTTAGCTCAGTTTTGGCGTGTCTTGAAGCCCGCGG GGAGTCTGTATTTATTCTGTGGCCACAGGTTAGCATCAGATATAGAG ATCATGATGCGTGAAAGGTTCAGTGTACTAAACCATATTATATGGGC GAAACCATCTGGAAGATGGAATGGCTGCAACAAAGAGTCTCTTAGA GCGTATTTTCCCGCCACAGAGCGTATTCTGTTTGCGGAGCACTACCA AGGTCCATATCGTCCAAAAGACGCTGGATATGAAGCTAAAGGAAGA GCCCTGAAACAGCACGTTATGGCCCCCCTTATAGCGTACTTTCGTGA TGCGCGTGCTGCTCTAGGCATCACTGCGAAGCAGATTGCAGATGCAA CAGGGAAGAAGAACATGGTGCCACATTGGTTCAGTGCAAGCCAATG GCAACTACCGAATGAATCAGATTACCTGAAATTGCAATCATTATTCG CTAGGGTTGCTGAGGAGAAGCACCAGAGAGGGGAGTTAGAGAAACC CCATCATCAACTGGTATCCACTTATTCTGAGTTGAACCGTAAATACA TGGAATTACTATCAGAATACAAAAACCTACGTAGATACTTCGGAGTG ACGGTGCAGGTGCCCTATACAGATGTATGGACTTACAAACCCGTGCA GTATTATCCGGGGAAGCATCCGTGTGAAAAACCCGCAGAGATGTTA CAACAGATCATAAGTGCATCCTCACGTCCCGGTGACTTGGTTGCGGA TTTCTTCATGGGCAGTGGCTCCACGGTCAAAGCTGCCATGGCATTGG GTAGGCGTGCCATTGGAGTTGAACTAGAGACTGGAAGATTCGAGCA GACAGTACGTGAGGTACAAGACCTTATCGTCtgaggcgcgccacttctaaataagc gaatttcttatgatttat

Chapter 3:

Mutations in the PCNA DNA polymerase clamp of *Saccharomyces* cerevisiae reveal complexities of the cell cycle and ploidy on heterochromatin assembly[1]

3.1 Abstract

In *Saccharomyces cerevisiae*, transcriptional silencing at *HML* and *HMR* maintains mating-type identity. The repressive chromatin structure at these loci is replicated every cell cycle and must be re-established quickly to prevent transcription of the genes at these loci. Mutations in a component of the replisome, the Proliferating Cell Nuclear Antigen (PCNA), encoded by *POL30*, cause a loss of transcriptional silencing at *HMR*. We used an assay that captures transient losses of silencing at *HML* and *HMR* to perform extended genetic analyses of the *pol30-6*, *pol30-8*, and *pol30-79* alleles. All three alleles destabilized silencing only transiently and only in cycling cells. Whereas *pol30-8* caused loss of silencing by disrupting the function of Chromatin Assembly Factor 1 (CAF-I), *pol30-6* and *pol30-79* acted through a separate genetic pathway but one still dependent on histone chaperones. Surprisingly, the silencing-loss phenotypes depended on ploidy but not on *POL30* dosage or mating-type identity. Separately from silencing loss, the *pol30-6* and *pol30-79* alleles also displayed high levels of mitotic recombination in diploids. These results established that histone trafficking involving PCNA at replication forks is crucial to the maintenance of chromatin state and genome stability during DNA replication. They also raised the possibility that increased ploidy may protect chromatin states when the replisome is perturbed.

3.2 Introduction

Eukaryotic genomes include tightly packaged and transcriptionally repressed domains referred to as heterochromatin. The nucleosomes in heterochromatin are enriched for particular chromatin marks made by specialized chromatin-modifying enzymes. The marks left by these enzymes are recognized by other proteins that silence gene transcription. Although the exact histone modifications and heterochromatin proteins differ from organism to organism, there are unifying characteristics of heterochromatin including independence from underlying DNA sequence, replication late in S phase, and structural compaction.

To maintain the repression of genes within heterochromatin, histone modifications and chromatin-binding proteins must be faithfully replicated onto both daughter strands during DNA replication. The process that is required for inheritance of chromatin state through DNA replication is unclear but requires the interaction of chromatin regulators with various factors in the eukaryotic replisome (reviewed in Alabert et al. 2017).

Proliferating Cell Nuclear Antigen (PCNA) is a DNA polymerase processivity clamp conserved from yeast to human (reviewed in Choe and Moldovan 2017). PCNA is a homotrimer that assembles around individual DNA molecules, and, through protein-protein interactions, coordinates many activities at the DNA replication fork, including the processivity of DNA polymerase, Okazaki fragment processing, and chromatin assembly and remodeling. PCNA is

[1] A version of this work was originally published as: Brothers M, Rine J. 2019. Mutations in the PCNA DNA Polymerase Clamp of Saccharomyces cerevisiae Reveal Complexities of the Cell Cycle and Ploidy on Heterochromatin Assembly. *Genetics* **213**: 449–463. http://dx.doi.org/10.1534/genetics.119.302452.

also required for many different DNA repair pathways. Many chromatin modifiers and remodelers are recruited to replication forks through direct and indirect interactions with PCNA.

PCNA has a direct role in the stability of heterochromatin. In mice, heterochromatin Protein 1 (HP1) is recruited to replication forks through direct interaction with the histone chaperone complex Chromatin Assembly Factor 1 (CAF-I) (Murzina et al. 1999), which itself is recruited to replication forks through direct interaction with PCNA (Shibahara and Stillman 1999; Zhang et al. 2000; Ben-Shahar et al. 2009). PCNA, in concert with CAF-I, is also required for the asymmetric specification of cell fate in the *C. elegans* nervous system, an epigenetic process (Nakano et al. 2011). Additionally, the maintenance of transcriptional silencing requires functional and stable DNA-bound PCNA in *Saccharomyces cerevisiae* (Zhang et al. 2000; Miller et al. 2008; Janke et al. 2018). These results suggest an important role for PCNA and CAF-I in the inheritance of chromatin states through DNA replication.

Circumstantial evidence for the importance of PCNA in the assembly of heterochromatin is also found in humans and *D. melanogaster.* In humans, Histone Deacetylase 1 (HDAC1), which is associated with transcriptional repression, interacts with PCNA *in vitro* and colocalizes with PCNA at replication forks *in vivo* (Milutinovic et al. 2002). In *D. melanogaster*, Polycomb Group (PcG) proteins, required for the establishment and maintenance of facultative heterochromatin, transiently associate with PCNA and CAF-I during DNA replication (Petruk et al. 2012).

Saccharomyces cerevisiae contains well-characterized heterochromatin domains that we used here to study the role of PCNA in epigenetic inheritance through DNA replication. Two of these loci, *HML* and *HMR,* share characteristics of heterochromatin in other organisms. Silencing of *HML* and *HMR* requires the activity of the SIR (Silent Information Regulator) complex, composed of Sir2, Sir3, and Sir4. The Sir proteins are recruited first to the *E* and *I* silencers, nucleation sites flanking *HML* and *HMR,* and subsequently bind to nucleosomes that span the entire 3-4kb region between the silencers. Through the histone deacetylation activity of Sir2 and nucleosome-bridging ability of Sir3, the SIR complex creates a hypoacetylated, compact chromatin structure (reviewed in Gartenberg and Smith 2016).

In *S. cerevisiae*, alleles of PCNA, encoded by *POL30*, have been isolated that disrupt transcriptional silencing of reporter genes at telomeres and the silent mating-type locus, *HMR.* (Zhang et al. 2000). These alleles, *pol30-6*, *pol30-8*, and *pol30-79*, differ in phenotype and the degree of silencing loss they cause. Using the *ADE2* reporter at *HMR*, the *pol30-8* allele results in sectored colonies, suggesting the existence of two heritable states of gene expression: heritable silencing (*ADE2* expression off, resulting in red sectors), and heritable expression (*ADE2* expression on, resulting in white sectors). In contrast, colonies containing *pol30-6* or *pol30-79* are pink, suggesting a partial reduction of silencing in all cells (Zhang et al. 2000).

In combination with a deletion of *CAC1*, which encodes the large subunit of the histone chaperone CAF-I, the *pol30-6* and *pol30-79* alleles synergistically reduce silencing of *URA3* at telomere VII-L and of *ADE2* at *HMR*. However, the combination of *cac1*Δ and *pol30-8* result in similarly-sectored *ADE2* colonies as *pol30-8* alone and no further decrease in telomeric silencing than *pol30-8* alone. These two results suggest that PCNA may contribute to heritable silencing through at least two different mechanisms, one of which is through the histone-chaperone activity of CAF-I (Zhang et al. 2000).

Although reporter genes have a long history of successful use in genetic studies, the reliability of the *ADE2* and *URA3* reporters has been called into question, especially for situations involving DNA metabolism (Takahashi et al. 2011; Rossmann et al. 2011). Using a

silencing-reporter assay that more sensitively captures loss-of-silencing events, better maintains the gene structure of *HML* and *HMR*, and is free of the complications of nucleotide metabolism, we have re-evaluated earlier claims about the silencing phenotypes of *pol30-6*, *pol30-8*, and *pol30-79,* extended the analyses substantially, and have provided new interpretations of published observations.

3.3 Results

3.3.1 Mutants of *POL30* caused transient loss of silencing

We introduced alleles of *POL30* implicated in heterochromatic silencing, *pol30-6, pol30-8,* and *pol30-79* (Zhang et al. 2000) into a strain we previously constructed that allows sensitive detection of losses of heterochromatin silencing (Figure 3.1A, (Dodson and Rine 2015). In this strain, the *α2* coding sequence at *HMLα* or *HMRα* is replaced with the coding sequence of Cre recombinase. The *URA3* locus on chromosome V is replaced by *loxP* sites flanking the *RFP* gene and the selectable marker *hphMX* downstream of the strong *TDH3* promoter. Downstream of *loxP-RFP-hphMX-loxP* is a promoter-less *GFP* gene. Upon loss of silencing at *HMLα* or *HMRα*, Cre recombinase is expressed and excises the *RFP* and *hphMX* sequences, resulting in a permanent switch from expressing RFP to expressing GFP (Figure 3.1A). Within a colony, a sector of green cells represents a loss-of-silencing event in a cell born at the vertex with the sector representing growth of the descendants following the loss event. This assay is referred to as the CRASH assay (Cre-Reported Altered States of Heterochromatin, (Dodson and Rine 2015).

Each of the *pol30* mutants resulted in increased sectoring compared to wild-type *POL30* at both *HMLα* and *HMRα* (Figure 3.1B). We also quantified loss-of-silencing events in these strains using flow cytometry. The apparent silencing-loss rate was calculated as the number of yellow cells (cells that had recently excised the *RFP* gene) divided by the sum of all yellow cells *and* red cells. The loss rates from flow cytometry experiments mirrored qualitative assessments of loss rates from colony sectoring (Figure 3.1C). *pol30-8* cells had the most unstable silencing followed by *pol30-6* and then *pol30-79* (Figure 3.1B, 3.1C). There was no significant difference between silencing instability at *HML* and *HMR* for each of the mutants (Figure 3.1C).

The CRASH assay reveals how unstable transcriptional silencing is in a given strain, but because it is a permanent switch, the assay is unable to capture the heritability of the de-repressed state at *HML* and *HMR*. To determine how heritable the loss-of-silencing events were in strains with the *pol30-6*, *pol30-8*, and *pol30-79* alleles, we first performed an α-factor halo assay (Figure 3.1D). When *MATa* cells are exposed to the mating pheromone α-factor, they arrest in G1. On a lawn of *MATa* cells, this results in a halo of arrested cells surrounding the source of α-factor (Figure 3.1D, wild type) However, if *MATa* cells lose silencing at *HMLα,* they no longer arrest in response to α-factor (Figure 3.1D, *sir4*Δ). If the loss-of-silencing events created by the *pol30* mutants were heritable, colonies would grow within the halo, as noted for the *sir4*Δ strain. However, for all three alleles, we observed no cell growth within the halos (Figure 3.1D). In agreement with the α-factor halo results, strains containing *pol30-6, pol30-8,* or *pol30-79* also showed only low levels of *HMLα1*, *HMLα2*, and *HMRa1* transcripts by RT-qPCR (Figure 3.1E). Analysis of *cre* transcripts from CRASH strains with the *POL30* alleles also revealed only low levels of transcription (data not shown).

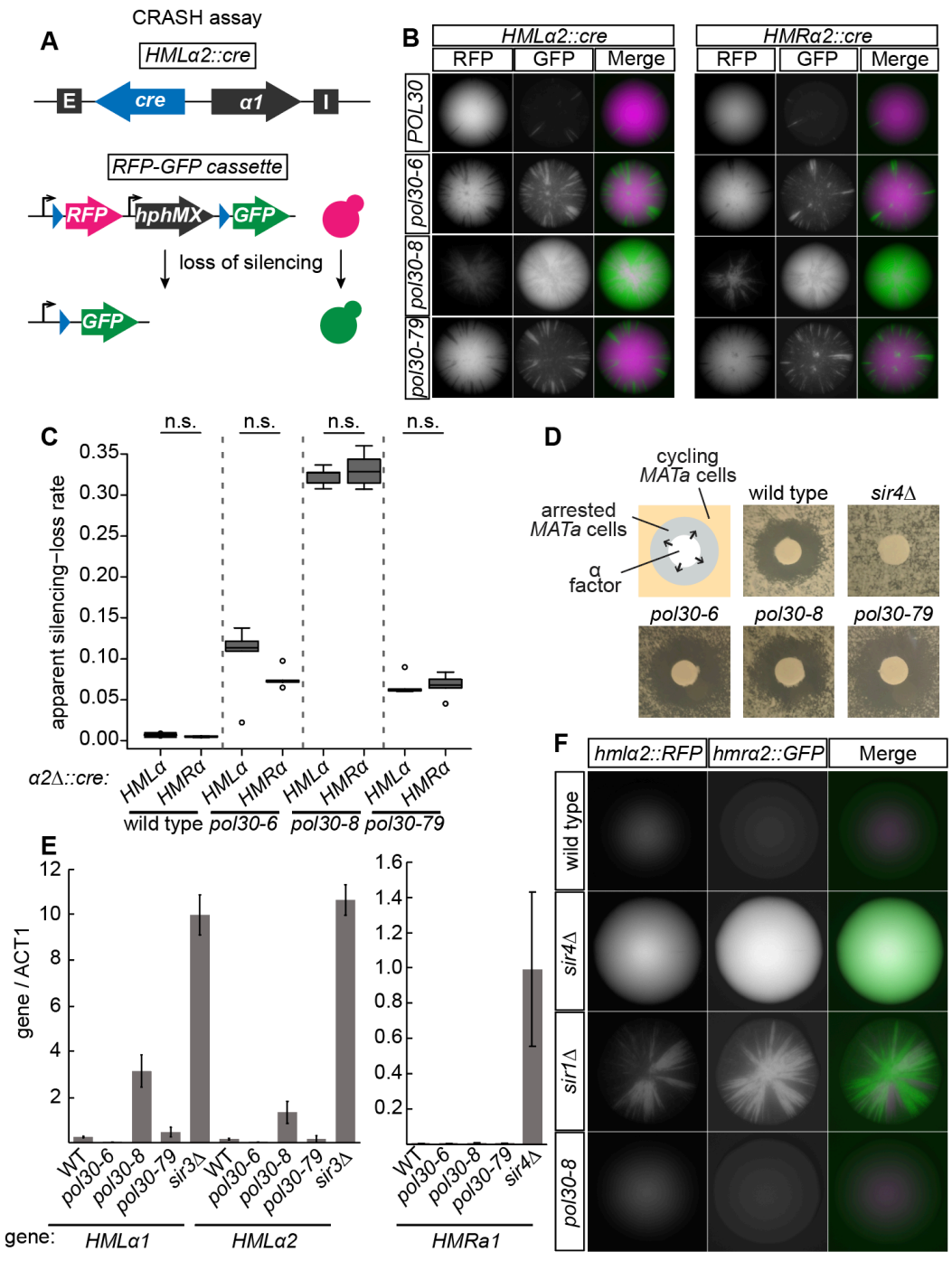

Figure 3.1. Mutants of *POL30* caused transient loss of silencing.
A) Schematic of the CRASH loss-of-silencing assay. Expression of *cre* from *HMLα2::cre* occurs when transcriptional silencing is disturbed. In cells that lose silencing even transiently, Cre causes a permanent switch from expressing RFP to expressing GFP. In a similar strain, *cre* is expressed from *HMRα2* to detect loss-of-silencing events at HMR. **B)** Colonies of *HMLα2::cre* (left panel) and *HMRα2::cre* (right panel) strains for each *POL30* allele. Each green sector represents a loss-of-silencing event. Wild-type strains (JRY10790, left and JRY10710, right) had few sectors. Strains containing *pol30-6* (JRY11137, left and JRY11186, right), *pol30-8* (JRY11188, left and JRY11187, right), or *pol30-79* (JRY11141, left and JRY11608, right) had elevated sectoring compared to wild type. **C)** The apparent silencing-loss rates for each of the strains in B were quantified by flow cytometry as described
(continued on next page)

in *Materials and Methods* and in Janke *et al.* (2018). Significance (Nonsignificant difference = n.s.) was determined by one-way ANOVA and Tukey's honestly significant difference *post hoc* test. The center line of each box plot represents the median of at least five biological replicates. The boxes represent the 25th and 75th percentiles. Whiskers represent the range of values within 1.5× the interquartile range. Values extending past 1.5× the interquartile range are marked as outliers (circles). **D)** α-Factor halo assay. Filter papers soaked in the mating pheromone α-factor (200 μM in 100 mM sodium acetate) were placed onto a freshly spread lawn of *MATa* cells of each indicated genotype. *MATa* cells that maintain silencing at *HML*α will arrest in G1 phase around the filter paper, creating a "halo." Cells that heritably lose silencing at *HML*α do not arrest in response to α-factor. Representative images of wild type (JRY4012), *sir4*Δ (JRY4577), *pol30-6* (JRY11645), *pol30-8* (JRY11647), and *pol30-79* (JRY11649) are shown. **E)** Quantitative RT-PCR of α *1* and α*2* transcripts from *HML*α and *a1* from *HMRa*. Quantification was performed using a standard curve for each set of primers and normalized to *ACT1* transcript levels. Error bars represent SD. Bars represent the normalized average of three technical replicates of each indicated strain: WT (JRY11699 *mat*Δ), *sir3*Δ (JRY9624, *mat*Δ*hmr*Δ) *sir4*Δ (JRY12174 *MAT*α), *pol30-6* (JRY11700 *mat* Δ), *pol30-8* (JRY11701 *mat*Δ), and *pol30-79* (JRY11702 *mat*Δ). **F)** Genes encoding fluorescence reporters were placed at *HML*α*2* (RFP) and *HMR*α*2* (GFP) to report on transcription from the two loci. Shown are representative images of colonies from each strain: WT (JRY11129), *sir4*Δ (JRY11131), *sir1*Δ (JRY11130) *pol30-8* (JRY11132). WT, wild type.

The absence of a notable increase in transcripts from *HML* and *HMR* was particularly surprising for *pol30-8*, which had an extremely high CRASH sectoring rate (Figure 3.1B, 3.1C) and was previously suggested to have bi-stable epigenetic states based upon the *HMR::ADE2* reporter (Zhang et al. 2000; Miller et al. 2010). Therefore, we also placed this allele in another reporter strain that encodes *GFP* at *HMRα2* and *RFP* at *HMLα2*. In *sir4*Δ colonies, every cell expresses both *RFP* and *GFP*, whereas *sir1*Δ colonies have *GFP* and *RFP* sectors (Figure 3.1F), representing the bi-stable epigenetic states characteristic of this deletion (Pillus and Rine 1989). If the *pol30-8* allele resulted in a population of cells with stable expression from *HML* or *HMR*, we would expect fluorescent sectors, just like *sir1*Δ (Figure 3.1F). Instead, *pol30-8* colonies were not sectored, meaning that any transcription occurring from the locus following a loss-of-silencing event was not stable (Figure 3.1F).

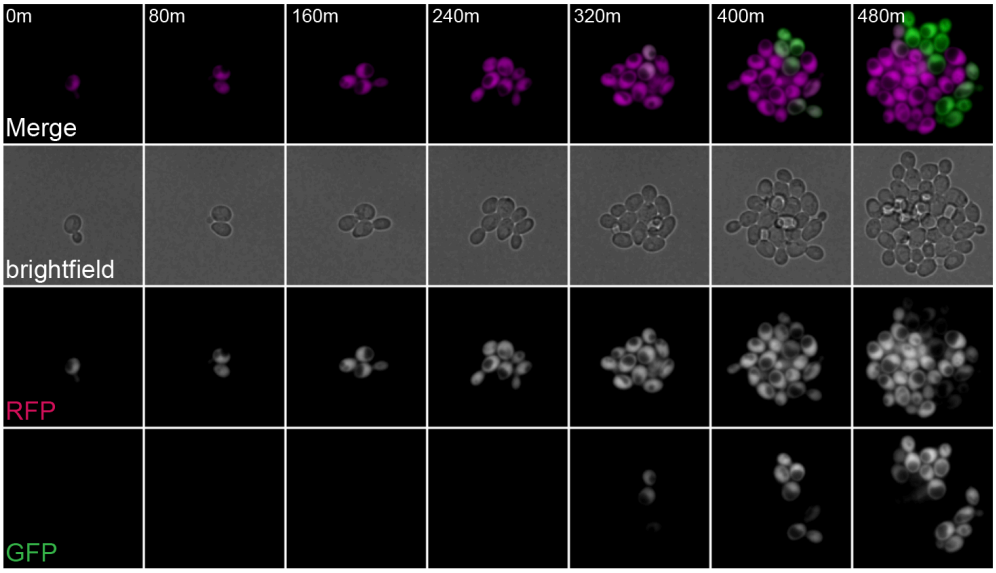

Figure 3.2. Loss-of-silencing events in strains with defective *POL30* alleles occurred predominantly in cycling cells.
Representative images of two loss-of-silencing events in one micro-clone of cycling cells in the *HML*α*2*::*cre* CRASH assay containing the *pol30-8* allele (JRY11635, *bar1*Δ). See Table 1 for calculation of switching rates for all *POL30* alleles.

3.3.2 Loss-of-silencing events in strains with defective *POL30* alleles occurred predominantly in cycling cells

Given the major role of PCNA in DNA replication, we considered that the loss-of-silencing events may occur only during S-phase. Alternatively, because PCNA is involved in replication-independent roles such as DNA repair, it was possible that heterochromatin assembled in the *pol30* mutants might be unstable at any point in the cell cycle. We performed time-lapse microscopy using CRASH strains to compare the rate that silencing is lost in G1-arrested cells to the rate in cycling cells. As an example, in cycling *pol30-8* cells, switches were readily visible over the time-course of 8 hours (Figure 3.2). In wild-type cells, the rate of switching was about the same for arrested versus cycling cells. However, in cells containing each of the *pol30* mutants, losses of silencing predominantly occurred in cycling cells. Arrested *pol30* mutants exhibited a low frequency of silencing loss comparable to that seen in wild type (Table 1). These results suggested that the *pol30-6*, *pol30-8*, and *pol30-79* alleles caused only transient losses of silencing in actively cycling cells, with quick re-establishment of the silent state.

3.3.3 Silencing loss caused by *POL30* alleles was dependent on ploidy

To determine whether each of the *pol30* mutants disrupted silencing in the CRASH assay through the same mechanism, we performed pairwise complementation testing among the three alleles. As a necessary prerequisite, we tested each allele in a diploid in combination with wild-type *POL30. pol30-6, pol30-8,* and *pol30-79* were all recessive to *POL30* by this assay (Figure 3.3A).

If two recessive *pol30* mutants disrupt heterochromatin through different mechanisms, then the combination of those two alleles in the diploid should complement, decreasing the frequency of RFP-to-GFP switches compared to each allele alone. All three combinations of *pol30* mutants in heteroallelic diploids decreased sectoring relative to haploids with each allele individually, most dramatically evident in the *pol30-6 / pol30-8* diploid (Figure 3.3B, 3.3C). Because the sectoring phenotype of *pol30-79* was weak on its own, its effect in combination with the other alleles was not as striking but still noticeably in combination with both *pol30-6* and *pol30-8* (Figure 3.3B, 3.3C).

In the simplest manifestation of the complementation test in yeast genetics, the phenotype of haploids containing each mutant of interest is compared to the phenotype of diploids containing both mutations, often ignoring potential complications of ploidy in assessing whether the mutations complement. Surprisingly, homozygosity of each allele at least partially suppressed the loss-of-silencing phenotype as measured by the CRASH assay (Figure 3.4A, 3.4B, 3.4C).

To test whether the phenotypic suppression of *pol30* mutations reflected mating-type differences between haploids and diploids, we created *MATα / mat*Δ diploids homozygous for each *POL30* allele. These cells, though diploid, express only *α*-specific genes and therefore behave as *MATα* haploids. If mating-type were the cause of sectoring suppression in the *pol30-6, pol30-8, and pol30-79* diploids, then *MATα / mat*Δ diploids would be expected to increase the sectoring rate back to the same level as the haploids. For all three alleles, changing the mating type had little or no effect on the reduced sectoring phenotype of diploids (Figure 3.4A, 3.4C).

Therefore, mating type was not responsible for the difference between haploid and diploid *pol30* mutants.

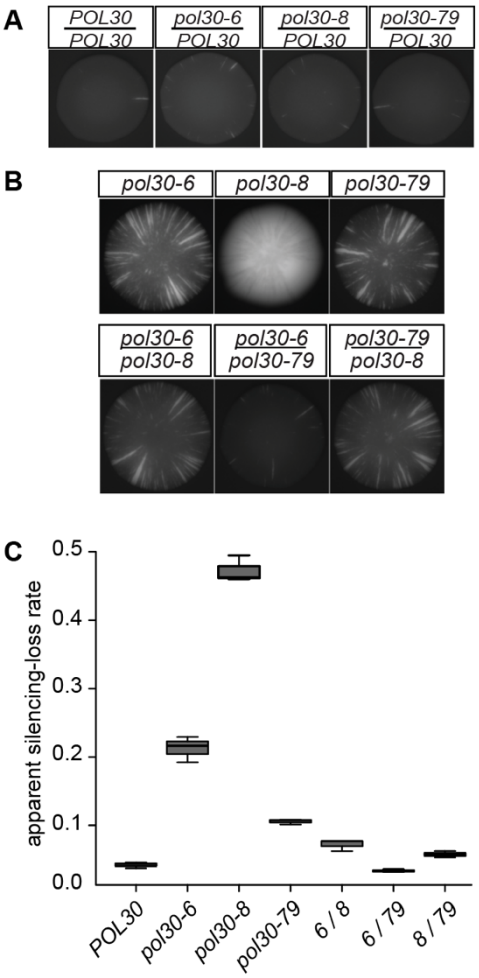

Figure 3.3. *POL30* alleles complemented in diploids.
A) Each *pol30* allele was recessive to wild-type *POL30* in the CRASH assay *POL30/POL30* (JRY11159), *pol30-6/POL30* (JRY11160), *pol30-8/POL30* (JRY11169), and *pol30-79/POL30* (JRY11161). Only the GFP channel is shown. These diploid strains contained only one *HMLα2*::*cre* and one *RFP-hphMX-GFP* cassette. **B)** Complementation of *pol30-6*, *pol30-8*, and *pol30-79* in the CRASH assay. Only the GFP channel is shown. The top row shows representative haploid colonies containing the indicated allele: *pol30-6* (JRY11137), *pol30-8* (JRY11188), and *pol30-79* (JRY11141). The bottom row shows representative diploid colonies containing a combination of the indicated alleles: *pol30-6/pol30-8* (JRY11656), *pol30-6/pol30-79* (JRY11657), and *pol30-8/pol30-79* (JRY11658). Diploid strains contained only one *HMLα 2*::*cre* and one *RFP-hphMX-GFP* cassette. **C)** The apparent silencing-loss rates for each of the strains in B and *POL30* (JRY10790) were quantified by flow cytometry as described in Figure 3.1C.

Alternatively, the reduced sectoring in diploids could reflect a difference in gene dosage of *POL30* between haploids and diploids. We therefore created hemizygotes for each allele in which diploids contained only one copy of the allele instead of two. Although hemizygosity did not increase the sectoring rate to the same level as the haploid, the *pol30-8* hemizygote had a statistically significant increase in the loss of silencing rate compared to the homozygote (Figure 3.4C). In contrast to *pol30-8*, the *pol30-6* and *pol30-79* hemizygotes had only minor, statistically-insignificant increases in sectoring (Figure 3.4B, 3.4C). Immunoblot of Pol30 protein levels and qRT-PCR of *POL30* RNA levels in the various mutants revealed that *pol30-6* and *pol30-79* expression was comparable in hemizygotes and homozygotes, whereas wild-type *POL30* and *pol30-8* expression decreased by half at both the protein and RNA level (Figure 3.4D, 3.4E).

The effect of *pol30* mutants on heterochromatin stability was different in haploids and diploids, and this difference was independent of mating type and largely independent of gene dosage. Moreover, silencing in tetraploid cells with just one copy of *POL30* was as stable as in haploids and homozygous or hemizygous diploids (Figure 3.4F), even with a quarter the expression of *POL30* relative to the amount of chromatin the cell (Figure 3.4D, 3.4E).

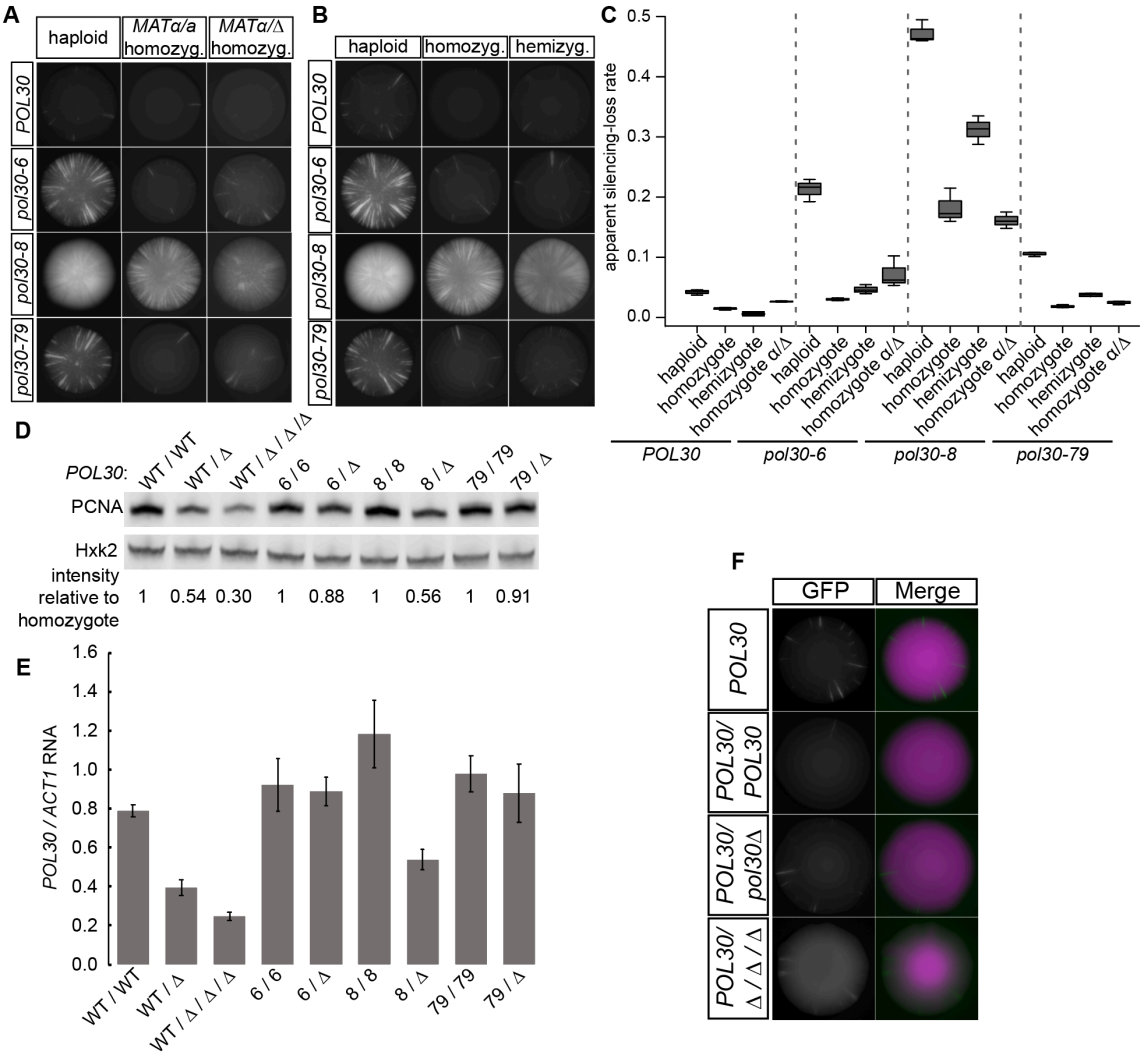

Figure 3.4. The effect of *POL30* mutants on silencing was dependent on ploidy.
A) Representative images of haploids, *MATα/MATa* homozygotes, and *MATα/mat*Δ homozygotes for each indicated *POL30* allele in the CRASH assay. Homozygous diploid strains contained two copies of each indicated allele. Only the GFP channel is shown. Diploid strains contained only one *HMLα 2*::*cre* and one *RFP-hphMX-GFP* cassette. *POL30* row: JRY10790, JRY11159, and JRY11718. *pol30-6* row: JRY11137, JRY11686, and JRY11719. *pol30-8* row: JRY11188, JRY11687, and JRY11744. *pol30-79* row: JRY11141, JRY11688, and JRY11720. **B)** Representative images of haploids, homozygotes, and hemizygotes for each indicated *POL30* allele in the CRASH assay. Homozygotes are diploid strains containing two copies of each indicated allele. Hemizygotes are diploid strains containing one copy of the indicated allele over a deletion of *POL30* (*pol30*Δ). Diploid strains contained only one *HMLα2*::*cre* and one *RFP-hphMX-GFP* cassette. *POL30* row: JRY10790, JRY11159, and JRY11745. *pol30-6* row: JRY11137, JRY11686, and JRY11822. *pol30-8* row: JRY11188, JRY11687, and JRY11749. *pol30-79* row: JRY11141, JRY11688, and JRY11823. **C)** The apparent silencing-loss rates for each of the strains in A and B were quantified by flow cytometry as described in Figure 3.1C. **D)** Immunoblot analysis of PCNA protein levels in homozygotes and hemizygotes of each allele (same strains as B) as well as a tetraploid containing just one copy of wild-type *POL30* (WT/Δ/Δ/Δ, JRY12026). The tetraploid contained two copies of *HMLα2*::*cre* and the *RFP-hphMX-GFP* cassette. Hxk2 levels served as a loading control. *POL30* allele nomenclature was abbreviated. Each PCNA band intensity was normalized to Hxk2 intensity. After normalization to Hxk2, the relative intensity of each lane to its corresponding *POL30*, *pol30-6*, *pol30-8*, or *pol30-79* homozygote was calculated and displayed. **E)** Quantitative RT-PCR analysis of *POL30* RNA levels in homozygotes and hemizygotes
(continued on next page)

of each allele and a tetraploid with one copy of wild-type *POL30* (same strains as B and D). Quantification was performed as in Figure 3.1E. **F)** Representative images of a wild-type haploid (*POL30* JRY10790), homozygote (*POL30/POL30* JRY11159), hemizygote (*POL30/*Δ JRY11745), and tetraploid with one copy of *POL30* (*POL30/*Δ/Δ/Δ JRY12026). The haploids and diploids contained only one *HMLα2*::*cre* and one *RFP-hphMX-GFP* cassette. The tetraploid contained two copies of *HMLα2*::*cre* and the *RFP-hphMX-GFP* cassette. The increased background in the GFP channel of the tetraploid was due to loop-out of one *RFP-hphMX* cassette, leaving just one *RFP-hphMX-GFP* cassette able to switch. WT, wild type.

3.3.4 *pol30-6* and *pol30-79* caused high rates of mitotic recombination and gene conversion in diploids

In the course of characterizing the *POL30* mutants, we found that *pol30-6* and *pol30-79* homozygous diploids had high rates of mitotic recombination/gene conversion in diploids that was dependent on mating type but not on *POL30* gene dosage. CRASH colonies of *pol30-6* and *pol30-79* homozygotes revealed mitotic recombination of the *RFP-GFP* cassette through the existence of sectors that were twice as bright and sectors that were non-fluorescent suggesting duplication and loss of the cassette, respectively (Figure 3.5A). *pol30-8* homozygotes did not display mitotic recombination (data not shown). In *mat*Δ */ MATα* diploids homozygous for *pol30-6* and *pol30-79,* this phenotype was suppressed (Figure 3.5A). Hemizygosity for *pol30-6* or *pol30-79* did not suppress the high levels of mitotic recombination seen in homozygous diploids (Figure 3.5A).

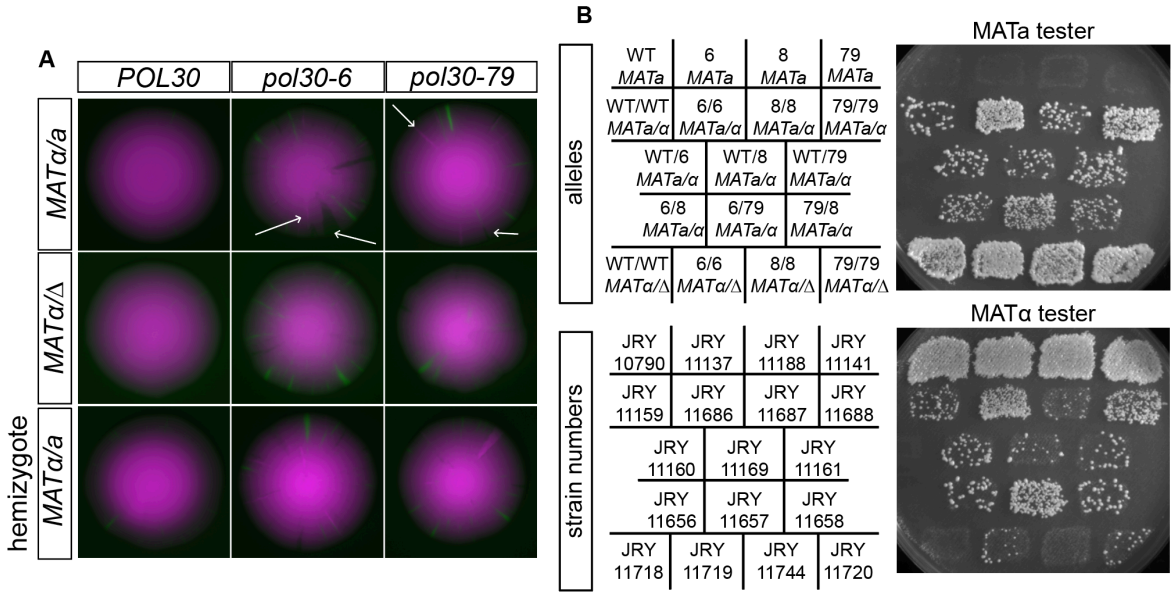

Figure 3.5. *pol30-6* and *pol30-79* caused high rates of mitotic recombination and gene conversion in diploids. **A)** Representative CRASH colonies of each indicated genotype. The *pol30-6* homozygote *MATa/MAT*α diploid (JRY11686) and the *pol30-79* homozygote *MATa/MAT*α diploid (JRY11688) both had extrabright sectors and nonfluorescent sectors (examples illustrated by arrows). No, or very few, sectors were observed in *POL30 MATa/MAT*α (JRY11159), *POL30 mat*Δ*/ MAT*α (JRY11718), *pol30-6 mat*Δ*/MAT*α (JRY11719), or *pol30-79 mat*Δ*/MAT*α (JRY11720). Hemizygosity of *POL30* (JRY11745), *pol30-6* (JRY11822), or *pol30-79* (JRY11823) in *MATa/ MAT*α diploids had no effect on the mitotic recombination phenotype. **B)** Patch-mating assay. Each indicated strain was patched onto complete medium plates seeded with a freshly plated lawn of either *MATa* or *MAT*α haploid cells with complementary auxotrophies. After ~18 hr, mating patches were replica plated onto minimal medium plates. Growth occurs within the patch only if the indicated strains mated with the mating tester lawn. WT, wild type.

Both homozygotes and hemizygotes of *pol30-6* and *pol30-79* had higher rates of spore inviability than expected whereas wild type and *pol30-8* did not (Table 2). The *pol30-6* and *pol30-79* alleles complemented one another by this assay, and their combination with *pol30-8* also reduced the high levels of spore inviability (Table 2). The consistency between spore inviability and recombination of the GFP cassette in *pol30-6* and *pol30-79* diploids suggested that the increased spore death might be a result of high levels of mitotic recombination. The inviability was suggestive of unequal or intra-chromosomal crossing over, since well-aligned reciprocal recombination would not be expected to cause inviability.

Further evidence of genome instability of *pol30-6* and *pol30-79* mutants came from mating-type testing of diploids homozygous for these alleles. Diploid cells express both *MATa* and *MATα* information, which prevents them from mating. However, if they undergo mitotic recombination between the centromere and *MAT* or gene conversion event at the *MAT* locus, they could become *MATa / MATa* or *MATα / MATα*, resulting in some cells in a patch of cells gaining the ability to mate with *MATα* or *MATa* tester lawns, respectively. We patched each strain onto normal growth medium with a lawn of either *MATa* or *MATα* haploids with complementary auxotrophies. After allowing time for mating, we replica plated these patches onto minimal media, selecting for diploid cells by the complementation of auxotrophic markers.

As expected, haploid *MATa* strains mated only with the *MATα* tester (Figure 3.5B, top row). Additionally, *MATα / mat*Δ diploids mated robustly with the *MATa* tester (Figure 3.5B, bottom row). There is some mitotic recombination/gene conversion that occurs in wild-type diploids allowing them to mate inefficiently with *MATa* and *MATα* cells (Figure 3.5B, WT/WT MATa/α). However, *pol30-6* and *pol30-79* homozygous diploids had much higher levels of mitotic recombination/gene conversion, demonstrated by the greater density of colonies in those patches (Figure 3.5B, row 2).

Combination of *pol30-6* or *pol30-79* with a wild-type *POL30* allele or the *pol30-8* allele reduced the mating efficiency back to wild-type levels (Figure 3.5B, rows 3 and 4). Although still elevated compared to wild-type, *MATα / mat*Δ diploids of *pol30-6* and *pol30-79* had lower amounts of mitotic recombination/gene conversion. Mutations that elevate the rate of chromosome loss would be expected to have a similar phenotype, but the involvement of mating type was suggestive of recombination events rather than chromosome losses being elevated in the homozygous diploids.

In contrast to the spore inviability results, where *pol30-6* and *pol30-79* complemented one another, there was no detectable complementation by this assay: The diploids with both *pol30-6* with *pol30-79* still had increased ability to mate as a diploid (Figure 3.5B, row 4) compared to the wild-type diploid.

3.3.5 Coordination of histone chaperones at replication forks by PCNA was required for full transcriptional silencing

Because the *pol30* mutants appeared to have separable defects in heterochromatic silencing, we combined each of the alleles with known mutants affecting histone chaperone events at the replication fork: *cac1*Δ*, dpb3*Δ*,* and *mcm2-3A*. We made each combination in a CRASH assay strain and compared the sectoring phenotype of the double mutants with the corresponding single mutants.

CAC1 is a subunit of the histone chaperone complex CAF-I. CAF-I deposits newly synthesized H3/H4 tetramers on daughter strands of DNA during replication (Smith and Stillman

1989; Serra-Cardona and Zhang 2018). Previous double-mutant analyses using a different silencing assay concluded that *pol30-8* results in loss of silencing through a defect in CAF-I activity, but that *pol30-6* and *pol30-79* act through a different mechanism (Zhang et al. 2000). In contrast to previous reports of a weak silencing defect for *cac1*Δ (Zhang et al. 2000; Huang et al. 2005), it had a severe sectoring phenotype in the CRASH assay, comparable to that of *pol30-8* alone (Figure 3.6A, 3.6B). The combination of *cac1*Δ with *pol30-8* was similar in phenotype to the single mutants, in agreement with previous results and the hypothesis that *pol30-8* and *cac1*Δ decrease silencing stability through the same mechanism (Figure 3.6A, 3.6B). Also, in agreement with previous results, the combination of *cac1*Δ with *pol30-6* or *pol30-79* worsened their phenotype significantly, suggesting that *pol30-6* and *pol30-79* had defects distinct from *cac1*Δ (Figure 3.6A, 3.6B).

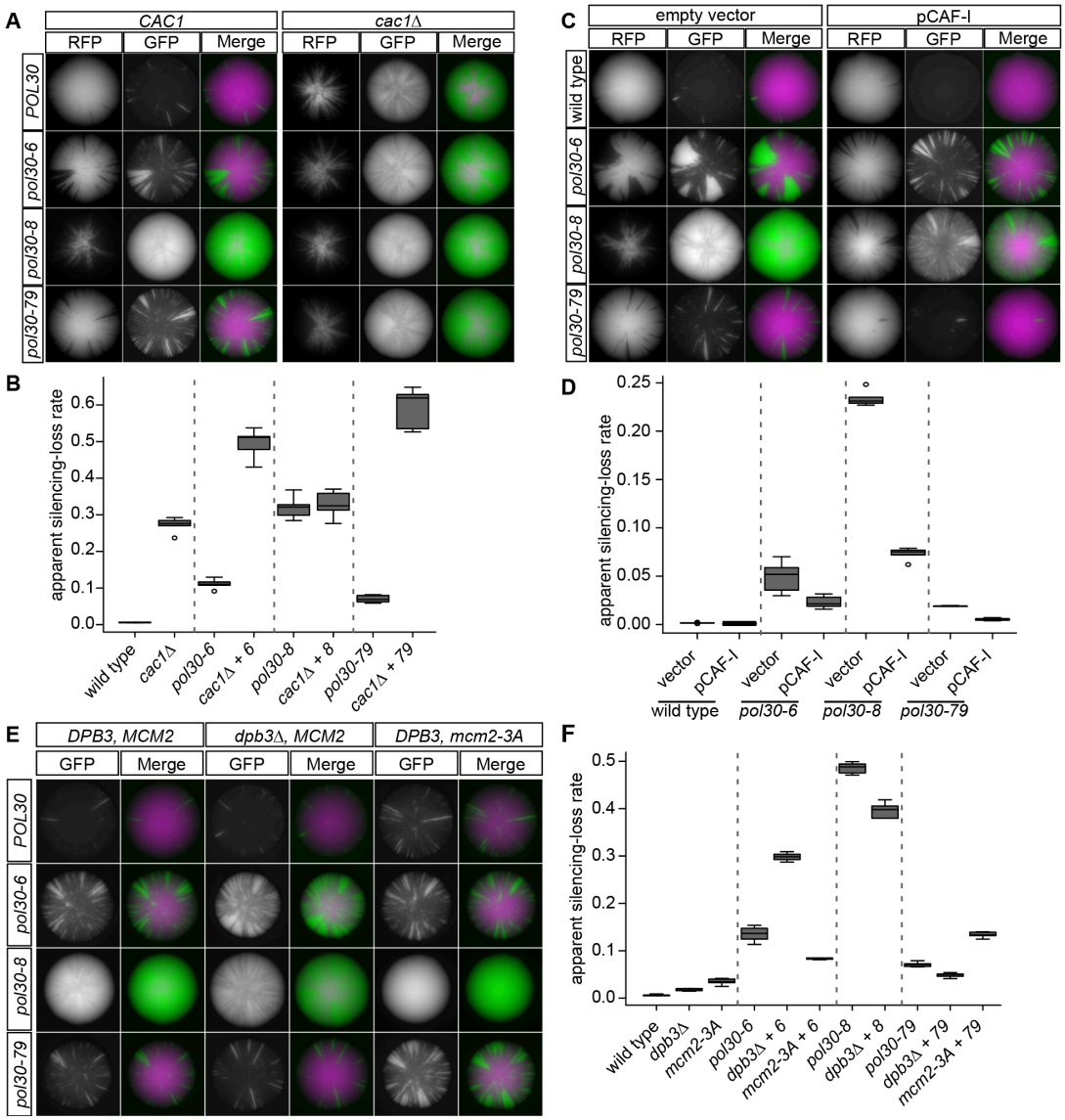

Figure 3.6. Coordination of histone chaperones by PCNA was required for transcriptional silencing.
A) Double-mutant analysis of *POL30* alleles with *cac1*Δ. Representative images of CRASH colonies. The left panel shows colonies with each of the *POL30* alleles with wild-type *CAC1* strain: *POL30* (JRY10790), *pol30-6*

(continued on next page)

(JRY11137), *pol30-8* (JRY11188), and *pol30-79* (JRY11141). The right panel shows colonies with each of the *POL30* alleles in combination with deletion of *CAC1* (*cac1* Δ): *POL30 cac1*Δ (JRY11193), *pol30-6 cac1*Δ (JRY11192), *pol30-8 cac1*Δ (JRY11189), and *pol30-79 cac1*Δ (JRY11163). **B)** The apparent silencing-loss rates for each of the strains in A were quantified by flow cytometry as described in Figure 3.1C. **C)** Overexpression of the CAF-1 complex in combination with *POL30* alleles. Representative images of CRASH colonies. The left panel shows colonies with each of the *POL30* alleles in combination with a 2μ vector (pRS425): *POL30* (JRY11175), *pol30-6* (JRY11176), *pol30-8* (JRY11177), and *pol30-79* (JRY11178). The right panel shows colonies with each of the *POL30* alleles in combination with a 2μ plasmid expressing all three subunits of the CAF-1 complex, *CAC1*, *CAC2*, and *CAC3* (pJR3418): *POL30* pCAF-1 (JRY11165), *pol30-6* pCAF-1 (JRY11166), *pol30-8* pCAF-1 (JRY11167), and *pol30-79* pCAF-1 (JRY11168). **D)** The apparent silencing-loss rates for each of the strains in C were quantified by flow cytometry as described in Figure 3.1C. **E)** Double-mutant analysis of *POL30* alleles with *dpb3*Δ and *mcm2-3A* alleles. Representative images of CRASH colonies. In the left panel are each of the *POL30* alleles in a wild-type strain: *POL30* (JRY10790), *pol30-6* (JRY11137), *pol30-8* (JRY11188), and *pol30-79* (JRY11141). In the middle panel are each of the *POL30* alleles in combination with deletion of *DPB3* (*dpb3*Δ): *POL30 dpb3*Δ (JRY11760), *pol30-6 dpb3*Δ (JRY11806), *pol30-8 dpb3*Δ (JRY11808), and *pol30-79 dpb3*Δ (JRY11810). In the right panel are each of the *POL30* alleles in combination with the *mcm2-3A allele*: *POL30 mcm2-3A* (JRY11812), *pol30-6 mcm2-3A* (JRY11987), *pol30-8 mcm2-3A* (JRY11989), and *pol30-79 mcm2-3A* (JRY11991). **F)** The apparent silencing-loss rates for each of the strains in E were quantified by flow cytometry as described in Figure 3.1C. The silencing-loss rate for *pol30-8 mcm2-3A* double mutant could not be quantified because it uniformly expressed GFP.

To further test each allele's dependence on CAF-I for their silencing phenotype, we overexpressed the three subunits of CAF-I, *CAC1, CAC2,* and *CAC3*, from a 2μ plasmid (pCAF-I, pJR3418, Janke *et al.* 2018). If overexpression of CAF-I could suppress or rescue the phenotype of a *pol30* mutant, it would be strong evidence that the *pol30* mutant weakened silencing through reduced CAF-I activity. Compared to an empty vector control, overexpression of CAF-I strongly suppressed the phenotype of *pol30-8* (Figure 3.6C, 3.6D), in agreement with the conclusion from the double-mutant analysis between *pol30-8* and *cac1*Δ (Figure 3.6A, 3.6B). In contrast, overexpression of CAF-I in strains harboring *pol30-6* and *pol30-79* had no statistically significant effect on their silencing defects (Figure 3.6C, 3.6D).

Whereas CAF-I chaperones newly-synthesized histones, recent evidence implicates both Dpb3 and Mcm2 as having a role in chaperoning parental histones at the replication fork. Dpb3 and Dpb4 are part of DNA polymerase ε, the leading strand polymerase, and re-deposit parental (old) histones onto the leading strand during DNA replication (He et al. 2017; Bellelli et al. 2018). Mcm2 is a subunit of the replicative helicase MCM2-7 and is responsible for re-deposition of parental histones onto the lagging strand during DNA replication (Petryk et al. 2018; Gan et al. 2018). Because *MCM2* is an essential gene in yeast, we used the *mcm2-3A* allele, which has a defect in its histone chaperone activity but not in its helicase activity (Foltman et al. 2013).

In the CRASH assay, *dpb3*Δ and *mcm2-3A* on their own had minor but statistically insignificant sectoring phenotypes (Figure 3.6E, 3.6F). Their combination with different *pol30* mutants showed an interesting pattern: If combination of an allele with *dpb3*Δ enhanced the sectoring phenotype, then combination with *mcm2-3A* weakened it, and vice versa (Figure 3.6F). Except for the *pol30-6 dpb3*Δ combination, the differences in phenotype between the single and double mutants are modest, suggesting that these effects might be indirect.

3.4 Discussion

3.4.1 The *pol30-8* allele did not cause epigenetically bi-stable states as was previously reported

Previous studies of transcriptional silencing in strains carrying *pol30-8* used the *ADE2* gene within the *HMR* locus as a reporter of gene silencing. When transcriptional silencing is disrupted, cells expressed *ADE2* and are white instead of red. *pol30-8* colonies have red sectors and white sectors, previously thought to represent two stable populations of cells: silencing *ADE2* or expressing *ADE2*. Surprisingly, even though *pol30-8* had highly unstable silencing in the CRASH assay, we found no evidence of bi-stable populations in strains carrying the *pol30-8* allele. The CRASH assay relies on alleles of *HML* and *HMR* that more closely resemble the native structure of those loci; it uses the native α*2* promoter and leaves the 5' and 3' UTRs and the *α1* gene intact (Dodson and Rine 2015), none of which is true for the previously used *HMR::ADE2* reporter. Moreover, the α-factor halo assay failed to reveal any clonally stable populations of cells expressing *HML* in any of the *pol30* mutants, nor did the *HMLα2::RFP, HMRα2::GFP* reporter. Therefore, the *ADE2* sectors were likely an artifact of the metabolically responsive *ADE2* reporter in this context (Rossmann et al. 2011), as we found no evidence of bi-stability among *pol30* mutants by two independent and metabolically neutral assays.

3.4.2 Defective assembly versus maintenance of silenced chromatin *POL30* mutants

Although the expression of PCNA is highest in S phase and its major role in the cell occurs at replication forks, it is still present at lower levels in all stages of the cell cycle, functioning in DNA damage signaling and repair (Bauer and Burgers 1990). By monitoring loss-of-silencing events in unsynchronized cycling cells and cells arrested in G1 over time, we found that all three of the *pol30* mutants increased loss of silencing rates compared to wild type *POL30* only in cycling cells.

As the replication fork progresses, nucleosomes in front of the fork are disassembled and reassembled onto daughter strands and newly-synthesized nucleosomes are also deposited onto daughter strands. Sir proteins must reassemble on nucleosomes to re-set the heterochromatin state. Heterochromatin is then maintained through G2, M, and G1 until it is assembled again in the next round of replication. Since *pol30-6*, *pol30-8*, and *pol30-79* only caused loss of silencing in actively cycling cells, the predominant role of PCNA in silencing stability is most likely through heterochromatin assembly during S phase.

3.4.3 Histone chaperones ensure the stability of heterochromatin through DNA replication

Previous results and supporting results in the CRASH assay shown here suggest that the unstable silencing caused by *pol30-8* is due to a defect in new histone deposition by the replication-coupled histone chaperone complex CAF-I (Zhang et al. 2000). Genetic evidence also suggests an interaction between two other histone chaperones, Hir1 and Asf1, and the *pol30-6* and *pol30-79* alleles (Sharp et al. 2001). If the *pol30* mutants caused slower or defective histone deposition during DNA replication, with fewer nucleosomes to bind, the SIR complex would be less able to properly block transcription at *HML* and *HMR* until the chromatin state was restored.

We explored the possibility that the *pol30* mutants might affect histone recycling from the mother DNA duplex to daughter strands chromatids by performing double-mutant analysis with *dpb3*Δ and *mcm2-3A*. The effects on CRASH sectoring phenotypes were minor but displayed an intriguing pattern: *mcm2-3A* and *dpb3*Δ had opposite effects for each given *pol30*

mutant. These results could be interpreted as a leading strand or lagging strand bias for each allele. Biochemical studies of *pol30-79* show that it has a defect in binding to DNA polymerase δ (DNA Pol δ), the lagging-strand polymerase, but not DNA polymerase ε (DNA Pol ε), the leading-strand polymerase (Eissenberg et al. 1997). In contrast to *pol30-79, pol30-6* is completely unable to bind DNA Pol ε, with only reduced binding to DNA Pol δ (Ayyagari et al. 1995). Its CRASH phenotype in combination with *mcm2-3A* and *dpb3*Δ also mirror *pol30-79* analyses. Binding studies between the DNA polymerases and *pol30-8* have not been done, but the phenotype of the double-mutant analyses, interpreted in the light of a strand-bias model, suggested that *pol30-8* may exhibit weakened binding to DNA Pol δ but not Pol ε.

3.4.4 A surprising effect of ploidy on silencing instability

Complementation tests revealed that any combination of *pol30-6, pol30-8*, or *pol30-79* in diploids complemented, resulting in colonies with fewer sectors in the CRASH assay than the haploids with each allele alone. These results suggested that *POL30* contributed at least two, and maybe three, separable roles in the assembly of stable silent chromatin. However, we also found that diploids carrying homozygous copies of *pol30-6* or *pol30-79* displayed no CRASH phenotype, and diploids homozygous for *pol30-8* had fewer sectors than a *pol30-8* haploid. Diploids homozygous for *POL30* alleles and expressing only *MATα* mating type information all displayed the same suppression, establishing that the phenotype was not an unexpected manifestation of mating-type regulation. Likewise, hemizygosity of each allele in diploids failed to restore their CRASH sectoring phenotype back to haploids levels. Thus ploidy, independently of mating type and dosage of PCNA, changed the sensitivity of diploid cells to defects in histone deposition caused by the *pol30* mutant. To our knowledge, this wrinkle is unique among complementation tests, though we caution that most complementation tests are inadequately powered to detect the impact of ploidy. We note that none of the genes studied here are among the set shown to have ploidy-dependent impacts on their expression (Storchová et al. 2006).

HML and *HMR* cluster at the nuclear periphery with a higher local concentration of Sir proteins in the cluster than in the rest of the nucleoplasm (Gotta et al. 1996; Bystricky et al. 2009; Miele et al. 2009; Kirkland and Kamakaka 2013). The two copies of *HML* and *HMR* and the *SIR* genes in diploids might increase the local concentration of Sir proteins, despite the larger volume associated with increases in ploidy, enough that it could overcome a brief disruption in histone deposition during DNA replication in *pol30* mutants. Even though tethering to the nuclear periphery is not required for silencing in an otherwise wild-type strain (Gartenberg et al. 2004), the *pol30* mutants might create a sensitized background that is more dependent on clustering of the SIR complex with *HML* and *HMR* for maintenance of silencing through replication.

3.4.5 A note on PCNA expression in hemizygotes

Compared to expression in homozygotes, the expression of PCNA in *pol30-6* and *pol30-79* strains did not decrease by half, whereas PCNA levels in *POL30* and *pol30-8* strains did. The expression of *POL30* is cell-cycle regulated (Bauer and Burgers 1990) and increases in response to DNA damage (Jelinsky and Samson 1999; Lee et al. 2007a). Differences in cell-cycle distribution or levels of DNA damage in *pol30-6* and *pol30-79* hemizygotes compared to

homozygotes would be compatible explanations for observations on PCNA levels produced by the various alleles.

3.4.6 High levels of DNA damage and defective repair in *pol30-6* and *pol30-79*

The high rates of mitotic recombination and gene conversion we observed in *pol30-6* and *pol30-79* diploids presumably reflected higher levels of DNA damage in these mutants. Work from multiple labs shows that all three alleles, and especially *pol30-6* and *pol30-79,* are more sensitive to DNA damaging agents (Ayyagari et al. 1995; Eissenberg et al. 1997; Zhang et al. 2000; Miller et al. 2008). Additionally, *pol30-79* causes higher rates of substitutions and small insertions and deletions compared to wild-type cells (Eissenberg et al. 1997).

The published studies were done using haploid cells, where mitotic recombination is seldom detected. *MATa / MATα* diploids avoid non-homologous end-joining because the a1-α2 transcription factor represses required genes *NEJ1* and *LIF1* (Åström and Rine 1999; Lee et al. 1999; Frank-Vaillant and Marcand 2001; Kegel et al. 2001; Valencia et al. 2001). Deleting *MATa* in the *pol30-6* and *pol30-79* homozygous diploids suppressed the increase in mitotic recombination, suggesting that the higher rates of mitotic recombination and gene conversion might be caused by homology-directed repair in lieu of non-homologous end-joining. We observed synthetic lethality in the haploid double mutants *pol30-6 rad54*Δ*, pol30-79 rad54*Δ*,* and *pol30-6 rad9*Δ and synthetic growth defects in the double mutants *pol30-79 rad9*Δ*, pol30-6 H3K56R,* and *pol30-79 H3K56R* (data not shown). These synthetic phenotypes fit with a higher DNA damage load in strains carrying *pol30-6* and *pol30-79*. Our work in diploids provided more evidence that the *pol30-6* and *pol30-79* alleles have DNA damage and repair defects. It is unlikely that the mitotic recombination and silencing phenotypes of the *pol30-6* and *pol30-8* alleles are directly related since one phenotype was dependent on mating type (mitotic recombination) and the other was not (silencing).

The mutants *pol30-6* and *pol30-79* alleles reduce global levels of histone H3 lysine 56 (H3K56) acetylation (Recht et al. 2006; Miller et al. 2008), a histone modification that increases the affinity of CAF-I for H3/H4 dimers (Masumoto et al. 2005; Recht et al. 2006; Li et al. 2008). Misregulation of H3K56 acetylation, both hypoacetylation and hyperacetylation, is associated with increased DNA damage and sensitivity to DNA-damaging agents (Hyland et al. 2005; Masumoto et al. 2005; Recht et al. 2006; Clemente-Ruiz et al. 2011; Wurtele et al. 2012). Additionally, Many DNA repair factors contain PCNA-Interacting Protein (PIP) or PIP-like motifs (reviewed in Boehm and Washington 2016). The *pol30-6* and *pol30-79* mutations disrupt the cleft of PCNA that bind PIP motifs (Kondratick et al. 2018), which could prevent the recruitment of DNA repair factors to sites of DNA damage. These results could explain the high levels of DNA damage and mitotic recombination in *pol30-6* and *pol30-79*. Furthermore, the recessive nature of these alleles in all of our assays suggests that PCNA trimers containing both mutant and wild-type alleles are fully functional for DNA repair and transcriptional silencing.

3.5 Materials and Methods

Yeast Strains

All strains in this study were derived from W303 and are listed in Table S1. Plasmids used in this study are listed in Table 3.2. Gene deletions (except for *bar1*Δ) were created by one-step integration of PCR-amplified disruption cassettes (Goldstein and McCusker 1999; Gueldener et

al. 2002), using primers listed in Table 3.3. The *pol30-8* (R61A, D63A) allele, *mcm2-3A* (Y79A, Y82A, Y91A) allele, and *bar1*Δ were introduced using Cas9 technology. Guide RNAs targeting *POL30*, *MCM2,* and *BAR1* are listed in Table 3.3. The sgRNA dropout-Cas9 expression plasmid (pJR3428) was assembled using a toolkit from (Lee et al. 2015). The gRNA target and non-target strands were integrated into pJR3428 by Golden Gate cloning using the restriction enzyme *Bsm*BI as described in Lee *et al.* 2015. The repair templates were made by annealing oligos in Table 3.3 and extending the 3' ends using Phusion Polymerase (New England Biolabs).

Creation of pol30-6 and pol30-79 by URA3 swap
The *pol30-6* (D41A, D42A) and *pol30-79* (L126A, I128A) alleles were created by integration of two overlapping gene blocks (gBlocks, Integrated DNA Technologies) at the *POL30* locus. Two gene blocks were used because the full sequence needed was too long to synthesize. One block contained the *pol30-6* or *pol30-79* allele followed by the first two-thirds of the *Candida albicans URA3* gene and the other contained the second two-thirds of the *Candida albicans URA3* gene followed by the *pol30-6* or *pol30-79* allele. The sequence of gene blocks is in Table 3.3. Selection for pop-out of the *URA3* gene was performed using the drug 5-fluoroorotic acid. Confirmation of the *pol30-6* and *pol30-8* allele was performed by PCR-amplification of the entire *POL30* locus followed by Sanger sequencing.

Creation of POL30 hemizygotes
Hemizygotes were created by mating between *MATα* strains containing *POL30* (JRY11131), *pol30-6* (JRY11133), *pol30-8* (JRY11135), or *pol30-79* (JRY11137) with a *MATa* strain with a deletion of *POL30* (*pol30*Δ) complemented by a plasmid carrying *POL30* with a *TRP1* marker (ZGY5-0, Zhang *et al.* 2000). The resulting diploids were streaked out for single colonies twice and checked for tryptophan auxotrophy, indicating they had lost the *POL30* plasmid. Hemizygosity for *POL30* was further confirmed by sporulation and tetrad analysis. Each strain resulted in at least 50% spore inviability (*POL30* is an essential gene) and no spores grew on CSM – Trp plates, indicating they did not carry the *POL30, TRP1* plasmid.

Creation of tetraploid
The tetraploid *POL30 / pol30*Δ */ pol30*Δ */ pol30*Δ strain (JRY12026) was created in multiple steps. First, a *POL30* hemizygous diploid carrying a *POL30, TRP1* plasmid was screened for spontaneous *MATa/MATa* diploids by ability to mate with a haploid *MATα* mating tester. The resulting *MATa/MATa* diploid was confirmed by sporulation in the presence of nicotinamide and tetrad analysis; all spores mated only with a *MATα* mating tester. The remaining chromosomal copy of *POL30* in this strain was deleted and replaced with a *Kluyveromyces lactis LEU2* gene, leaving a *MATa/MATa* diploid with the only *POL30* gene present on a plasmid. This *MATa/MATa; pol30*Δ*/pol30*Δ diploid was mated with a *MATα/MATα POL30/pol30*Δ hemizygous diploid (screened in the same manner as above for spontaneous *MATα/MATα* diploids). The resulting tetraploid was streaked out for single colonies twice and checked for tryptophan auxotrophy, indicating they had lost the *POL30* plasmid. The final strain, JRY12026, was confirmed by sporulation and tetrad dissection.

Colony Growth and Imaging
Strains were patched onto YPD and grown overnight. CRASH strains were first patched onto selective medium plates to select for cells expressing *hphMX*, and thus had not lost silencing and

excised the RFP-hphMX cassette (Figure 3.1A): YPD containing 200µg/mL G418 (Geneticin; Life Technologies) for strains carrying the kanMX cassette or YPD containing 300µg/mL Hygromycin B (MilliporeSigma) for strains carrying the hphMX cassette. Cells were then resuspended in water and plated onto Complete Supplement Mixture (CSM) or CSM –Trp (Sunrise Science Products), 1.5% agar, at a density of ~30 cells per plate. Colonies were imaged after 5-6 days of growth at 30°C. At least 10 colonies per genotype were imaged using a Leica M205FA fluorescence stereomicroscope, a Leica DFC3000G CCD camera, and a PlanApo 0.63X Objective. Image analysis and assembly was performed using ImageJ software (Fiji, (Schindelin et al. 2012).

Quantification of Silencing Loss by Flow Cytometry

For each strain, 3-5 single colonies were inoculated in 1mL in selective media to select for cells that had not lost silencing. These 1mL cultures were grown in deep 96-well plates (VWR) at 30°C overnight to saturation. Overnight cultures were diluted into 1mL of fresh, non-selective YPD to ~10^5 cells/mL in a deep 96-well plate and grown for 5-6 hours before flow cytometry. For each culture, a minimum of 15,000 events were collected using a BD High-Throughput Sampler on a BD LSR Fortessa X20 Cell Analyzer. Gating and quantification were performed as previously described (Janke et al. 2018).

α-factor Halo Assay

MATa strains were scraped from a YPD plate with a toothpick, resuspended in water, and ~150,000 cells were freshly spread onto Complete Supplement Mixture plates (CSM, Sunrise Science Products). Hole-punched Whatman filter papers were soaked for ~5 sec in 200µg/uL α-factor in 100mM sodium acetate and then placed onto the plates. Three soaked filter-paper circles were placed on each plate. Plates were incubated at 30°C for 36-48 hours before imaging.

RNA preparation for quantitative qPCR

Cells were grown to mid-log phase in YPD and RNA was extracted using hot acidic phenol and chloroform (Collart and Oliviero 2001). Samples were treated with DNase I (New England Biolabs) and subsequently purified using the Qiagen RNeasy Mini Kit. Complementary DNA (cDNA) was synthesized using the SuperScript III First-Strand Synthesis System (Invitrogen) and oligo(dT) primers. Quantitative PCR of cDNA was performed using the DyNAmo HS SYBR Green kit (Thermo Fisher Scientific) on an Mx3000P machine (Stratagene) using the primers listed in Table 3.3. Standard curves were generated using the *sir3*Δ *mat*Δ *hmr*Δ (JRY9624) or *sir4*Δ strain (JRY12714).

Live-cell Imaging

All single-cell microscopy images were collected on a Zeiss Axio Observer Z1 inverted microscope equipped with a Plan-Apochromat 63x oil-immersion objective (Zeiss) and the Definite Focus System for maintenance of focus over time. yEGFP was excited with the 420-500nm spectrum range at 20% intensity, and yEmRFP was excited with the 500-755nm spectrum range at 20% intensity from a CoolLED pE-300 ultra and collected with the Multiband Semrock Filter (LF405/488/594-A-ZHE). Images were acquired with a Teledyne Photometrics Prime 95B sCMOS camera. For time-lapse experiments, images were collected every 5 or 7 minutes, using an exposure time of 20msec for brightfield, 50msec for yEGFP, and 200msec for yEmRFP. At each time point, multiple stage positions were collected using an ASI MS-2000 XYZ piezo stage.

The microscope, camera, and stage were controlled with the Micro-manager software (Edelstein et al. 2014). Image analysis and assembly was performed using Fiji software (Schindelin et al. 2012).

For the CRASH time course setup, each strain was inoculated in 5mL of selective media to select for cells that had not lost silencing. Cultures were grown to saturation overnight at 30°C. Overnight cultures were diluted back to 10^6 cells/mL in 10mL of YPD containing G418 or Hygromycin B and grown to early-log phase (~ 4 x 10^6 cells/mL). The culture was then split into 5mL of YPD containing G418 or Hygromycin B and 40nM α-factor in 100mM sodium acetate, and 5mL of YPD containing G418 or Hygromycin B. The cultures were grown for another 90 minutes (~1 doubling). The cells were then harvested and resuspended in water. The resuspended cells were diluted to ~2 x 10^7 cells/mL, and 5uL were pipetted onto a 1cm x 1cm square of CSM – Trp + 2% agar with or without 40nM α-factor in 100mM sodium acetate. Both agar pads were placed into a 27mm glass dish (Thermo Scientific) and mounted in a Pecon Incubator XL with Heating Unit XL S (Zeiss) controlled by TempModule S (Zeiss) and kept at 30°C for the duration of the experiment. To calculate the number of switches per 10,000 cells in the arrested condition, the number of cells that were RFP-expressing at time zero were counted. The total number of switches (RFP-to-GFP) were counted for all of those cells and divided by the total number of RFP-expressing cells at time zero. To calculate the number of switches per 10,000 divisions in the cycling condition, the number of switches over the entire time course was divided by the calculated total number of divisions. The number of divisions was calculated using the following formula:

$$D = n_0 * 2^{tf} - n_0$$

value t: total number of minutes in the time course (480 minutes for an 8hr time course)
value f: division rate (per minute). To determine this value, the time from small bud to the next small bud for five cells at the beginning of the time course, five cells at the end of the time course in the center of a micro-colony, and five cells at the end of the time course at the edge of a micro-colony was averaged to get the time for one division.
value n_0: number of RFP-expressing cells at time 0

Protein Isolation and Immunoblotting

Each strain was inoculated in 5mL of YPD and grown overnight to saturation. Overnight cultures were diluted to ~2 x 10^5 cells/mL in fresh YPD and grown to mid-log phase, and ~10^8 cells were harvested and pelleted. Pellets were resuspended in 1mL of 5% trichloroacetic acid and incubated at 4°C for 90 minutes. The precipitates were pelleted, washed twice with 1mL of 100% acetone, and air-dried. Dried pellets were resuspended in 100uL of protein breakage buffer (50mM Tris-HCl pH 7.5, 1mM EDTA, 3mM DTT) and an equal volume of 0.5mm zirconium ceramic beads (BioSpec Products) followed by five cycles of vortexing, 1min bursts with 1min of incubation on ice between each cycle. 50µL of 3X SDS sample buffer (188mM Tris-HCl pH 6.8, 30% glycerol, 150mM DTT, 6% SDS, 0.03% bromophenol blue, 2% BME) was added to each sample and incubated at 95°C for 5min. Insoluble material was pelleted by centrifugation and an equal volume of the soluble fraction from each sample was run on an SDS-Polyacrylamide gel (Mini-PROTEAN TGX Any kD pre-cast gel, BioRad) and transferred to a nitrocellulose membrane using a TransBlot Turbo Transfer Pack (BioRad) on the Mixed MW

setting of a TransBlot Turbo machine (BioRad). The membrane was cut horizontally in half between the 50kD and 37kD markers and separated to blot for Hxk2 on the top half and PCNA on the bottom half. The membranes were blocked in Odyssey Blocking Buffer (LI-COR Biosciences), and the following primary antibodies and dilutions were used for detection: PCNA (Abcam ab221196, 1:1000), Hxk2 (Rockland #100-4159, 1:10,000). The secondary antibody used was IRDyeCW800 goat anti-rabbit (LI-COR Biosciences, 1:20,000), and the membrane was imaged on a Li-Cor Odyssey Imager. All washing steps were performed with Phosphate Buffered Saline + 0.1% Tween-20. Quantitative analysis was performed using Fiji software (Schindelin et al. 2012): The area under the intensity peak above background for each band was used for normalization to Hxk2 followed by comparison between lanes.

Tetrad Analysis

Diploid cells were sporulated on 1% potassium acetate, 2% agar, 0.25X CSM plates for 2-3 days at room temperature. Tetrads were dissected onto YPD plates using a micromanipulator and grown for 2 days before replica plating and scoring.

Patch Mating Assay

All strains were patched on YPD and grown at 30°C for 3 days. A small sample of yeast was scraped from the center of each patch and patched onto a fresh YPD plate and grown overnight at 30°C. The following day, the YPD plate was replica plated onto a YPD plate with a fresh lawn of *MATa* haploid testers and a YPD plate with a fresh lawn of *MATα* haploid testers. The replica plates were grown overnight and then replica plated onto minimal media plates the next day. Minimal media plates were grown for 2 days at 30°C and then imaged.

Data Availability

All data necessary for confirming the conclusions presented in the article are represented fully within the article. Supplemental material has been uploaded to the GSA figshare public repository. Table 3.1 contains details about the yeast strains used in this study. Table 3.2 contains the plasmids used in this study. Table 3.3 contains oligonucleotides used in this study.

Table 3.1. Strains used in this study.
All strains listed were derived from the W303 background. Unless otherwise noted, all strains are *can1-100, his3-11,15, leu2-3,112, lys2, ura3-1*. Genotypes with [ ] denote a strain that carries the plasmid designated within the brackets. *K.l.* stands for *Kluyveromyces lactis*. *"RFP-GFP(KanMX)"* refers to the cassette containing *GPDpro-loxP-yEmRFP-CYC1term-kanMX-loxP-yEGFP-ADH1term. "RFP-GFP(HphMX)"* refers to the cassette containing *GPDpro-loxP-yEmRFP-CYC1term-hphMX-loxP-yEGFP-ADH1term*.

Strain Number	***MAT***	**Genotype**
JRY4012	*a*	*trp1-1*
JRY4577	*a*	*trp1-1, sir4Δ::HIS3*
JRY9624	Δ	*trp1-1, matΔ::kanMX, hmrΔ::hygMX, sir3Δ::K.l.URA3*
JRY10710	*α*	*hmrα2Δ::cre, ura3Δ::RFP-GFP(KanMX)*
JRY10790	*a*	*hmrα2Δ::cre, ura3Δ::RFP-GFP(HphMX)*
JRY11129	*a*	*trp1-1, hmlα2Δ::yEmRFP, hmrα2Δ::yEGFP*
JRY11131	*a*	*trp1-1, sir4Δ::HIS3, hmlα2Δ::yEmRFP, hmrα2Δ::yEGFP*
JRY11132	*a*	*trp1-1, pol30-8, hmlα2Δ::yEmRFP, hmrα2Δ::yEGFP*
JRY11137	*a*	*hmlα2Δ::cre, ura3Δ::RFP-GFP(HphMX), pol30-6*
JRY11141	*a*	*hmlα2Δ::cre, ura3Δ::RFP-GFP(HphMX), pol30-79*
JRY11159	*a/α*	*TRP1/trp1-1, hmlα2Δ::cre/HML, ura3Δ::RFP-GFP(HphMX)/ura3-1*
JRY11160	*a/α*	*TRP1/trp1-1, hmlα2Δ::cre/HML, ura3Δ::RFP-GFP(HphMX)/ura3-1, POL30/pol30-6*
JRY11161	*a/α*	*TRP1/trp1-1, hmlα2Δ::cre/HML, ura3Δ::RFP-GFP(HphMX)/ura3-1, POL30/pol30-79*
JRY11163	*a*	*hmlα2Δ::cre, ura3Δ::RFP-GFP(HphMX), cac1Δ::K.l.URA3, pol30-79*
JRY11165	*a*	*hmlα2Δ::cre, ura3Δ::RFP-GFP(HphMX), [pJR3418]*
JRY11166	*a*	*hmlα2Δ::cre, ura3Δ::RFP-GFP(HphMX), pol30-6, [pJR3418]*
JRY11167	*a*	*hmlα2Δ::cre, ura3Δ::RFP-GFP(HphMX), pol30-8, [pJR3418]*
JRY11168	*a*	*hmlα2Δ::cre, ura3Δ::RFP-GFP(HphMX), pol30-79, [pJR3418]*
JRY11169	*a/α*	*TRP1/trp1-1, hmlα2Δ::cre/HML, ura3Δ::RFP-GFP(HphMX)/ura3-1, POL30/pol30-8*
JRY11175	*a*	*hmlα2Δ::cre, ura3Δ::RFP-GFP(HphMX), [pRS425]*
JRY11176	*a*	*hmlα2Δ::cre, ura3Δ::RFP-GFP(HphMX), pol30-6, [pRS425]*
JRY11177	*a*	*hmlα2Δ::cre, ura3Δ::RFP-GFP(HphMX), pol30-8, [pRS425]*
JRY11178	*a*	*hmlα2Δ::cre, ura3Δ::RFP-GFP(HphMX), pol30-79, [pRS425]*
JRY11186	*α*	*HMRα, hmrα2Δ::CRE, ura3Δ::RFP-GFP(KanMX), pol30-6*
JRY11187	*α*	*HMRα, hmrα2Δ::CRE, ura3Δ::RFP-GFP(KanMX), pol30-8*
JRY11188	*a*	*hmlα2Δ::cre, ura3Δ::RFP-GFP(HphMX), pol30-8*
JRY11189	*a*	*hmlα2Δ::cre, ura3Δ::RFP-GFP(HphMX), cac1Δ::K.l.URA3, pol30-8*
JRY11192	*a*	*hmlα2Δ::cre, ura3Δ::RFP-GFP(HphMX), cac1Δ::K.l.URA3, pol30-6*
JRY11193	*α*	*hmlα2Δ::cre, ura3Δ::RFP-GFP(HphMX), cac1Δ::K.l.URA3*
JRY11597	*a*	*hmlα2Δ::cre, ura3Δ::RFP-GFP(HphMX), bar1Δ*
JRY11599	*a*	*hmlα2Δ::cre, ura3Δ::RFP-GFP(HphMX), bar1Δ, pol30-79*
JRY11608	*α*	*HMRα, hmrα2Δ::CRE, ura3Δ::RFP-GFP(KanMX), pol30-79*
JRY11635	*a*	*hmlα2Δ::cre, ura3Δ::RFP-GFP(HphMX), bar1Δ, pol30-8*

JRY11645	*a*	*pol30-6*
JRY11647	*a*	*pol30-8*
JRY11649	*a*	*pol30-79*
JRY11656	*a/α*	*TRP1/trp1-1, hmlα2Δ::cre/HML, ura3Δ::RFP-GFP(HphMX)/ura3-1, pol30-6/pol30-8*
JRY11657	*a/α*	*TRP1/trp1-1, hmlα2Δ::cre/HML, ura3Δ::RFP-GFP(HphMX)/ura3-1, pol30-6/pol30-79*
JRY11658	*a/α*	*TRP1/trp1-1, hmlα2Δ::cre/HML, ura3Δ::RFP-GFP(HphMX)/ura3-1, pol30-79/pol30-8*
JRY11682	*a*	*hmlα2Δ::cre, ura3Δ::RFP-GFP(HphMX), bar1Δ, pol30-6*
JRY11685	*a/α*	*TRP1/trp1-1, hmlα2Δ::cre/HML, ura3Δ::RFP-GFP(KanMX)/ura3-1, pol30-6/pol30-79*
JRY11686	*a/α*	*TRP1/TRP1, hmlα2Δ::cre/HML, ura3Δ::RFP-GFP(KanMX)/ura3-1, pol30-6/pol30-6*
JRY11687	*a/α*	*TRP1/trp1-1, hmlα2Δ::cre/HML, ura3Δ::RFP-GFP(HphMX)/ura3-1, pol30-8/pol30-8*
JRY11688	*a/α*	*TRP1/trp1-1, hmlα2Δ::cre/HML, ura3Δ::RFP-GFP(HphMX)/ura3-1, pol30-79/pol30-79*
JRY11699	Δ	*trp1-1, matΔ::K.l.LEU2*
JRY11700	Δ	*matΔ::K.l.LEU2, pol30-6*
JRY11701	Δ	*trp1-1, matΔ::K.l.LEU2, pol30-8*
JRY11702	Δ	*trp1-1, matΔ::K.l.LEU2, pol30-79*
JRY11714	*a/α*	*TRP1/TRP1, hmlα2Δ::cre/HML, ura3Δ::RFP-GFP(KanMX)/ura3-1, pol30-6/pol30-6*
JRY11715	*a/α*	*hmlα2Δ::cre/HML, ura3Δ::RFP-GFP(HphMX)/ura3-1, pol30-6/pol30-6*
JRY11716	*a/α*	*TRP1/trp1-1, hmlα2Δ::cre/HML, ura3Δ::RFP-GFP(HphMX)/ura3-1, pol30-79/pol30-79*
JRY11717	*a/α*	*TRP1/trp1-1, hmlα2Δ::cre/HML, ura3Δ::RFP-GFP(HphMX)/ura3-1, pol30-79/pol30-79*
JRY11718	Δ/*α*	*TRP1/trp1-1, hmlα2Δ::cre/HML, ura3Δ::RFP-GFP(HphMX)/ura3-1, MATα/matΔ::K.l.LEU2*
JRY11719	Δ/*α*	*TRP1/trp1-1, hmlα2Δ::cre/HML, ura3Δ::RFP-GFP(HphMX)/ura3-1, MATα/matΔ::K.l.LEU2, pol30-6/pol30-6*
JRY11720	Δ/*α*	*TRP1/trp1-1, hmlα2Δ::cre/HML, ura3Δ::RFP-GFP(HphMX)/ura3-1, MATα/matΔ::K.l.LEU2, pol30-79/pol30-79*
JRY11744	Δ/*α*	*TRP1/trp1-1, hmlα2Δ::cre/HML, ura3Δ::RFP-GFP(HphMX)/ura3-1, MATα/matΔ::K.l.LEU2, pol30-8/pol30-8*
JRY11745	*a/α*	*trp1-1/trp1-1, ADE2/ade2-1, HMR/hmr::ADE2, hmlα2Δ::cre/HML, ura3Δ::RFP-GFP(HphMX)/ura3-1, POL30/pol30Δ*
JRY11746	*a/α*	*trp1-1/trp1-1, ADE2/ade2-1, HMR/hmr::ADE2, hmlα2Δ::cre/HML, ura3Δ::RFP-GFP(HphMX)/ura3-1, POL30/pol30Δ*
JRY11747	*a/α*	*trp1-1/trp1-1, ADE2/ade2-1, HMR/hmr::ADE2, hmlα2Δ::cre/HML, ura3Δ::RFP-GFP(HphMX)/ura3-1, pol30-6/pol30Δ*
JRY11748	*a/α*	*trp1-1/trp1-1, ADE2/ade2-1, HMR/hmr::ADE2, hmlα2Δ::cre/HML, ura3Δ::RFP-GFP(HphMX)/ura3-1, pol30-6/pol30Δ*
JRY11749	*a/α*	*trp1-1/trp1-1, ADE2/ade2-1, HMR/hmr::ADE2, hmlα2Δ::cre/HML, ura3Δ::RFP-GFP(HphMX)/ura3-1, pol30-8/pol30Δ*
JRY11750	*a/α*	*trp1-1/trp1-1, ADE2/ade2-1, HMR/hmr::ADE2, hmlα2Δ::cre/HML, ura3Δ::RFP-GFP(HphMX)/ura3-1, pol30-8/pol30Δ*
JRY11751	*a/α*	*trp1-1/trp1-1, ADE2/ade2-1, HMR/hmr::ADE2, hmlα2Δ::cre/HML, ura3Δ::RFP-GFP(HphMX)/ura3-1, pol30-79/pol30Δ*
JRY11752	*a/α*	*trp1-1/trp1-1, ADE2/ade2-1, HMR/hmr::ADE2, hmlα2Δ::cre/HML, ura3Δ::RFP-GFP(HphMX)/ura3-1, pol30-79/pol30Δ*
JRY11760	*a*	*hmlα2Δ::cre, ura3Δ::RFP-GFP(HphMX), dpb3Δ::hisMX*
JRY11806	*a*	*hmlα2Δ::cre, ura3Δ::RFP-GFP(HphMX), dpb3Δ::hisMX, pol30-6*
JRY11808	*a*	*hmlα2Δ::cre, ura3Δ::RFP-GFP(HphMX), dpb3Δ::hisMX, pol30-8*

JRY11810	*a*	*hmlα2Δ::cre, ura3Δ::RFP-GFP(HphMX), dpb3Δ::hisMX, pol30-79*
JRY11812	*a*	*hmlα2Δ::cre, ura3Δ::RFP-GFP(HphMX), mcm2-3A*
JRY11822	*a/α*	*trp1-1/trp1-1, ADE2/ade2-1, HMR/hmr::ADE2, hmlα2Δ::cre/HML, ura3Δ::RFP-GFP(HphMX)/ura3-1, pol30-6/pol30Δ*
JRY11823	*a/α*	*trp1-1/trp1-1, ADE2/ade2-1, HMR/hmr::ADE2, hmlα2Δ::cre/HML, ura3Δ::RFP-GFP(HphMX)/ura3-1, pol30-79/pol30Δ*
JRY11987	*a*	*hmlα2Δ::cre, ura3Δ::RFP-GFP(HphMX), mcm2-3A, pol30-6*
JRY11989	*a*	*hmlα2Δ::cre, ura3Δ::RFP-GFP(HphMX), mcm2-3A, pol30-8*
JRY11991	*a*	*hmlα2Δ::cre, ura3Δ::RFP-GFP(HphMX), mcm2-3A, pol30-79*
JRY12174	*α*	*trp1-1, sir4Δ::TRP1*
JRY12026	*a/a/α/α*	*trp1-1, ade2-1/ADE2/ade2-1/ADE2, LYS2/lys2/LYS2/lys2, hmr::ADE2/HMR/hmr::ADE2/HMR, HML/hmlα2Δ::cre/HML/hmlα2Δ::cre, ura3-1/ura3Δ::RFP-GFP(HphMX)/ura3-1/ura3Δ::RFP-GFP(HphMX), POL30/pol30Δ/pol30Δ/pol30Δ::K.l.LEU2*

Table 3.2 Plasmids used in this study

Plasmid	Description	Published Source
pBL230-0	*POL30, TRP1, ampR, CEN/ARS*	(Ayyagari et al. 1995)
pJR3418	*CAC1, CAC2, CAC3, LEU2, ampR, 2μ*	(Janke et al. 2018)
pJR3428	*cas9, URA3, ARS4, KanR*	This study, (Lee et al. 2015)
pRS425	*LEU2, ampR, 2μ*	(Sikorski and Hieter 1989)

Table 3.3 Oligonucleotides used in this study

Name	Sequence (5'-3')
Oligonucleotides used for cassette knockouts	
pol30Δ::K.l.LEU2 fwd	CTTCAATATCTAATTATTTAGCATTTTTCTTCTCCATCCGgctgtgaagatcccagcaaa
pol30Δ::K.l.LEU2 rev	TTGGAAACAAAGCAATATTCCATTTGGAAGGGTTCATAGCaaccggaacctgtattattt
matΔ::K.l.LEU2 fwd	CTCACTATCTTGCCAATAAGACTCTACCCAGATTTGTATTgctgtgaagatcccagcaaa
matΔ::K.l.LEU2 rev	GGTTAAGATAAGAACAAAGAATGATGCTAAGAATTGATTGaaccggaacctgtattattt
dpb3Δ::hisMX fwd	TGATAAAAACAAGCAAGGGTCAACCGTGTTGCAAAAAAAgacatggaggcccagaatacc
dpb3Δ::hisMX rev	CATCGAATAGTAATTACATAGCAATAATAGCAATAACAcagtatagcgaccagcattcac
cac1Δ::K.l.URA3 fwd	TGAACCTCAAGACAGAAGAGAATCGAAAGGAAAAGGGAAAcccaatacaacagatcacgt
cac1Δ::K.l.URA3 rev	GTTTATCTGTATGTTTCTATATACTAAAGATCCGTTCAAGctgggtagaagatcggtctg
guide RNA sequences used for CRISPR-Cas9 editing	
POL30 top	gactttCCATACCTAACGTAACAGGA
POL30 bottom	aaacTCCTGTTACGTTAGGTATGGaa
MCM2 top	gactttTAATATGTATGACGATTATG
MCM2 bottom	aaacCATAATCGTCATACATATTAaa
BAR1 top	gactttAAATAAAAAGAGTGTCTAGA
BAR1 bottom	aaacTCTAGACACTCTTTTTATTTaa

CRISPR repair templates	
pol30-8 top	TCTATTGGTCTCCTTGGAAATAGGTGTCGAAGCCTTCCAAGAATATGCTTGTGCTCATCC
pol30-8 bottom	ATTTTACTTAGTGAGGTTAGATCCATACCTAACGTAACAGGATGAGCACAAGCATATTCT
mcm2-3A top	AACGAAGTAGATTTGATGGACGATAATATGGCTGACGATGCAGCAGCTGATCATAATAGA
mcm2-3A bottom	TTGTTCCCTGTCGTCAACTTGATCTGGATCAGCTCTATCTCTATTATGATCAGCTGCTGC
*bar1*Δ top	CGTGATTTAATTCTAGTGGTTCGTATCGCCTAAAATCATAGAAATCTGGA
*bar1*Δ bottom	TGATATTTATATGCTATAAAAAAATTGTACTCCAGATTTCTATGATTTTA
primers used for quantitative PCR	
ACT1 fwd	TTTTGTCCTTGTACTCTTCCGGTAGAAC
ACT1 rev	CCAAATCGATTCTCAAAATGGCGTGAG
POL30 fwd	GATCAACCTGTCGACTTGAC
POL30 rev	GGAATAAAGCAGGAGCTTCG
HMLα1 fwd	TCACAGGATAGCGTCTGGAA
HMLα1 rev	TCAGCGAGCAGAGAAGACAA
HMLα2 fwd	TCCACAAATCACAGATGAGT
HMLα2 rev	GTTGGCCCTAGATAAGAATCC
HMRa1 fwd	GGCGGAAAACATAAACAGAAC
HMRa1 rev	GGGTGATATTGATGATTTTCCC
gene blocks for *pol30-6* and *pol30-79* URA3 swap	

pol30-6 5'	GCGAAACGCGTAACTTTTTTTTTTTGGATTTCAACTGATAGTTTTCGTACTTT GCTTCCTCTGGTACATAAAATTATATATAAGAAACACTTTTGCTTTAGCCTT CCTTTCTTTCCACTTGCACCTTTCACTTTCGCCGTCCTTTTTCACTCACAGCA ACAAGCAGCAAGCACTAAGTACGCAGTCAAAAGAGAGAAAAAATGTTAGA AGCAAAATTTGAAGAAGCATCCCTTTTCAAGAGAATAATTGATGGTTTCAA AGATTGTGTCCAGTTGGTCAATTTCCAATGTAAAGAAGATGGTATCATTGCA CAAGCTGTCGCTGCTTCAAGAGTTCTATTGGTCTCCTTGGAAATAGGTGTCG AAGCCTTCCAAGAATATAGATGTGACCATCCTGTTACGTTAGGTATGGATCT AACCTCACTAAGTAAAATCCTACGTTGTGGTAACAACACCGATACATTAAC ACTAATTGCTGACAACACACCGGATTCCATCATCTTATTATTTGAGGATACC AAGAAAGACCGTATAGCCGAATACTCTCTGAAATTGATGGATATCGATGCT GATTTCTTAAAGATTGAAGAATTACAGTACGACTCCACCCTGTCATTGCCAT CTTCCGAATTCTCTAAAATTGTTCGTGACTTGTCCCAATTGAGTGATTCTATT AATATCATGATCACCAAAGAAACAATAAAGTTTGTAGCTGACGGTGATATC GGATCAGGTTCAGTCATAATAAAACCATTCGTGGATATGGAACATCCTGAA ACAAGCATCAAACTTGAAATGGATCAACCTGTCGACTTGACGTTCGGAGCT AAATATTTATTGGACATCATTAAGGGCTCCTCCCTTTCTGATAGAGTTGGTA TCAGGCTCTCCAGCGAAGCTCCTGCTTTATTCCAATTTGATTTGAAGAGTGG GTTCCTACAGTTTTTCTTGGCTCCTAAATTTAATGACGAAGAATAAGACATG GAGGCCCAGAATACCCTCCTTGACAGTCTTGACGTGCGCAGCTCAGGGGCA TGATGTGACTGTCGCCCGTACATTTAGCCCATACATCCCCATGTATAATCAT TTGCATCCATACATTTTGATGGCCGCACGGCGCGAAGCAAAAATTACGGCT CCTCGCTGCAGACCTGCGAGCAGGGAAACGCTCCCCTCACAGACGCGTTGA ATTGTCCCCACGCCGCGCCCCTGTAGAGAAATATAAAAGGTTAGGATTTGC CACTGAGGTTCTTCTTTCATATACTTCCTTTTAAAATCTTGCTAGGATACAGT TCTCACATCACATCCGAACATAAACAACCATGACAGTCAACACTAAGACCT ATAGTGAGAGAGCAGAAACTCATGCCTCACCAGTAGCACAGCGATTATTTC GATTAATGGAACTGAAGAAAACCAATTTATGTGCATCAATTGACGTTGATA CCACTAAGGAATTCCTTGAATTAATTGATAAATTAGGTCCTTATGTATGCTT AATCAAGACTCATATTGATATAATCAATGATTTTTCCTATGAATCCACTATT GAACCATTATTAGAACTTTCACGTAAACATCAATTTATGATTTTTGAAGATA GAAAATTTGCTGATATTGGTAATACCGTAAAGAAACAATATATTGGTGGAG TTTATAAAATTAGTAGTTGGGCAGATATTACCAATGCTCATGGTGTCACTGG GAATGGAGTGGTTGAAGGATTAAA

pol30-6 3'	TCAACACTAAGACCTATAGTGAGAGAGCAGAAACTCATGCCTCACCAGTAG CACAGCGATTATTTCGATTAATGGAACTGAAGAAAACCAATTTATGTGCAT CAATTGACGTTGATACCACTAAGGAATTCCTTGAATTAATTGATAAATTAGG TCCTTATGTATGCTTAATCAAGACTCATATTGATATAATCAATGATTTTTCCT ATGAATCCACTATTGAACCATTATTAGAACTTTCACGTAAACATCAATTTAT GATTTTTGAAGATAGAAAATTTGCTGATATTGGTAATACCGTAAAGAAACA ATATATTGGTGGAGTTTATAAAATTAGTAGTTGGGCAGATATTACCAATGCT CATGGTGTCACTGGGAATGGAGTGGTTGAAGGATTAAAACAGGGAGCTAAA GAAACCACCACCAACCAAGAGCCAAGAGGGTTATTGATGTTAGCTGAATTA TCATCAGTGGGATCATTAGCATATGGAGAATATTCTCAAAAAACTGTTGAA ATTGCTAAATCCGATAAGGAATTTGTTATTGGATTTATTGCCCAACGTGATA TGGGTGGCCAAGAAGAAGGATTTGATTGGCTTATTATGACACCTGGAGTTG GATTAGATGATAAAGGTGATGGATTAGGACAACAATATAGAACTGTTGATG AAGTTGTTAGCACTGGAACTGATATTATCATTGTTGGTAGAGGATTGTTTGG TAAAGGAAGAGATCCAGATATTGAAGGTAAAAGGTATAGAAATGCTGGTTG GAATGCTTATTTGAAAAAGACTGGCCAATTATAATCAGTACTGACAATAAA AAGATTCTTGTTTTCAAGAACTTGTCATTTGTATAGTTTTTTTATATTGTAGT TGTTCTATTTTAATCAAATGTTAGCGTGATTTATATTTTTTTTCGCCTCGACA TCATCTGCCCAGATGCGAAGTTAAGTGCGCAGAAAGTAATATCATGCGTCA ATCGTATGTGAATGCTGGTCGCTATACTGATGTTAGAAGCAAAATTTGAAG AAGCATCCCTTTTCAAGAGAATAATTGATGGTTTCAAAGATTGTGTCCAGTT GGTCAATTTCCAATGTAAAGAAGATGGTATCATTGCACAAGCTGTCGCTGCT TCAAGAGTTCTATTGGTCTCCTTGGAAATAGGTGTCGAAGCCTTCCAAGAAT ATAGATGTGACCATCCTGTTACGTTAGGTATGGATCTAACCTCACTAAGTAA AATCCTACGTTGTGGTAACAACACCGATACATTAACACTAATTGCTGACAA CACACCGGATTCCATCATCTTATTATTTGAGGATACCAAGAAAGACCGTATA GCCGAATACTCTCTGAAATTGATGGATATCGATGCTGATTTCTTAAAGATTG AAGAATTACAGTACGACTCCACCCTGTCATTGCCATCTTCCGAATTCTCTAA AATTGTTCGTGACTTGTCCCAATTGAGTGATTCTATTAATATCATGATCACC AAGGAGACAATAAAGTTTGTAGCTGACGGTGATATCG

pol30-79 5'	ATGTTAGAAGCAAAATTTGAAGAAGCATCCCTTTTCAAGAGAATAATTGAT GGTTTCAAAGATTGTGTCCAGTTGGTCAATTTCCAATGTAAAGAAGATGGTA TCATTGCACAAGCTGTCGATGACTCAAGAGTTCTATTGGTCTCCTTGGAAAT AGGTGTCGAAGCCTTCCAAGAATATAGATGTGACCATCCTGTTACGTTAGGT ATGGATCTAACCTCACTAAGTAAAATCCTACGTTGTGGTAACAACACCGAT ACATTAACACTAATTGCTGACAACACACCGGATTCCATCATCTTATTATTTG AGGATACCAAGAAAGACCGTATAGCCGAATACTCTCTGAAATTGATGGATA TCGATGCTGATTTCGCTAAGGCTGAAGAATTACAGTACGACTCCACCCTGTC ATTGCCATCTTCCGAATTCTCTAAAATTGTTCGTGACTTGTCCCAATTGAGT GATTCTATTAATATCATGATCACCAAAGAAACAATAAAGTTTGTAGCTGAC GGTGATATCGGATCAGGTTCAGTCATAATAAAACCATTCGTGGATATGGAA CATCCTGAAACAAGCATCAAACTTGAAATGGATCAACCTGTCGACTTGACG TTCGGAGCTAAATATTTATTGGACATCATTAAGGGCTCCTCCCTTTCTGATA GAGTTGGTATCAGGCTCTCCAGCGAAGCTCCTGCTTTATTCCAATTTGATTT GAAGAGTGGGTTCCTACAGTTTTTCTTGGCTCCTAAATTTAATGACGAAGAA TAAGACATGGAGGCCCAGAATACCCTCCTTGACAGTCTTGACGTGCGCAGC TCAGGGGCATGATGTGACTGTCGCCCGTACATTTAGCCCATACATCCCCATG TATAATCATTTGCATCCATACATTTTGATGGCCGCACGGCGCGAAGCAAAA ATTACGGCTCCTCGCTGCAGACCTGCGAGCAGGGAAACGCTCCCCTCACAG ACGCGTTGAATTGTCCCCACGCCGCGCCCCTGTAGAGAAATATAAAAGGTT AGGATTTGCCACTGAGGTTCTTCTTTCATATACTTCCTTTTAAAATCTTGCTA GGATACAGTTCTCACATCACATCCGAACATAAACAACCATGACAGTCAACA CTAAGACCTATAGTGAGAGAGCAGAAACTCATGCCTCACCAGTAGCACAGC GATTATTTCGATTAATGGAACTGAAGAAAACCAATTTATGTGCATCAATTGA CGTTGATACCACTAAGGAATTCCTTGAATTAATTGATAAATTAGGTCCTTAT GTATGCTTAATCAAGACTCATATTGATATAATCAATGATTTTTCCTATGAAT CCACTATTGAACCATTATTAGAACTTTCACGTAAACATCAATTTATGATTTT TGAAGATAGAAAATTTGCTGATATTGGTAATACCGTAAAGAAACAATATAT TGGTGGAGTTTATAAAATTAGTAGTTGGGCAGATATTACCAATGCTCATGGT GTCACTGGGAATGGAGTGGTTGAAGGATTAAAACAGGGAGCTAAAGAAAC CACCA

pol30-79 3'	AGAGCAGAAACTCATGCCTCACCAGTAGCACAGCGATTATTTCGATTAATG GAACTGAAGAAAACCAATTTATGTGCATCAATTGACGTTGATACCACTAAG GAATTCCTTGAATTAATTGATAAATTAGGTCCTTATGTATGCTTAATCAAGA CTCATATTGATATAATCAATGATTTTTCCTATGAATCCACTATTGAACCATT ATTAGAACTTTCACGTAAACATCAATTTATGATTTTTGAAGATAGAAAATTT GCTGATATTGGTAATACCGTAAAGAAACAATATATTGGTGGAGTTTATAAA ATTAGTAGTTGGGCAGATATTACCAATGCTCATGGTGTCACTGGGAATGGA GTGGTTGAAGGATTAAAACAGGGAGCTAAAGAAACCACCACCAACCAAGA GCCAAGAGGGTTATTGATGTTAGCTGAATTATCATCAGTGGGATCATTAGC ATATGGAGAATATTCTCAAAAAACTGTTGAAATTGCTAAATCCGATAAGGA ATTTGTTATTGGATTTATTGCCCAACGTGATATGGGTGGCCAAGAAGAAGG ATTTGATTGGCTTATTATGACACCTGGAGTTGGATTAGATGATAAAGGTGAT GGATTAGGACAACAATATAGAACTGTTGATGAAGTTGTTAGCACTGGAACT GATATTATCATTGTTGGTAGAGGATTGTTTGGTAAAGGAAGAGATCCAGAT ATTGAAGGTAAAAGGTATAGAAATGCTGGTTGGAATGCTTATTTGAAAAAG ACTGGCCAATTATAATCAGTACTGACAATAAAAAGATTCTTGTTTTCAAGAA CTTGTCATTTGTATAGTTTTTTTATATTGTAGTTGTTCTATTTTAATCAAATGT TAGCGTGATTTATATTTTTTTTCGCCTCGACATCATCTGCCCAGATGCGAAG TTAAGTGCGCAGAAAGTAATATCATGCGTCAATCGTATGTGAATGCTGGTC GCTATACTGATGTTAGAAGCAAAATTTGAAGAAGCATCCCTTTTCAAGAGA ATAATTGATGGTTTCAAAGATTGTGTCCAGTTGGTCAATTTCCAATGTAAAG AAGATGGTATCATTGCACAAGCTGTCGATGACTCAAGAGTTCTATTGGTCTC CTTGGAAATAGGTGTCGAAGCCTTCCAAGAATATAGATGTGACCATCCTGTT ACGTTAGGTATGGATCTAACCTCACTAAGTAAAATCCTACGTTGTGGTAACA ACACCGATACATTAACACTAATTGCTGACAACACACCGGATTCCATCATCTT ATTATTTGAGGATACCAAGAAAGACCGTATAGCCGAATACTCTCTGAAATT GATGGATATCGATGCTGATTTCGCTAAGGCTGAAGAATTACAGTACGACTC CACCCTGTCATTGCCATCTTCCGAATTCTCTAAAATTGTTCGTGACTTGTCCC AATTGAGTGATTCTATTAATATCATGATCACCAAAGAAACAATAAAGTTTGT AGCTGACGGTGATATCGGATCAGGTTCAGTCATAATAAAACCATTCGTGGA TATGGAACATCCTGAAACAAGCATCAAACTTGAAATGGATCAACCTGTCGA CTTGACGTTCGGAGCTAAATATTTATTGGACATCATTAAGGGCTCCTCCCTT TCTGATAGAGTTGGTATCAGGCTCTCCAGCGAAGCTCCTGCTTTATTCCAAT TTGATTTGAAGAGTGGGTTCCTACAGTTTTTCTTGGCTCCTAAATTTAATGA CGAAGAATAA

References

Abdulhay NJ, McNally CP, Hsieh LJ, Kasinathan S, Keith A, Estes LS, Karimzadeh M, Underwood JG, Goodarzi H, Narlikar GJ, et al. 2020. Massively multiplex single-molecule oligonucleosome footprinting. *Elife* **9**. http://dx.doi.org/10.7554/eLife.59404.

Abraham J, Nasmyth KA, Strathern JN, Klar AJS, Hicks HB. 1984. Regulation of mating-type information in yeast: Negative control requiring sequences both 5' and 3' to the regulated region. *J Mol Biol* **176**: 307–331.

Akoury E, Ma G, Demolin S, Brönner C, Zocco M, Cirilo A, Ivic N, Halic M. 2019. Disordered region of H3K9 methyltransferase Clr4 binds the nucleosome and contributes to its activity. *Nucleic Acids Res* **47**: 6726–6736. http://dx.doi.org/10.1093/nar/gkz480.

Alabert C, Jasencakova Z, Groth A. 2017. Chromatin Replication and Histone Dynamics. *Adv Exp Med Biol* **1042**: 311–333. http://dx.doi.org/10.1007/978-981-10-6955-0_15.

Albig C, Tikhonova E, Krause S, Maksimenko O, Regnard C, Becker PB. 2019. Factor cooperation for chromosome discrimination in Drosophila. *Nucleic Acids Res* **47**: 1706–1724. http://dx.doi.org/10.1093/nar/gky1238.

Albritton SE, Ercan S. 2018. Caenorhabditis elegans Dosage Compensation: Insights into Condensin-Mediated Gene Regulation. *Trends Genet* **34**: 41–53. http://dx.doi.org/10.1016/j.tig.2017.09.010.

Albritton SE, Kranz A-L, Winterkorn LH, Street LA, Ercan S. 2017. Cooperation between a hierarchical set of recruitment sites targets the X chromosome for dosage compensation. *Elife* **6**. http://dx.doi.org/10.7554/eLife.23645.

Alekseyenko AA, Larschan E, Lai WR, Park PJ, Kuroda MI. 2006. High-resolution ChIP-chip analysis reveals that the Drosophila MSL complex selectively identifies active genes on the male X chromosome. *Genes Dev* **20**: 848–857. http://dx.doi.org/10.1101/gad.1400206.

Alekseyenko AA, Peng S, Larschan E, Gorchakov AA, Lee O-K, Kharchenko P, McGrath SD, Wang CI, Mardis ER, Park PJ, et al. 2008. A sequence motif within chromatin entry sites directs MSL establishment on the Drosophila X chromosome. *Cell* **134**: 599–609. http://dx.doi.org/10.1016/j.cell.2008.06.033.

Allshire RC, Ekwall K. 2015. Epigenetic Regulation of Chromatin States in Schizosaccharomyces pombe. *Cold Spring Harb Perspect Biol* **7**: a018770. http://dx.doi.org/10.1101/cshperspect.a018770.

Al-Sady B, Madhani HD, Narlikar GJ. 2013. Division of labor between the chromodomains of HP1 and Suv39 methylase enables coordination of heterochromatin spread. *Mol Cell* **51**: 80–91. http://dx.doi.org/10.1016/j.molcel.2013.06.013.

Altaf M, Auger A, Covic M, Côté J. 2009. Connection between histone H2A variants and chromatin remodeling complexes. *Biochem Cell Biol* **87**: 35–50. http://dx.doi.org/10.1139/O08-140.

Altaf M, Utley RT, Lacoste N, Tan S, Briggs SD, Côté J. 2007. Interplay of chromatin modifiers on a short basic patch of histone H4 tail defines the boundary of telomeric heterochromatin. *Mol Cell* **28**: 1002–1014. http://dx.doi.org/10.1016/j.molcel.2007.12.002.

Altemose N, Maslan A, Smith OK, Sundararajan K, Brown RR, Detweiler AM, Neff N, Miga KH, Straight AF, Streets A. 2021. DiMeLo-seq: a long-read, single-molecule method for mapping protein-DNA interactions genome-wide. *bioRxiv* 2021.07.06.451383. https://www.biorxiv.org/content/10.1101/2021.07.06.451383v1.

Anderson EC, Frankino PA, Higuchi-Sanabria R, Yang Q, Bian Q, Podshivalova K, Shin A, Kenyon C, Dillin A, Meyer BJ. 2019. X Chromosome Domain Architecture Regulates Caenorhabditis elegans Lifespan but Not Dosage Compensation. *Dev Cell* **51**: 192-207.e6. http://dx.doi.org/10.1016/j.devcel.2019.08.004.

Armache K-J, Garlick JD, Canzio D, Narlikar GJ, Kingston RE. 2011. Structural basis of silencing: Sir3 BAH domain in complex with a nucleosome at 3.0 Å resolution. *Science* **334**: 977–982. http://dx.doi.org/10.1126/science.1210915.

Åström SU, Rine J. 1999. Yeast cell-type regulation of DNA repair. *Nature* **397**: 310.

Audergon PN, Catania S, Kagansky A, Tong P, Shukla M, Pidoux AL, Allshire RC. 2015. Restricted epigenetic inheritance of H3K9 methylation. *Science* **348**: 132–135.

Augui S, Nora EP, Heard E. 2011. Regulation of X-chromosome inactivation by the X-inactivation centre. *Nat Rev Genet* **12**: 429–442. http://dx.doi.org/10.1038/nrg2987.

Ayoub N, Noma K-I, Isaac S, Kahan T, Grewal SIS, Cohen A. 2003. A novel jmjC domain protein modulates heterochromatization in fission yeast. *Mol Cell Biol* **23**: 4356–4370. http://dx.doi.org/10.1128/mcb.23.12.4356-4370.2003.

Ayyagari R, Impellizzeri KJ, Yoder BL, Gary SL, Burgers PM. 1995. A mutational analysis of the yeast proliferating cell nuclear antigen indicates distinct roles in DNA replication and DNA repair. *Mol Cell Biol* **15**: 4420–4429. http://dx.doi.org/10.1128/mcb.15.8.4420.

Babiarz JE, Halley JE, Rine J. 2006. Telomeric heterochromatin boundaries require NuA4-dependent acetylation of histone variant H2A.Z in Saccharomyces cerevisiae. *Genes Dev* **20**: 700–710. http://dx.doi.org/10.1101/gad.1386306.

Balaton BP, Brown CJ. 2016. Escape Artists of the X Chromosome. *Trends Genet* **32**: 348–359. http://dx.doi.org/10.1016/j.tig.2016.03.007.

Bannister AJ, Zegerman P, Partridge JF, Miska EA, Thomas JO, Allshire RC, Kouzarides T. 2001. Selective recognition of methylated lysine 9 on histone H3 by the HP1 chromo domain. *Nature* **410**: 120–124. http://dx.doi.org/10.1038/35065138.

Barr ML, Bertram EG. 1949. A morphological distinction between neurones of the male and female, and the behaviour of the nucleolar satellite during accelerated nucleoprotein synthesis. *Nature* **163**: 676. http://dx.doi.org/10.1038/163676a0.

Bauer GA, Burgers PM. 1990. Molecular cloning, structure and expression of the yeast proliferating cell nuclear antigen gene. *Nucleic Acids Res* **18**: 261–265. http://dx.doi.org/10.1093/nar/18.2.261.

Behrouzi R, Lu C, Currie MA, Jih G, Iglesias N, Moazed D. 2016. Heterochromatin assembly by interrupted Sir3 bridges across neighboring nucleosomes. *Elife* **5**. http://dx.doi.org/10.7554/eLife.17556.

Bell O, Conrad T, Kind J, Wirbelauer C, Akhtar A, Schübeler D. 2008. Transcription-coupled methylation of histone H3 at lysine 36 regulates dosage compensation by enhancing recruitment of the MSL complex in Drosophila melanogaster. *Mol Cell Biol* **28**: 3401–3409. http://dx.doi.org/10.1128/MCB.00006-08.

Bellelli R, Belan O, Pye VE, Clement C, Maslen SL, Skehel JM, Cherepanov P, Almouzni G, Boulton SJ. 2018. POLE3-POLE4 Is a Histone H3-H4 Chaperone that Maintains Chromatin Integrity during DNA Replication. *Mol Cell* **72**: 112-126.e5. http://dx.doi.org/10.1016/j.molcel.2018.08.043.

Ben-Shahar TR, Castillo AG, Osborne MJ, Borden KLB, Kornblatt J, Verreault A. 2009. Two Fundamentally Distinct PCNA Interaction Peptides Contribute to Chromatin Assembly Factor 1 Function. *Mech Chem Biosyst* **29**: 6353–6365. https://mcb.asm.org/content/29/24/6353.

Bi X, Yu Q, Sandmeier JJ, Zou Y. 2004. Formation of boundaries of transcriptionally silent chromatin by nucleosome-excluding structures. *Mol Cell Biol* **24**: 2118–2131. http://dx.doi.org/10.1128/mcb.24.5.2118-2131.2004.

Bian Q, Anderson EC, Yang Q, Meyer BJ. 2020. Histone H3K9 methylation promotes formation of genome compartments in Caenorhabditis elegans via chromosome compaction and perinuclear anchoring. *Proc Natl Acad Sci U S A* **117**: 11459–11470. http://dx.doi.org/10.1073/pnas.2002068117.

Boehm EM, Washington MT. 2016. R.I.P. to the PIP: PCNA-binding motif no longer considered specific: PIP motifs and other related sequences are not distinct entities and can bind multiple proteins involved in genome maintenance. *Bioessays* **38**: 1117–1122. http://dx.doi.org/10.1002/bies.201600116.

Bone JR, Lavender J, Richman R, Palmer MJ, Turner BM, Kuroda MI. 1994. Acetylated histone H4 on the male X chromosome is associated with dosage compensation in Drosophila. *Genes Dev* **8**: 96–104. http://dx.doi.org/10.1101/gad.8.1.96.

Borra MT, Langer MR, Slama JT, Denu JM. 2004. Substrate Specificity and Kinetic Mechanism of the Sir2 Family of NAD+-Dependent Histone/Protein Deacetylases. *Biochemistry* **43**: 9877–9887. https://doi.org/10.1021/bi049592e.

Brand AH, Breeden L, Abraham J, Sternglanz R, Nasmyth K. 1985. Characterization of a "silencer" in yeast: A DNA sequence with properties opposite to those of a transcriptional enhancer. *Cell* **41**: 41–48. http://dx.doi.org/10.1016/0092-8674(85)90059-5.

Braunstein M, Rose AB, Holmes SG, Allis CD, Broach JR. 1993. Transcriptional silencing in yeast is associated with reduced nucleosome acetylation. *Genes Dev* **7**: 592–604. http://dx.doi.org/10.1101/gad.7.4.592.

Braunstein M, Sobel RE, Allis CD, Turner BM, Broach JR. 1996. Efficient transcriptional silencing in Saccharomyces cerevisiae requires a heterochromatin histone acetylation pattern. *Mol Cell Biol* **16**: 4349–4356. http://dx.doi.org/10.1128/mcb.16.8.4349.

Brejc K, Bian Q, Uzawa S, Wheeler BS, Anderson EC, King DS, Kranzusch PJ, Preston CG, Meyer BJ. 2017. Dynamic Control of X Chromosome Conformation and Repression by a Histone H4K20 Demethylase. *Cell* **171**: 85-102.e23. http://dx.doi.org/10.1016/j.cell.2017.07.041.

Brockdorff N. 2019. Localized accumulation of Xist RNA in X chromosome inactivation. *Open Biol* **9**: 190213. http://dx.doi.org/10.1098/rsob.190213.

Brockdorff N, Bowness JS, Wei G. 2020. Progress toward understanding chromosome silencing by Xist RNA. *Genes Dev* **34**: 733–744. http://genesdev.cshlp.org/content/34/11-12/733.full.pdf+html (Accessed June 1, 2020).

Brothers M, Rine J. 2019. Mutations in the PCNA DNA Polymerase Clamp of Saccharomyces cerevisiae Reveal Complexities of the Cell Cycle and Ploidy on Heterochromatin Assembly. *Genetics* **213**: 449–463. http://dx.doi.org/10.1534/genetics.119.302452.

Brown CJ, Willard HF. 1989. Noninactivation of a selectable human X-linked gene that complements a murine temperature-sensitive cell cycle defect. *Am J Hum Genet* **45**: 592–598. https://www.ncbi.nlm.nih.gov/pubmed/2491017.

Buchanan L, Durand-Dubief M, Roguev A, Sakalar C, Wilhelm B, Strålfors A, Shevchenko A, Aasland R, Shevchenko A, Ekwall K, et al. 2009. The Schizosaccharomyces pombe JmjC-protein, Msc1, prevents H2A.Z localization in centromeric and subtelomeric chromatin domains. *PLoS Genet* **5**: e1000726. http://dx.doi.org/10.1371/journal.pgen.1000726.

Buchberger JR, Onishi M, Li G, Seebacher J, Rudner AD, Gygi SP, Moazed D. 2008. Sir3-Nucleosome Interactions in Spreading of Silent Chromatin in Saccharomyces cerevisiae. *Mech Chem Biosyst* **28**: 6903–6918. https://mcb.asm.org/content/28/22/6903.

Buchman AR, Kimmerly WJ, Rine J, Kornberg RD. 1988. Two DNA-binding factors recognize specific sequences at silencers, upstream activating sequences, autonomously replicating sequences, and telomeres in Saccharomyces cerevisiae. *Mol Cell Biol* **8**: 210–225. http://dx.doi.org/10.1128/mcb.8.1.210.

Buck SW, Shore D. 1995. Action of a RAP1 carboxy-terminal silencing domain reveals an underlying competition between HMR and telomeres in yeast. *Genes Dev* **9**: 370–384.

Bühler M, Verdel A, Moazed D. 2006. Tethering RITS to a nascent transcript initiates RNAi- and heterochromatin-dependent gene silencing. *Cell* **125**: 873–886. http://dx.doi.org/10.1016/j.cell.2006.04.025.

Bystricky K, Van Attikum H, Montiel M-D, Dion V, Gehlen L, Gasser SM. 2009. Regulation of Nuclear Positioning and Dynamics of the Silent Mating Type Loci by the Yeast Ku70/Ku80 Complex. *Mech Chem Biosyst* **29**: 835–848. https://mcb.asm.org/content/29/3/835.

Cam HP, Sugiyama T, Chen ES, Chen X, FitzGerald PC, Grewal SIS. 2005. Comprehensive analysis of heterochromatin- and RNAi-mediated epigenetic control of the fission yeast genome. *Nat Genet* **37**: 809–819. http://dx.doi.org/10.1038/ng1602.

Canzio D, Liao M, Naber N, Pate E, Larson A, Wu S, Marina DB, Garcia JF, Madhani HD, Cooke R, et al. 2013. A conformational switch in HP1 releases auto-inhibition to drive heterochromatin assembly. *Nature* **496**: 377–381. http://dx.doi.org/10.1038/nature12032.

Carmen AA, Milne L, Grunstein M. 2002. Acetylation of the yeast histone H4 N terminus regulates its binding to heterochromatin protein SIR3. *J Biol Chem* **277**: 4778–4781. http://dx.doi.org/10.1074/jbc.M110532200.

Carrel L, Willard HF. 2005. X-inactivation profile reveals extensive variability in X-linked gene expression in females. *Nature* **434**: 400–404. http://dx.doi.org/10.1038/nature03479.

Cattanach BM. 1961. A chemically-induced variegated-type position effect in the mouse. *Zeitschrift fiir Vererbungslehre* **92**: 165–182. https://link.springer.com/content/pdf/10.1007/BF00890283.pdf.

Chang J-F, Hall BE, Tanny JC, Moazed D, Filman D, Ellenberger T. 2003. Structure of the coiled-coil dimerization motif of Sir4 and its interaction with Sir3. *Structure* **11**: 637–649. http://dx.doi.org/10.1016/s0969-2126(03)00093-5.

Charlton SJ, Jørgensen MM, Thon G. 2020. Integrity of a heterochromatic domain ensured by its boundary elements. *Proc Natl Acad Sci U S A*. http://dx.doi.org/10.1073/pnas.2010062117.

Chen L, Widom J. 2005. Mechanism of transcriptional silencing in yeast. *Cell* **120**: 37–48. http://dx.doi.org/10.1016/j.cell.2004.11.030.

Cheng TH, Gartenberg MR. 2000. Yeast heterochromatin is a dynamic structure that requires silencers continuously. *Genes Dev* **14**: 452–463. https://www.ncbi.nlm.nih.gov/pubmed/10691737.

Chereji RV, Ramachandran S, Bryson TD, Henikoff S. 2018. Precise genome-wide mapping of single nucleosomes and linkers in vivo. *Genome Biol* **19**: 19. http://dx.doi.org/10.1186/s13059-018-1398-0.

Cheutin T, Gorski SA, May KM, Singh PB, Misteli T. 2004. In vivo dynamics of Swi6 in yeast: evidence for a stochastic model of heterochromatin. *Mol Cell Biol* **24**: 3157–3167. http://dx.doi.org/10.1128/mcb.24.8.3157-3167.2004.

Cheutin T, McNairn AJ, Jenuwein T, Glibert DM, Singh PB, Misteli T. 2003. Maintenanceof Stable Heterochromatin Domainsby Dynamic HP1 Binding. *Science* **299**: 721–725.

Choe KN, Moldovan G-L. 2017. Forging Ahead through Darkness: PCNA, Still the Principal Conductor at the Replication Fork. *Mol Cell* **65**: 380–392. http://dx.doi.org/10.1016/j.molcel.2016.12.020.

Chuang PT, Lieb JD, Meyer BJ. 1996. Sex-specific assembly of a dosage compensation complex on the nematode X chromosome. *Science* **274**: 1736–1739. http://dx.doi.org/10.1126/science.274.5293.1736.

Clemente-Ruiz M, González-Prieto R, Prado F. 2011. Histone H3K56 acetylation, CAF1, and Rtt106 coordinate nucleosome assembly and stability of advancing replication forks. *PLoS Genet* **7**: e1002376. http://dx.doi.org/10.1371/journal.pgen.1002376.

Cockell M, Palladino F, Laroche T, Kyrion G, Liu C, Lustig AJ, Gasser SM. 1995. The carboxy termini of Sir4 and Rap1 affect Sir3 localization: evidence for a multicomponent complex required for yeast telomeric silencing. *J Cell Biol* **129**: 909–924. http://dx.doi.org/10.1083/jcb.129.4.909.

Collart MA, Oliviero S. 2001. Preparation of yeast RNA. *Curr Protoc Mol Biol* **Chapter 13**: Unit13.12. http://dx.doi.org/10.1002/0471142727.mb1312s23.

Colmenares SU, Buker SM, Buhler M, Dlakić M, Moazed D. 2007. Coupling of double-stranded RNA synthesis and siRNA generation in fission yeast RNAi. *Mol Cell* **27**: 449–461. http://dx.doi.org/10.1016/j.molcel.2007.07.007.

Conrad T, Cavalli FMG, Holz H, Hallacli E, Kind J, Ilik I, Vaquerizas JM, Luscombe NM, Akhtar A. 2012. The MOF chromobarrel domain controls genome-wide H4K16 acetylation and spreading of the MSL complex. *Dev Cell* **22**: 610–624. http://dx.doi.org/10.1016/j.devcel.2011.12.016.

Crane E, Bian Q, McCord RP, Lajoie BR, Wheeler BS, Ralston EJ, Uzawa S, Dekker J, Meyer BJ. 2015. Condensin-driven remodelling of X chromosome topology during dosage compensation. *Nature* **523**: 240–244. http://dx.doi.org/10.1038/nature14450.

Csankovszki G, McDonel P, Meyer BJ. 2004. Recruitment and spreading of the C. elegans dosage compensation complex along X chromosomes. *Science* **303**: 1182–1185. http://dx.doi.org/10.1126/science.1092938.

Dahlsveen IK, Gilfillan GD, Shelest VI, Lamm R, Becker PB. 2006. Targeting determinants of dosage compensation in Drosophila. *PLoS Genet* **2**: e5. http://dx.doi.org/10.1371/journal.pgen.0020005.

Davis TL, Meyer BJ. 1997. SDC-3 coordinates the assembly of a dosage compensation complex on the nematode X chromosome. *Development* **124**: 1019–1031. https://www.ncbi.nlm.nih.gov/pubmed/9056777.

Dawes HE, Berlin DS, Lapidus DM, Nusbaum C, Davis TL, Meyer BJ. 1999. Dosage compensation proteins targeted to X chromosomes by a determinant of hermaphrodite fate. *Science* **284**: 1800–1804. http://dx.doi.org/10.1126/science.284.5421.1800.

de Bruin D, Kantrow SM, Liberatore RA, Zakian VA. 2000. Telomere folding is required for the stable maintenance of telomere position effects in yeast. *Mol Cell Biol* **20**: 7991–8000. http://dx.doi.org/10.1128/mcb.20.21.7991-8000.2000.

Demakova OV, Kotlikova IV, Gordadze PR, Alekseyenko AA, Kuroda MI, Zhimulev IF. 2003. The MSL complex levels are critical for its correct targeting to the chromosomes in Drosophila melanogaster. *Chromosoma* **112**: 103–115. http://dx.doi.org/10.1007/s00412-003-0249-1.

Deng X, Koya SK, Kong Y, Meller VH. 2009. Coordinated regulation of heterochromatic genes in Drosophila melanogaster males. *Genetics* **182**: 481–491. http://dx.doi.org/10.1534/genetics.109.102087.

Dhillon N, Raab J, Guzzo J, Szyjka SJ, Gangadharan S, Aparicio OM, Andrews B, Kamakaka RT. 2009. DNA polymerase epsilon, acetylases and remodellers cooperate to form a specialized chromatin structure at a tRNA insulator. *EMBO J* **28**: 2583–2600. http://dx.doi.org/10.1038/emboj.2009.198.

Djupedal I, Portoso M, Spåhr H, Bonilla C, Gustafsson CM, Allshire RC, Ekwall K. 2005. RNA Pol II subunit Rpb7 promotes centromeric transcription and RNAi-directed chromatin silencing. *Genes Dev* **19**: 2301–2306. http://dx.doi.org/10.1101/gad.344205.

Dodson AE, Rine J. 2016. Donor Preference Meets Heterochromatin: Moonlighting Activities of a Recombinational Enhancer in Saccharomyces cerevisiae. *Genetics* **204**: 1065–1074. http://dx.doi.org/10.1534/genetics.116.194696.

Dodson AE, Rine J. 2015. Heritable capture of heterochromatin dynamics in Saccharomyces cerevisiae. *Elife* **4**: e05007. http://dx.doi.org/10.7554/eLife.05007.

Donohoe ME, Zhang L-F, Xu N, Shi Y, Lee JT. 2007. Identification of a Ctcf cofactor, Yy1, for the X chromosome binary switch. *Mol Cell* **25**: 43–56. http://dx.doi.org/10.1016/j.molcel.2006.11.017.

Donze D, Adams CR, Rine J, Kamakaka RT. 1999. The boundaries of the silenced HMR domain in Saccharomyces cerevisiae. *Genes Dev* **13**: 698–708. http://dx.doi.org/10.1101/gad.13.6.698.

Donze D, Kamakaka RT. 2001. RNA polymerase III and RNA polymerase II promoter complexes are heterochromatin barriers in Saccharomyces cerevisiae. *EMBO J* **20**: 520–531. http://dx.doi.org/10.1093/emboj/20.3.520.

Edelstein AD, Tsuchida MA, Amodaj N, Pinkard H, Vale RD, Stuurman N. 2014. Advanced methods of microscope control using μManager software. *J Biol Methods* **1**. http://dx.doi.org/10.14440/jbm.2014.36.

Ehrentraut S, Hassler M, Oppikofer M, Kueng S, Weber JM, Mueller JW, Gasser SM, Ladurner AG, Ehrenhofer-Murray AE. 2011. Structural basis for the role of the Sir3 AAA+ domain in silencing: interaction with Sir4 and unmethylated histone H3K79. *Genes Dev* **25**: 1835–1846. http://dx.doi.org/10.1101/gad.17175111.

Ehrentraut S, Weber JM, Dybowski JN, Hoffmann D, Ehrenhofer-Murray AE. 2010. Rpd3-dependent boundary formation at telomeres by removal of Sir2 substrate. *Proc Natl Acad Sci U S A* **107**: 5522–5527. http://dx.doi.org/10.1073/pnas.0909169107.

Eissenberg JC, Ayyagari R, Gomes XV, Burgers PM. 1997. Mutations in yeast proliferating cell nuclear antigen define distinct sites for interaction with DNA polymerase delta and DNA polymerase epsilon. *Mol Cell Biol* **17**: 6367–6378. http://dx.doi.org/10.1128/mcb.17.11.6367.

Ekwall K, Javerzat JP, Lorentz A, Schmidt H, Cranston G, Allshire R. 1995. The chromodomain protein Swi6: a key component at fission yeast centromeres. *Science* **269**: 1429–1431. http://dx.doi.org/10.1126/science.7660126.

Ellahi A, Thurtle DM, Rine J. 2015. The Chromatin and Transcriptional Landscape of Native Saccharomyces cerevisiae Telomeres and Subtelomeric Domains. *Genetics* **200**: 505–521. http://dx.doi.org/10.1534/genetics.115.175711.

Engreitz JM, Pandya-Jones A, McDonel P, Shishkin A, Sirokman K, Surka C, Kadri S, Xing J, Goren A, Lander ES, et al. 2013. The Xist lncRNA exploits three-dimensional genome architecture to spread across the X chromosome. *Science* **341**: 1237973. http://dx.doi.org/10.1126/science.1237973.

Ercan S, Dick LL, Lieb JD. 2009. The C. elegans dosage compensation complex propagates dynamically and independently of X chromosome sequence. *Curr Biol* **19**: 1777–1787. http://dx.doi.org/10.1016/j.cub.2009.09.047.

Ercan S, Giresi PG, Whittle CM, Zhang X, Green RD, Lieb JD. 2007. X chromosome repression by localization of the C. elegans dosage compensation machinery to sites of transcription initiation. *Nat Genet* **39**: 403–408. http://dx.doi.org/10.1038/ng1983.

Ercan S, Lieb JD. 2009. C. elegans dosage compensation: a window into mechanisms of domain-scale gene regulation. *Chromosome Res* **17**: 215–227. http://dx.doi.org/10.1007/s10577-008-9011-0.

Fan X, Struhl K. 2009. Where does mediator bind in vivo? *PLoS One* **4**: e5029. http://dx.doi.org/10.1371/journal.pone.0005029.

Feldman JB, Hicks JB, Broach JR. 1984. Identification of sites required for repression of a silent mating type locus in yeast. *Journal of Molecular Biology* **178**: 815–834. http://dx.doi.org/10.1016/0022-2836(84)90313-9.

Festenstein R, Pagakis SN, Hiragami K, Lyon D, Verreault A, Sekkali B, Kioussis D. 2003. Modulation of Heterochromatin Protein 1 Dynamics in Primary Mammalian Cells. *Science* **299**: 719–721.

Fischle W, Wang Y, Jacobs SA, Kim Y, Allis CD, Khorasanizadeh S. 2003. Molecular basis for the discrimination of repressive methyl-lysine marks in histone H3 by Polycomb and HP1 chromodomains. *Genes Dev* **17**: 1870–1881. http://dx.doi.org/10.1101/gad.1110503.

Foltman M, Evrin C, De Piccoli G, Jones RC, Edmondson RD, Katou Y, Nakato R, Shirahige K, Labib K. 2013. Eukaryotic replisome components cooperate to process histones during chromosome replication. *Cell Rep* **3**: 892–904. http://dx.doi.org/10.1016/j.celrep.2013.02.028.

Fourel G, Revardel E, Koering CE, Gilson E. 1999. Cohabitation of insulators and silencing elements in yeast subtelomeric regions. *EMBO J* **18**: 2522–2537. http://dx.doi.org/10.1093/emboj/18.9.2522.

Frank-Vaillant M, Marcand S. 2001. NHEJ regulation by mating type is exercised through a novel protein, Lif2p, essential to the ligase IV pathway. *Genes Dev* **15**: 3005–3012. http://dx.doi.org/10.1101/gad.206801.

Froberg JE, Pinter SF, Kriz AJ, Jégu T, Lee JT. 2018. Megadomains and superloops form dynamically but are dispensable for X-chromosome inactivation and gene escape. *Nat Commun* **9**: 5004. http://dx.doi.org/10.1038/s41467-018-07446-w.

Funabiki H, Hagan I, Uzawa S, Yanagida M. 1993. Cell cycle-dependent specific positioning and clustering of centromeres and telomeres in fission yeast. *J Cell Biol* **121**: 961–976. http://dx.doi.org/10.1083/jcb.121.5.961.

Galupa R, Heard E. 2018. X-Chromosome Inactivation: A Crossroads Between Chromosome Architecture and Gene Regulation. *Annu Rev Genet* **52**: 535–566. http://dx.doi.org/10.1146/annurev-genet-120116-024611.

Gan H, Serra-Cardona A, Hua X, Zhou H, Labib K, Yu C, Zhang Z. 2018. The Mcm2-Ctf4-Polα Axis Facilitates Parental Histone H3-H4 Transfer to Lagging Strands. *Mol Cell* **72**: 140-151.e3. http://dx.doi.org/10.1016/j.molcel.2018.09.001.

Gao L, Gross DS. 2008. Sir2 Silences Gene Transcription by Targeting the Transition between RNA Polymerase II Initiation and Elongation. *Mech Chem Biosyst* **28**: 3979–3994. https://mcb.asm.org/content/28/12/3979.

Garcia JF, Al-Sady B, Madhani HD. 2015. Intrinsic Toxicity of Unchecked Heterochromatin Spread Is Suppressed by Redundant Chromatin Boundary Functions in Schizosacchromyces pombe. *G3* **5**: 1453–1461. http://dx.doi.org/10.1534/g3.115.018663.

Garcia JF, Dumesic PA, Hartley PD, El-Samad H, Madhani HD. 2010. Combinatorial, site-specific requirement for heterochromatic silencing factors in the elimination of nucleosome-free regions. *Genes Dev* **24**: 1758–1771. http://dx.doi.org/10.1101/gad.1946410.

Gartenberg MR, Neumann FR, Laroche T, Blaszczyk M, Gasser SM. 2004. Sir-mediated repression can occur independently of chromosomal and subnuclear contexts. *Cell* **119**: 955–967. http://dx.doi.org/10.1016/j.cell.2004.11.008.

Gartenberg MR, Smith JS. 2016. The Nuts and Bolts of Transcriptionally Silent Chromatin in Saccharomyces cerevisiae. *Genetics* **203**: 1563–1599. http://dx.doi.org/10.1534/genetics.112.145243.

Gelbart ME, Larschan E, Peng S, Park PJ, Kuroda MI. 2009. Drosophila MSL complex globally acetylates H4K16 on the male X chromosome for dosage compensation. *Nat Struct Mol Biol* **16**: 825–832. http://dx.doi.org/10.1038/nsmb.1644.

Georgel PT, Palacios DeBeer MA, Pietz G, Fox CA, Hansen JC. 2001. Sir3-dependent assembly of supramolecular chromatin structures in vitro. *Proc Natl Acad Sci U S A* **98**: 8584–8589. http://dx.doi.org/10.1073/pnas.151258798.

Ghidelli S, Donze D, Dhillon N, Kamakaka RT. 2001. Sir2p exists in two nucleosome-binding complexes with distinct deacetylase activities. *EMBO J* **20**: 4522–4535. http://dx.doi.org/10.1093/emboj/20.16.4522.

Giaimo BD, Ferrante F, Herchenröther A, Hake SB, Borggrefe T. 2019. The histone variant H2A.Z in gene regulation. *Epigenetics Chromatin* **12**: 37. http://dx.doi.org/10.1186/s13072-019-0274-9.

Gilfillan GD, Straub T, de Wit E, Greil F, Lamm R, van Steensel B, Becker PB. 2006. Chromosome-wide gene-specific targeting of the Drosophila dosage compensation complex. *Genes Dev* **20**: 858–870. http://dx.doi.org/10.1101/gad.1399406.

Giorgetti L, Lajoie BR, Carter AC, Attia M, Zhan Y, Xu J, Chen CJ, Kaplan N, Chang HY, Heard E, et al. 2016. Structural organization of the inactive X chromosome in the mouse. *Nature* **535**: 575–579. http://dx.doi.org/10.1038/nature18589.

Goldstein AL, McCusker JH. 1999. Three new dominant drug resistance cassettes for gene disruption in Saccharomyces cerevisiae. *Yeast* **15**: 1541–1553. http://dx.doi.org/10.1002/(SICI)1097-0061(199910)15:14<1541::AID-YEA476>3.0.CO;2-K.

Goodnight D, Rine J. 2020. S-phase-independent silencing establishment in Saccharomyces cerevisiae. *Elife* **9**. http://dx.doi.org/10.7554/eLife.58910.

Gotta M, Laroche T, Formenton A, Maillet L, Scherthan H, Gasser SM. 1996. The clustering of telomeres and colocalization with Rap1, Sir3, and Sir4 proteins in wild-type Saccharomyces cerevisiae. *J Cell Biol* **134**: 1349–1363. http://dx.doi.org/10.1083/jcb.134.6.1349.

Gotta M, Palladino F, Gasser SM. 1998. Functional characterization of the N terminus of Sir3p. *Mol Cell Biol* **18**: 6110–6120. http://dx.doi.org/10.1128/MCB.18.10.6110.

Gottschling DE. 1992. Telomere-proximal DNA in Saccharomyces cerevisiae is refractory to methyltransferase activity in vivo.pdf. *Proc Natl Acad Sci U S A* **89**: 4062–4065.

Gottschling DE, Aparicio OM, Billington BL, Zakian VA. 1990. Position effect at S. cerevisiae telomeres: reversible repression of Pol II transcription. *Cell* **63**: 751–762. http://dx.doi.org/10.1016/0092-8674(90)90141-z.

Greenstein RA, Jones SK, Spivey EC, Rybarski JR, Finkelstein IJ, Al-Sady B. 2018. Noncoding RNA-nucleated heterochromatin spreading is intrinsically labile and requires accessory elements for epigenetic stability. *Elife* **7**. http://dx.doi.org/10.7554/eLife.32948.

Grimaud C, Becker PB. 2009. The dosage compensation complex shapes the conformation of the X chromosome in Drosophila. *Genes Dev* **23**: 2490–2495. http://dx.doi.org/10.1101/gad.539509.

Gu W, Szauter P, Lucchesi JC. 1998. Targeting of MOF, a putative histone acetyltransferase to the X chromosome of Drosophila melanogaster. *Dev Genetics* **22**: 56–64. https://onlinelibrary.wiley.com/doi/abs/10.1002/%28SICI%291520-6408%281998%2922%3A1%3C56%3A%3AAID-DVG6%3E3.0.CO%3B2-6.

Gu W, Wei X, Pannuti A, Lucchesi JC. 2000. Targeting the chromatin-remodeling MSL complex of Drosophila to its sites of action on the X chromosome requires both acetyl transferase and ATPase activities. *EMBO J* **19**: 5202–5211. http://dx.doi.org/10.1093/emboj/19.19.5202.

Gueldener U, Heinisch J, Koehler GJ, Voss D, Hegemann JH. 2002. A second set of loxP marker cassettes for Cre-mediated multiple gene knockouts in budding yeast. *Nucleic Acids Res* **30**: e23. http://dx.doi.org/10.1093/nar/30.6.e23.

Hall IM, Shankaranarayana GD, Noma K-I, Ayoub N, Cohen A, Grewal SIS. 2002. Establishment and maintenance of a heterochromatin domain. *Science* **297**: 2232–2237. http://dx.doi.org/10.1126/science.1076466.

He H, Li Y, Dong Q, Chang A-Y, Gao F, Chi Z, Su M, Zhang F, Ban H, Martienssen R, et al. 2017. Coordinated regulation of heterochromatin inheritance by Dpb3-Dpb4 complex. *Proc Natl Acad Sci U S A* **114**: 12524–12529. http://dx.doi.org/10.1073/pnas.1712961114.

Hecht A, Laroche T, Strahl-Bolsinger S, Gasser SM, Grunstein M. 1995. Histone H3 and H4 N-termini interact with SIR3 and SIR4 proteins: a molecular model for the formation of heterochromatin in yeast. *Cell* **80**: 583–592. http://dx.doi.org/10.1016/0092-8674(95)90512-x.

Hecht A, Strahl-Bolsinger S, Grunstein M. 1996. Spreading of transcriptional repressor SIR3 from telomeric heterochromatin. *Nature* **383**: 92–96.

Helbo AS, Lay FD, Jones PA, Liang G, Grønbæk K. 2017. Nucleosome Positioning and NDR Structure at RNA Polymerase III Promoters. *Sci Rep* **7**: 41947. http://dx.doi.org/10.1038/srep41947.

Henikoff S. 1996. Dosage-dependent modification of position-effect variegation in Drosophila. *Bioessays* **18**: 401–409.

Hentges P, Van Driessche B, Tafforeau L, Vandenhaute J, Carr AM. 2005. Three novel antibiotic marker cassettes for gene disruption and marker switching in Schizosaccharomyces pombe. *Yeast* **22**: 1013–1019. http://dx.doi.org/10.1002/yea.1291.

Hocher A, Ruault M, Kaferle P, Descrimes M, Garnier M, Morillon A, Taddei A. 2018. Expanding heterochromatin reveals discrete subtelomeric domains delimited by chromatin landscape transitions. *Genome Res* **28**: 1867–1881. http://dx.doi.org/10.1101/gr.236554.118.

Hofmann JFX, Laroche T, Brand AH, Gasser SM. 1989. RAP-1 Factor Is Necessary for DNA Loop Formation In Vitro at the Silent Mating Type Locus HML. *Cell* **57**: 725–737.

Hoggard T, Müller CA, Nieduszynski CA, Weinreich M, Fox CA. 2020. Sir2 mitigates an intrinsic imbalance in origin licensing efficiency between early- and late-replicating euchromatin. *Proc Natl Acad Sci U S A* **117**: 14314–14321. http://dx.doi.org/10.1073/pnas.2004664117.

Hoggard TA, Chang F, Perry KR, Subramanian S, Kenworthy J, Chueng J, Shor E, Hyland EM, Boeke JD, Weinreich M, et al. 2018. Yeast heterochromatin regulators Sir2 and Sir3 act directly at euchromatic DNA replication origins. *PLoS Genet* **14**: e1007418. http://dx.doi.org/10.1371/journal.pgen.1007418.

Hoppe GJ, Tanny JC, Rudner AD, Gerber SA, Danaie S, Gygi SP, Moazed D. 2002. Steps in assembly of silent chromatin in yeast: Sir3-independent binding of a Sir2/Sir4 complex to silencers and role for Sir2-dependent deacetylation. *Mol Cell Biol* **22**: 4167–4180. http://dx.doi.org/10.1128/mcb.22.12.4167-4180.2002.

Horvath LM, Li N, Carrel L. 2013. Deletion of an X-inactivation boundary disrupts adjacent gene silencing. *PLoS Genet* **9**: e1003952. http://dx.doi.org/10.1371/journal.pgen.1003952.

Hou H, Wang Y, Kallgren SP, Thompson J, Yates JR 3rd, Jia S. 2010. Histone variant H2A.Z regulates centromere silencing and chromosome segregation in fission yeast. *J Biol Chem* **285**: 1909–1918. http://dx.doi.org/10.1074/jbc.M109.058487.

Hsu H-C, Wang C-L, Wang M, Yang N, Chen Z, Sternglanz R, Xu R-M. 2013. Structural basis for allosteric stimulation of Sir2 activity by Sir4 binding. *Genes Dev* **27**: 64–73. http://dx.doi.org/10.1101/gad.208140.112.

Huang S, Zhou H, Katzmann D, Hochstrasser M, Atanasova E, Zhang Z. 2005. Rtt106p is a histone chaperone involved in heterochromatin-mediated silencing. *Proc Natl Acad Sci U S A* **102**: 13410–13415. http://dx.doi.org/10.1073/pnas.0506176102.

Hyland EM, Cosgrove MS, Molina H, Wang D, Pandey A, Cottee RJ, Boeke JD. 2005. Insights into the role of histone H3 and histone H4 core modifiable residues in Saccharomyces cerevisiae. *Mol Cell Biol* **25**: 10060–10070. http://dx.doi.org/10.1128/MCB.25.22.10060-10070.2005.

Iida T, Kobayashi T. 2019. RNA Polymerase I Activators Count and Adjust Ribosomal RNA Gene Copy Number. *Mol Cell* **73**: 645-654.e13. http://dx.doi.org/10.1016/j.molcel.2018.11.029.

Imai S, Armstrong CM, Kaeberlein M, Guarente L. 2000. Transcriptional silencing and longevity protein Sir2 is an NAD-dependent histone deacetylase. *Nature* **403**: 795–800. http://dx.doi.org/10.1038/35001622.

Ivanova AV, Bonaduce MJ, Ivanov SV, Klar AJ. 1998. The chromo and SET domains of the Clr4 protein are essential for silencing in fission yeast. *Nat Genet* **19**: 192–195. http://dx.doi.org/10.1038/566.

Iyer V, Struhl K. 1995. Poly(dA:dT), a ubiquitous promoter element that stimulates transcription via its intrinsic DNA structure. *EMBO J* **14**: 2570–2579. https://www.ncbi.nlm.nih.gov/pubmed/7781610.

Janke R, King GA, Kupiec M, Rine J. 2018. Pivotal roles of PCNA loading and unloading in heterochromatin function. *Proc Natl Acad Sci U S A* **115**: E2030–E2039. http://dx.doi.org/10.1073/pnas.1721573115.

Jans J, Gladden JM, Ralston EJ, Pickle CS, Michel AH, Pferdehirt RR, Eisen MB, Meyer BJ. 2009. A condensin-like dosage compensation complex acts at a distance to control expression throughout the genome. *Genes Dev* **23**: 602–618. http://dx.doi.org/10.1101/gad.1751109.

Jelinsky SA, Samson LD. 1999. Global response of Saccharomyces cerevisiae to an alkylating agent. *Proc Natl Acad Sci U S A* **96**: 1486–1491. http://dx.doi.org/10.1073/pnas.96.4.1486.

Jeon Y, Lee JT. 2011. YY1 tethers Xist RNA to the inactive X nucleation center. *Cell* **146**: 119–133. http://dx.doi.org/10.1016/j.cell.2011.06.026.

Jia S, Noma K-I, Grewal SIS. 2004. RNAi-independent heterochromatin nucleation by the stress-activated ATF/CREB family proteins. *Science* **304**: 1971–1976. http://dx.doi.org/10.1126/science.1099035.

Johnson A, Li G, Sikorski TW, Buratowski S, Woodcock CL, Moazed D. 2009. Reconstitution of heterochromatin-dependent transcriptional gene silencing. *Mol Cell* **35**: 769–781. http://dx.doi.org/10.1016/j.molcel.2009.07.030.

Johnson A, Wu R, Peetz M, Gygi SP, Moazed D. 2013. Heterochromatic gene silencing by activator interference and a transcription elongation barrier. *J Biol Chem* **288**: 28771–28782. http://dx.doi.org/10.1074/jbc.M113.460071.

Johnson LM, Kayne PS, Kahn ES, Grunstein M. 1990. Genetic evidence for an interaction between SIR3 and histone H4 in the repression of the silent mating loci in Saccharomyces cerevisiae. *Proc Natl Acad Sci USA* **87**: 6286–6290.

Joshi SS, Meller VH. 2017. Satellite Repeats Identify X Chromatin for Dosage Compensation in Drosophila melanogaster Males. *Curr Biol* **27**: 1393-1402.e2. http://dx.doi.org/10.1016/j.cub.2017.03.078.

Kanoh J, Sadaie M, Urano T, Ishikawa F. 2005. Telomere binding protein Taz1 establishes Swi6 heterochromatin independently of RNAi at telomeres. *Curr Biol* **15**: 1808–1819. http://dx.doi.org/10.1016/j.cub.2005.09.041.

Kato H, Goto DB, Martienssen RA, Urano T, Furukawa K, Murakami Y. 2005. RNA polymerase II is required for RNAi-dependent heterochromatin assembly. *Science* **309**: 467–469. http://dx.doi.org/10.1126/science.1114955.

Kegel A, Sjöstrand JO, Aström SU. 2001. Nej1p, a cell type-specific regulator of nonhomologous end joining in yeast. *Curr Biol* **11**: 1611–1617. http://dx.doi.org/10.1016/s0960-9822(01)00488-2.

Kelley RL, Kuroda MI. 2003. The Drosophila roX1 RNA gene can overcome silent chromatin by recruiting the male-specific lethal dosage compensation complex. *Genetics* **164**: 565–574. https://www.ncbi.nlm.nih.gov/pubmed/12807777.

Kelley RL, Lee O-K, Shim Y-K. 2008. Transcription rate of noncoding roX1 RNA controls local spreading of the Drosophila MSL chromatin remodeling complex. *Mech Dev* **125**: 1009–1019. http://dx.doi.org/10.1016/j.mod.2008.08.003.

Kelley RL, Meller VH, Gordadze PR, Roman G, Davis RL, Kuroda MI. 1999. Epigenetic spreading of the Drosophila dosage compensation complex from roX RNA genes into flanking chromatin. *Cell* **98**: 513–522. http://dx.doi.org/10.1016/s0092-8674(00)81979-0.

Kelsey AD, Yang C, Leung D, Minks J, Dixon-McDougall T, Baldry SEL, Bogutz AB, Lefebvre L, Brown CJ. 2015. Impact of flanking chromosomal sequences on localization and silencing by the human non-coding RNA XIST. *Genome Biol* **16**: 208. http://dx.doi.org/10.1186/s13059-015-0774-2.

Kilic S, Bachmann AL, Bryan LC, Fierz B. 2015. Multivalency governs HP1α association dynamics with the silent chromatin state. *Nat Commun* **6**: 7313. http://dx.doi.org/10.1038/ncomms8313.

Kim D, Blus BJ, Chandra V, Huang P, Rastinejad F, Khorasanizadeh S. 2010. Corecognition of DNA and a methylated histone tail by the MSL3 chromodomain. *Nat Struct Mol Biol* **17**: 1027–1029. http://dx.doi.org/10.1038/nsmb.1856.

Kim HS, Choi ES, Shin JA, Jang YK, Park SD. 2004. Regulation of Swi6/HP1-dependent heterochromatin assembly by cooperation of components of the mitogen-activated protein kinase pathway and a histone deacetylase Clr6. *J Biol Chem* **279**: 42850–42859. http://dx.doi.org/10.1074/jbc.M407259200.

Kim H-S, Vanoosthuyse V, Fillingham J, Roguev A, Watt S, Kislinger T, Treyer A, Carpenter LR, Bennett CS, Emili A, et al. 2009. An acetylated form of histone H2A.Z regulates chromosome architecture in Schizosaccharomyces pombe. *Nat Struct Mol Biol* **16**: 1286–1293. http://dx.doi.org/10.1038/nsmb.1688.

Kimmerly W, Buchman A, Kornberg R, Rine J. 1988. Roles of two DNA-binding factors in replication, segregation and transcriptional repression mediated by a yeast silencer. *EMBO J* **7**: 2241–2253. https://www.ncbi.nlm.nih.gov/pubmed/3046937.

Kimura A, Umehara T, Horikoshi M. 2002. Chromosomal gradient of histone acetylation established by Sas2p and Sir2p functions as a shield against gene silencing. *Nat Genet* **32**: 370–377. http://dx.doi.org/10.1038/ng993.

King DA, Hall BE, Iwamoto MA, Win KZ, Chang JF, Ellenberger T. 2006. Domain structure and protein interactions of the silent information regulator Sir3 revealed by screening a nested deletion library of protein fragments. *J Biol Chem* **281**: 20107–20119. http://dx.doi.org/10.1074/jbc.M512588200.

Kirkland JG, Kamakaka RT. 2013. Long-range heterochromatin association is mediated by silencing and double-strand DNA break repair proteins. *J Cell Biol* **201**: 809–826. http://dx.doi.org/10.1083/jcb.201211105.

Kirkland JG, Raab JR, Kamakaka RT. 2013. TFIIIC bound DNA elements in nuclear organization and insulation. *Biochim Biophys Acta* **1829**: 418–424. http://dx.doi.org/10.1016/j.bbagrm.2012.09.006.

Kondratick CM, Litman JM, Shaffer KV, Washington MT, Dieckman LM. 2018. Crystal structures of PCNA mutant proteins defective in gene silencing suggest a novel interaction site on the front face of the PCNA ring. *PLoS One* **13**: e0193333. http://dx.doi.org/10.1371/journal.pone.0193333.

Koya SK, Meller VH. 2015. Modulation of Heterochromatin by Male Specific Lethal Proteins and roX RNA in Drosophila melanogaster Males. *PLoS One* **10**: e0140259. http://dx.doi.org/10.1371/journal.pone.0140259.

Kramer M, Kranz A-L, Su A, Winterkorn LH, Albritton SE, Ercan S. 2015. Developmental Dynamics of X-Chromosome Dosage Compensation by the DCC and H4K20me1 in C. elegans. *PLoS Genet* **11**: e1005698. http://dx.doi.org/10.1371/journal.pgen.1005698.

Lachner M, O'Carroll D, Rea S, Mechtler K, Jenuwein T. 2001. Methylation of histone H3 lysine 9 creates a binding site for HP1 proteins. *Nature* **410**: 116–120.

Ladurner AG, Inouye C, Jain R, Tjian R. 2003. Bromodomains Mediate an Acetyl-Histone Encoded Antisilencing Function at Heterochromatin Boundaries. *Mol Cell* **11**: 365–376. http://www.sciencedirect.com/science/article/pii/S1097276503000352.

Landry J, Sutton A, Tafrov ST, Heller RC, Stebbins J, Pillus L, Sternglanz R. 2000. The silencing protein SIR2 and its homologs are NAD-dependent protein deacetylases. *Proc Natl Acad Sci U S A* **97**: 5807–5811. http://dx.doi.org/10.1073/pnas.110148297.

Langmead B, Salzberg SL. 2012. Fast gapped-read alignment with Bowtie 2. *Nat Methods* **9**: 357–359. http://dx.doi.org/10.1038/nmeth.1923.

Lantermann AB, Straub T, Strålfors A, Yuan G-C, Ekwall K, Korber P. 2010. Schizosaccharomyces pombe genome-wide nucleosome mapping reveals positioning mechanisms distinct from those of Saccharomyces cerevisiae. *Nat Struct Mol Biol* **17**: 251–257. http://dx.doi.org/10.1038/nsmb.1741.

Larschan E, Alekseyenko AA, Gortchakov AA, Peng S, Li B, Yang P, Workman JL, Park PJ, Kuroda MI. 2007. MSL complex is attracted to genes marked by H3K36 trimethylation using a sequence-independent mechanism. *Mol Cell* **28**: 121–133. http://dx.doi.org/10.1016/j.molcel.2007.08.011.

Larson AG, Elnatan D, Keenen MM, Trnka MJ, Johnston JB, Burlingame AL, Agard DA, Redding S, Narlikar GJ. 2017. Liquid droplet formation by HP1α suggests a role for phase separation in heterochromatin. *Nature* **547**: 236–240. http://dx.doi.org/10.1038/nature22822.

Lee ME, DeLoache WC, Cervantes B, Dueber JE. 2015. A Highly Characterized Yeast Toolkit for Modular, Multipart Assembly. *ACS Synth Biol* **4**: 975–986. http://dx.doi.org/10.1021/sb500366v.

Lee M-W, Kim B-J, Choi H-K, Ryu M-J, Kim S-B, Kang K-M, Cho E-J, Youn H-D, Huh W-K, Kim S-T. 2007a. Global protein expression profiling of budding yeast in response to DNA damage. *Yeast* **24**: 145–154. http://dx.doi.org/10.1002/yea.1446.

Lee SE, Pâques F, Sylvan J, Haber JE. 1999. Role of yeast SIR genes and mating type in directing DNA double-strand breaks to homologous and non-homologous repair paths. *Curr Biol* **9**: 767–770. http://dx.doi.org/10.1016/s0960-9822(99)80339-x.

Lee W, Tillo D, Bray N, Morse RH, Davis RW, Hughes TR, Nislow C. 2007b. A high-resolution atlas of nucleosome occupancy in yeast. *Nat Genet* **39**: 1235–1244. http://dx.doi.org/10.1038/ng2117.

Li M, Valsakumar V, Poorey K, Bekiranov S, Smith JS. 2013. Genome-wide analysis of functional sirtuin chromatin targets in yeast. *Genome Biol* **14**: R48. http://dx.doi.org/10.1186/gb-2013-14-5-r48.

Li Q, Zhou H, Wurtele H, Davies B, Horazdovsky B, Verreault A, Zhang Z. 2008. Acetylation of histone H3 lysine 56 regulates replication-coupled nucleosome assembly. *Cell* **134**: 244–255. http://dx.doi.org/10.1016/j.cell.2008.06.018.

Liaw H, Lustig AJ. 2006. Sir3 C-terminal domain involvement in the initiation and spreading of heterochromatin. *Mol Cell Biol* **26**: 7616–7631. http://dx.doi.org/10.1128/MCB.01082-06.

Liu T, Rechtsteiner A, Egelhofer TA, Vielle A, Latorre I, Cheung M-S, Ercan S, Ikegami K, Jensen M, Kolasinska-Zwierz P, et al. 2011. Broad chromosomal domains of histone modification patterns in C. elegans. *Genome Res* **21**: 227–236. http://dx.doi.org/10.1101/gr.115519.110.

Locke J, Kotarski MA, Tartof KD. 1988. Dosage-dependent modifiers of position effect variegation in Drosophila and a mass action model that explains their effect. *Genetics* **120**: 181–198. https://www.ncbi.nlm.nih.gov/pubmed/3146523.

Loda A, Brandsma JH, Vassilev I, Servant N, Loos F, Amirnasr A, Splinter E, Barillot E, Poot RA, Heard E, et al. 2017. Genetic and epigenetic features direct differential efficiency of Xist-mediated silencing at X-chromosomal and autosomal locations. *Nat Commun* **8**: 690. http://dx.doi.org/10.1038/s41467-017-00528-1.

Longtine MS, Wilson NM, Petracek ME, Berman J. 1989. A yeast telomere binding activity binds to two related telomere sequence motifs and is indistinguishable from RAP1. *Curr Genet* **16**: 225–239. http://dx.doi.org/10.1007/BF00422108.

Loo S, Rine J. 1994. Silencers and Domains of Generalized Repression. *Science* **264**: 1748–1771.

Lyman LM, Copps K, Rastelli L, Kelley RL, Kuroda MI. 1997. Drosophila male-specific lethal-2 protein: structure/function analysis and dependence on MSL-1 for chromosome association. *Genetics* **147**: 1743–1753. https://www.ncbi.nlm.nih.gov/pubmed/9409833.

Lynch PJ, Rusche LN. 2009. A Silencer Promotes the Assembly of Silenced Chromatin Independently of Recruitment. *Mech Chem Biosyst* **29**: 43–56. https://mcb.asm.org/content/29/1/43.

Mahoney DJ, Broach JR. 1989. The HML Mating-Type Cassette of Saccharomyces cerevisiae Is Regulated by Two Separate but Functionally Equivalent Silencers. *Mol Cell Biol* **9**: 4621–4630.

Makhlouf M, Ouimette J-F, Oldfield A, Navarro P, Neuillet D, Rougeulle C. 2014. A prominent and conserved role for YY1 in Xist transcriptional activation. *Nat Commun* **5**: 4878. http://dx.doi.org/10.1038/ncomms5878.

Marks H, Kerstens HHD, Barakat TS, Splinter E, Dirks RAM, van Mierlo G, Joshi O, Wang S-Y, Babak T, Albers CA, et al. 2015. Dynamics of gene silencing during X inactivation using allele-specific RNA-seq. *Genome Biol* **16**: 149. http://dx.doi.org/10.1186/s13059-015-0698-x.

Martienssen R, Moazed D. 2015. RNAi and heterochromatin assembly. *Cold Spring Harb Perspect Biol* **7**: a019323. http://dx.doi.org/10.1101/cshperspect.a019323.

Martino F, Kueng S, Robinson P, Tsai-Pflugfelder M, van Leeuwen F, Ziegler M, Cubizolles F, Cockell MM, Rhodes D, Gasser SM. 2009. Reconstitution of yeast silent chromatin: multiple contact sites and O-AADPR binding load SIR complexes onto nucleosomes in vitro. *Mol Cell* **33**: 323–334. http://dx.doi.org/10.1016/j.molcel.2009.01.009.

Masumoto H, Hawke D, Kobayashi R, Verreault A. 2005. A role for cell-cycle-regulated histone H3 lysine 56 acetylation in the DNA damage response. *Nature* **436**: 294–298. http://dx.doi.org/10.1038/nature03714.

Mavrich TN, Jiang C, Ioshikhes IP, Li X, Venters BJ, Zanton SJ, Tomsho LP, Qi J, Glaser RL, Schuster SC, et al. 2008. Nucleosome organization in the Drosophila genome. *Nature* **453**: 358–362. http://dx.doi.org/10.1038/nature06929.

McDonel P, Jans J, Peterson BK, Meyer BJ. 2006. Clustered DNA motifs mark X chromosomes for repression by a dosage compensation complex. *Nature* **444**: 614–618. http://dx.doi.org/10.1038/nature05338.

Meller VH, Rattner BP. 2002. The roX genes encode redundant male-specific lethal transcripts required for targeting of the MSL complex. *EMBO J* **21**: 1084–1091. http://dx.doi.org/10.1093/emboj/21.5.1084.

Mendez DL, Kim D, Chruszcz M, Stephens GE, Minor W, Khorasanizadeh S, Elgin SCR. 2011. The HP1a disordered C terminus and chromo shadow domain cooperate to select target peptide partners. *Chembiochem* **12**: 1084–1096. http://dx.doi.org/10.1002/cbic.201000598.

Meneghini MD, Wu M, Madhani HD. 2003. Conserved histone variant H2A.Z protects euchromatin from the ectopic spread of silent heterochromatin. *Cell* **112**: 725–736. http://dx.doi.org/10.1016/s0092-8674(03)00123-5.

Menon DU, Coarfa C, Xiao W, Gunaratne PH, Meller VH. 2014. siRNAs from an X-linked satellite repeat promote X-chromosome recognition in Drosophila melanogaster. *Proc Natl Acad Sci U S A* **111**: 16460–16465. http://dx.doi.org/10.1073/pnas.1410534111.

Meyer BJ. In press. Mechanisms of sex determination and X-chromosome dosage compensation. *Genetics*.

Meyer BJ, Casson LP. 1986. Caenorhabditis elegans compensates for the difference in X chromosome dosage between the sexes by regulating transcript levels. *Cell* **47**: 871–881. http://dx.doi.org/10.1016/0092-8674(86)90802-0.

Miele A, Bystricky K, Dekker J. 2009. Yeast silent mating type loci form heterochromatic clusters through silencer protein-dependent long-range interactions. *PLoS Genet* **5**: e1000478. http://dx.doi.org/10.1371/journal.pgen.1000478.

Miller A, Chen J, Takasuka TE, Jacobi JL, Kaufman PD, Irudayaraj JMK, Kirchmaier AL. 2010. Proliferating cell nuclear antigen (PCNA) is required for cell cycle-regulated silent chromatin on replicated and nonreplicated genes. *J Biol Chem* **285**: 35142–35154. http://dx.doi.org/10.1074/jbc.M110.166918.

Miller A, Yang B, Foster T, Kirchmaier AL. 2008. Proliferating cell nuclear antigen and ASF1 modulate silent chromatin in Saccharomyces cerevisiae via lysine 56 on histone H3. *Genetics* **179**: 793–809. http://dx.doi.org/10.1534/genetics.107.084525.

Miller AM, Nasmyth KA. 1984. Role of DNA replication in the repression of silent mating type loci in yeast. *Nature* **312**: 247–251.

Milutinovic S, Zhuang Q, Szyf M. 2002. Proliferating cell nuclear antigen associates with histone deacetylase activity, integrating DNA replication and chromatin modification. *J Biol Chem* **277**: 20974–20978. http://dx.doi.org/10.1074/jbc.M202504200.

Minks J, Baldry SE, Yang C, Cotton AM, Brown CJ. 2013. XIST-induced silencing of flanking genes is achieved by additive action of repeat A monomers in human somatic cells. *Epigenetics Chromatin* **6**: 23. http://dx.doi.org/10.1186/1756-8935-6-23.

Moore SA, Ferhatoglu Y, Jia Y, Al-Jiab RA, Scott MJ. 2010. Structural and biochemical studies on the chromo-barrel domain of male specific lethal 3 (MSL3) reveal a binding preference for mono- or dimethyllysine 20 on histone H4. *J Biol Chem* **285**: 40879–40890. http://dx.doi.org/10.1074/jbc.M110.134312.

Moretti P, Freeman K, Coodly L, Shore D. 1994. Evidence that a complex of SIR proteins interacts with the silencer and telomere-binding protein RAP1. *Genes Dev* **8**: 2257–2269. http://dx.doi.org/10.1101/gad.8.19.2257.

Moretti P, Shore D. 2001. Multiple interactions in Sir protein recruitment by Rap1p at silencers and telomeres in yeast. *Mol Cell Biol* **21**: 8082–8094. http://dx.doi.org/10.1128/MCB.21.23.8082-8094.2001.

Müller KP, Erdel F, Caudron-Herger M, Marth C, Fodor BD, Richter M, Scaranaro M, Beaudouin J, Wachsmuth M, Rippe K. 2009. Multiscale analysis of dynamics and interactions of heterochromatin protein 1 by fluorescence fluctuation microscopy. *Biophys J* **97**: 2876–2885. http://dx.doi.org/10.1016/j.bpj.2009.08.057.

Murray IA, Morgan RD, Luyten Y, Fomenkov A, Corrêa IR Jr, Dai N, Allaw MB, Zhang X, Cheng X, Roberts RJ. 2018. The non-specific adenine DNA methyltransferase M.EcoGII. *Nucleic Acids Res* **46**: 840–848. http://dx.doi.org/10.1093/nar/gkx1191.

Murzina N, Verreault A, Laue E, Stillman B. 1999. Heterochromatin dynamics in mouse cells: interaction between chromatin assembly factor 1 and HP1 proteins. *Mol Cell* **4**: 529–540. http://dx.doi.org/10.1016/s1097-2765(00)80204-x.

Nakano S, Stillman B, Horvitz HR. 2011. Replication-coupled chromatin assembly generates a neuronal bilateral asymmetry in C. elegans. *Cell* **147**: 1525–1536. http://dx.doi.org/10.1016/j.cell.2011.11.053.

Nakayama J, Rice JC, Strahl BD, Allis CD, Grewal SI. 2001. Role of histone H3 lysine 9 methylation in epigenetic control of heterochromatin assembly. *Science* **292**: 110–113. http://dx.doi.org/10.1126/science.1060118.

Ng HH, Ciccone DN, Morshead KB, Oettinger MA, Struhl K. 2003. Lysine-79 of histone H3 is hypomethylated at silenced loci in yeast and mammalian cells: a potential mechanism for position-effect variegation. *Proc Natl Acad Sci U S A* **100**: 1820–1825. http://dx.doi.org/10.1073/pnas.0437846100.

Ng HH, Feng Q, Wang H, Erdjument-Bromage H, Tempst P, Zhang Y, Struhl K. 2002. Lysine methylation within the globular domain of histone H3 by Dot1 is important for telomeric silencing and Sir protein association. *Genes Dev* **16**: 1518–1527. http://dx.doi.org/10.1101/gad.1001502.

Noma K, Allis CD, Grewal SI. 2001. Transitions in distinct histone H3 methylation patterns at the heterochromatin domain boundaries. *Science* **293**: 1150–1155. http://dx.doi.org/10.1126/science.1064150.

Noma K-I, Cam HP, Maraia RJ, Grewal SIS. 2006. A role for TFIIIC transcription factor complex in genome organization. *Cell* **125**: 859–872. http://dx.doi.org/10.1016/j.cell.2006.04.028.

Noma K-I, Sugiyama T, Cam H, Verdel A, Zofall M, Jia S, Moazed D, Grewal SIS. 2004. RITS acts in cis to promote RNA interference-mediated transcriptional and post-transcriptional silencing. *Nat Genet* **36**: 1174–1180. http://dx.doi.org/10.1038/ng1452.

Norris A, Bianchet MA, Boeke JD. 2008. Compensatory interactions between Sir3p and the nucleosomal LRS surface imply their direct interaction. *PLoS Genet* **4**: e1000301. http://dx.doi.org/10.1371/journal.pgen.1000301.

Oh H, Park Y, Kuroda MI. 2003. Local spreading of MSL complexes from roX genes on the Drosophila X chromosome. *Genes Dev* **17**: 1334–1339. http://dx.doi.org/10.1101/gad.1082003.

O'Hare K, Chadwick BP, Constantinou A, Davis AJ, Mitchelson A, Tudor M. 2002. A 5.9-kb tandem repeat at the euchromatin-heterochromatin boundary of the X chromosome of Drosophila melanogaster. *Mol Genet Genomics* **267**: 647–655. http://dx.doi.org/10.1007/s00438-002-0698-x.

Oki M, Kamakaka RT. 2005. Barrier function at HMR. *Mol Cell* **19**: 707–716. http://dx.doi.org/10.1016/j.molcel.2005.07.022.

Oki M, Valenzuela L, Chiba T, Ito T, Kamakaka RT. 2004. Barrier proteins remodel and modify chromatin to restrict silenced domains. *Mol Cell Biol* **24**: 1956–1967. http://dx.doi.org/10.1128/mcb.24.5.1956-1967.2004.

Onishi M, Liou G-G, Buchberger JR, Walz T, Moazed D. 2007. Role of the conserved Sir3-BAH domain in nucleosome binding and silent chromatin assembly. *Mol Cell* **28**: 1015–1028. http://dx.doi.org/10.1016/j.molcel.2007.12.004.

Oppikofer M, Kueng S, Keusch JJ, Hassler M, Ladurner AG, Gut H, Gasser SM. 2013. Dimerization of Sir3 via its C-terminal winged helix domain is essential for yeast heterochromatin formation. *EMBO J* **32**: 437–449. http://dx.doi.org/10.1038/emboj.2012.343.

Oppikofer M, Kueng S, Martino F, Soeroes S, Hancock SM, Chin JW, Fischle W, Gasser SM. 2011. A dual role of H4K16 acetylation in the establishment of yeast silent chromatin. *EMBO J* **30**: 2610–2621. http://dx.doi.org/10.1038/emboj.2011.170.

Osada S, Sutton A, Muster N, Brown CE, Yates JR 3rd, Sternglanz R, Workman JL. 2001. The yeast SAS (something about silencing) protein complex contains a MYST-type putative acetyltransferase and functions with chromatin assembly factor ASF1. *Genes Dev* **15**: 3155–3168. http://dx.doi.org/10.1101/gad.907201.

Ozsolak F, Song JS, Liu XS, Fisher DE. 2007. High-throughput mapping of the chromatin structure of human promoters. *Nat Biotechnol* **25**: 244–248. http://dx.doi.org/10.1038/nbt1279.

Park D, Lee Y, Bhupindersingh G, Iyer VR. 2013. Widespread misinterpretable ChIP-seq bias in yeast. *PLoS One* **8**: e83506. http://dx.doi.org/10.1371/journal.pone.0083506.

Park J-H, Cosgrove MS, Youngman E, Wolberger C, Boeke JD. 2002a. A core nucleosome surface crucial for transcriptional silencing. *Nat Genet* **32**: 273–279. http://dx.doi.org/10.1038/ng982.

Park Y, Kelley RL, Oh H, Kuroda MI, Meller VH. 2002b. Extent of chromatin spreading determined by roX RNA recruitment of MSL proteins. *Science* **298**: 1620–1623. http://dx.doi.org/10.1126/science.1076686.

Partridge JF, Borgstrøm B, Allshire RC. 2000. Distinct protein interaction domains and protein spreading in a complex centromere. *Genes Dev* **14**: 783–791. https://www.ncbi.nlm.nih.gov/pubmed/10766735.

Peeters SB, Cotton AM, Brown CJ. 2014. Variable escape from X-chromosome inactivation: identifying factors that tip the scales towards expression. *Bioessays* **36**: 746–756. http://dx.doi.org/10.1002/bies.201400032.

Petruk S, Sedkov Y, Johnston DM, Hodgson JW, Black KL, Kovermann SK, Beck S, Canaani E, Brock HW, Mazo A. 2012. TrxG and PcG proteins but not methylated histones remain associated with DNA through replication. *Cell* **150**: 922–933. http://dx.doi.org/10.1016/j.cell.2012.06.046.

Petryk N, Dalby M, Wenger A, Stromme CB, Strandsby A, Andersson R, Groth A. 2018. MCM2 promotes symmetric inheritance of modified histones during DNA replication. *Science* **361**: 1389–1392. http://dx.doi.org/10.1126/science.aau0294.

Petty EL, Collette KS, Cohen AJ, Snyder MJ, Csankovszki G. 2009. Restricting dosage compensation complex binding to the X chromosomes by H2A.Z/HTZ-1. *PLoS Genet* **5**: e1000699. http://dx.doi.org/10.1371/journal.pgen.1000699.

Pferdehirt RR, Kruesi WS, Meyer BJ. 2011. An MLL/COMPASS subunit functions in the C. elegans dosage compensation complex to target X chromosomes for transcriptional regulation of gene expression. *Genes Dev* **25**: 499–515. http://dx.doi.org/10.1101/gad.2016011.

Pillus L, Rine J. 1989. Epigenetic inheritance of transcriptional states in S. cerevisiae. *Cell* **59**: 637–647. http://dx.doi.org/10.1016/0092-8674(89)90009-3.

Pryde FE, Louis EJ. 1999. Limitations of silencing at native yeast telomeres. *EMBO J* **18**: 2538–2550. http://dx.doi.org/10.1093/emboj/18.9.2538.

Radman-Livaja M, Ruben G, Weiner A, Friedman N, Kamakaka R, Rando OJ. 2011. Dynamics of Sir3 spreading in budding yeast: secondary recruitment sites and euchromatic localization. *EMBO J* **30**: 1012–1026. http://dx.doi.org/10.1038/emboj.2011.30.

Ragunathan K, Jih G, Moazed D. 2015. Epigenetic inheritance uncoupled from sequence-specific recruitment. *Science* **348**: 1258699. http://dx.doi.org/10.1126/science.1258699.

Raisner RM, Hartley PD, Meneghini MD, Bao MZ, Liu CL, Schreiber SL, Rando OJ, Madhani HD. 2005. Histone variant H2A.Z marks the 5' ends of both active and inactive genes in euchromatin. *Cell* **123**: 233–248. http://dx.doi.org/10.1016/j.cell.2005.10.002.

Ramírez F, Lingg T, Toscano S, Lam KC, Georgiev P, Chung H-R, Lajoie BR, de Wit E, Zhan Y, de Laat W, et al. 2015. High-Affinity Sites Form an Interaction Network to Facilitate Spreading of the MSL Complex across the X Chromosome in Drosophila. *Mol Cell* **60**: 146–162. http://dx.doi.org/10.1016/j.molcel.2015.08.024.

Ranjan A, Mizuguchi G, FitzGerald PC, Wei D, Wang F, Huang Y, Luk E, Woodcock CL, Wu C. 2013. Nucleosome-free region dominates histone acetylation in targeting SWR1 to promoters for H2A.Z replacement. *Cell* **154**: 1232–1245. http://dx.doi.org/10.1016/j.cell.2013.08.005.

Ravindra A, Weiss K, Simpson RT. 1999. High-resolution structural analysis of chromatin at specific loci: Saccharomyces cerevisiae silent mating-type locus HMRa. *Mol Cell Biol* **19**: 7944–7950. http://dx.doi.org/10.1128/mcb.19.12.7944.

Recht J, Tsubota T, Tanny JC, Diaz RL, Berger JM, Zhang X, Garcia BA, Shabanowitz J, Burlingame AL, Hunt DF, et al. 2006. Histone chaperone Asf1 is required for histone H3 lysine 56 acetylation, a modification associated with S phase in mitosis and meiosis. *Proc Natl Acad Sci U S A* **103**: 6988–6993. http://dx.doi.org/10.1073/pnas.0601676103.

Renauld H, Aparicio OM, Zierath PD, Billington BL, Chhablani SK, Gottschling DE. 1993. Silent domains are assembled continuously from the telomere and are defined by promoter distance and strength, and by SIR3 dosage. *Genes & Development* **7**: 1133–1145.

Ridings-Figueroa R, Stewart ER, Nesterova TB, Coker H, Pintacuda G, Godwin J, Wilson R, Haslam A, Lilley F, Ruigrok R, et al. 2017. The nuclear matrix protein CIZ1 facilitates localization of Xist RNA to the inactive X-chromosome territory. *Genes Dev* **31**: 876–888. http://dx.doi.org/10.1101/gad.295907.117.

Rieder LE, Jordan WT 3rd, Larschan EN. 2019. Targeting of the Dosage-Compensated Male X-Chromosome during Early Drosophila Development. *Cell Rep* **29**: 4268-4275.e2. http://dx.doi.org/10.1016/j.celrep.2019.11.095.

Rine J, Herskowitz I. 1987. Four Genes Responsible for Position Effect on Expression From HML and HMR in Saccharomyces cerevisiae. *Genetics* **116**: 9–22.

Rossmann MP, Luo W, Tsaponina O, Chabes A, Stillman B. 2011. A common telomeric gene silencing assay is affected by nucleotide metabolism. *Mol Cell* **42**: 127–136. http://dx.doi.org/10.1016/j.molcel.2011.03.007.

Rudner AD, Hall BE, Ellenberger T, Moazed D. 2005. A nonhistone protein-protein interaction required for assembly of the SIR complex and silent chromatin. *Mol Cell Biol* **25**: 4514–4528. http://dx.doi.org/10.1128/MCB.25.11.4514-4528.2005.

Rusche LN, Kirchmaier AL, Rine J. 2002. Ordered Nucleation and Spreading of Silenced Chromatin in Saccharomyces cerevisiae. *Molecular Biology of the Cell* **13**: 2207–2222. http://dx.doi.org/10.1091/mbc.E02.

Russell LB, Bangham JW. 1961. Variegated-type position effects in the mouse. *Genetics* **46**: 509–525. https://www.ncbi.nlm.nih.gov/pubmed/13744850.

Samata M, Akhtar A. 2018. Dosage Compensation of the X Chromosome: A Complex Epigenetic Assignment Involving Chromatin Regulators and Long Noncoding RNAs. *Annu Rev Biochem* **87**: 323–350. http://dx.doi.org/10.1146/annurev-biochem-062917-011816.

Samel A, Rudner A, Ehrenhofer-Murray AE. 2017. Variants of the Sir4 Coiled-Coil Domain Improve Binding to Sir3 for Heterochromatin Formation in Saccharomyces cerevisiae. *G3* **7**: 1117–1126. http://dx.doi.org/10.1534/g3.116.037739.

Sampath V, Yuan P, Wang IX, Prugar E, van Leeuwen F, Sternglanz R. 2009. Mutational analysis of the Sir3 BAH domain reveals multiple points of interaction with nucleosomes. *Mol Cell Biol* **29**: 2532–2545. http://dx.doi.org/10.1128/MCB.01682-08.

Sanulli S, Trnka MJ, Dharmarajan V, Tibble RW, Pascal BD, Burlingame AL, Griffin PR, Gross JD, Narlikar GJ. 2019. HP1 reshapes nucleosome core to promote phase separation of heterochromatin. *Nature* **575**: 390–394. http://dx.doi.org/10.1038/s41586-019-1669-2.

Saxton DS, Rine J. 2019. Epigenetic memory independent of symmetric histone inheritance. *Elife* **8**. http://dx.doi.org/10.7554/eLife.51421.

Scherthan H, Bähler J, Kohli J. 1994. Dynamics of chromosome organization and pairing during meiotic prophase in fission yeast. *J Cell Biol* **127**: 273–285. http://dx.doi.org/10.1083/jcb.127.2.273.

Schindelin J, Arganda-Carreras I, Frise E, Kaynig V, Longair M, Pietzsch T, Preibisch S, Rueden C, Saalfeld S, Schmid B, et al. 2012. Fiji: an open-source platform for biological-image analysis. *Nat Methods* **9**: 676–682. http://dx.doi.org/10.1038/nmeth.2019.

Schnell R, Rine J. 1986. A position effect on the expression of a tRNA gene mediated by the SIR genes in Saccharomyces cerevisiae. *Mol Cell Biol* **6**: 494–501. http://dx.doi.org/10.1128/mcb.6.2.494-501.1986.

Schotta G, Ebert A, Krauss V, Fischer A, Hoffmann J, Rea S, Jenuwein T, Dorn R, Reuter G. 2002. Central role of Drosophila SU(VAR)3-9 in histone H3-K9 methylation and heterochromatic gene silencing. *EMBO J* **21**.

Scott KC, Merrett SL, Willard HF. 2006. A heterochromatin barrier partitions the fission yeast centromere into discrete chromatin domains. *Curr Biol* **16**: 119–129. http://dx.doi.org/10.1016/j.cub.2005.11.065.

Sekinger EA, Gross DS. 2001. Silenced chromatin is permissive to activator binding and PIC recruitment. *Cell* **105**: 403–414. http://dx.doi.org/10.1016/s0092-8674(01)00329-4.

Serra-Cardona A, Zhang Z. 2018. Replication-Coupled Nucleosome Assembly in the Passage of Epigenetic Information and Cell Identity. *Trends Biochem Sci* **43**: 136–148. http://dx.doi.org/10.1016/j.tibs.2017.12.003.

Sharp JA, Fouts ET, Krawitz DC, Kaufman PD. 2001. Yeast histone deposition protein Asf1p requires Hir proteins and PCNA for heterochromatic silencing. *Curr Biol* **11**: 463–473. http://dx.doi.org/10.1016/s0960-9822(01)00140-3.

Shibahara K, Stillman B. 1999. Replication-dependent marking of DNA by PCNA facilitates CAF-1-coupled inheritance of chromatin. *Cell* **96**: 575–585. http://dx.doi.org/10.1016/s0092-8674(00)80661-3.

Shipony Z, Marinov GK, Swaffer MP, Sinnott-Armstrong NA, Skotheim JM, Kundaje A, Greenleaf WJ. 2020. Long-range single-molecule mapping of chromatin accessibility in eukaryotes. *Nat Methods* **17**: 319–327. http://dx.doi.org/10.1038/s41592-019-0730-2.

Shogren-Knaak M, Ishii H, Sun J-M, Pazin MJ, Davie JR, Peterson CL. 2006. Histone H4-K16 Acetylation Controls Chromatin Structure and Protein Interactions. *Science* **311**: 844–847. https://science.sciencemag.org/content/311/5762/844.abstract (Accessed August 28, 2020).

Shore D, Nasmyth K. 1987. Purification and cloning of a DNA binding protein from yeast that binds to both silencer and activator elements. *Cell* **51**: 721–732. http://dx.doi.org/10.1016/0092-8674(87)90095-x.

Shore D, Stillman DJ, Brand AH, Nasmyth KA. 1987. Identification of silencer binding proteins from yeast: possible roles in SIR control and DNA replication. *EMBO J* **6**: 461–467. https://www.ncbi.nlm.nih.gov/pubmed/15981337.

Sikorski RS, Hieter P. 1989. A system of shuttle vectors and yeast host strains designed for efficient manipulation of DNA in Saccharomyces cerevisiae. *Genetics* **122**: 19–27. http://dx.doi.org/10.1093/genetics/122.1.19.

Simms TA, Dugas SL, Gremillion JC, Ibos ME, Dandurand MN, Toliver TT, Edwards DJ, Donze D. 2008. TFIIIC binding sites function as both heterochromatin barriers and chromatin insulators in Saccharomyces cerevisiae. *Eukaryot Cell* **7**: 2078–2086. http://dx.doi.org/10.1128/EC.00128-08.

Simon MD, Pinter SF, Fang R, Sarma K, Rutenberg-Schoenberg M, Bowman SK, Kesner BA, Maier VK, Kingston RE, Lee JT. 2013. High-resolution Xist binding maps reveal two-step spreading during X-chromosome inactivation. *Nature* **504**: 465–469. http://dx.doi.org/10.1038/nature12719.

Singh J, Klar AJ. 1992. Active genes in budding yeast display enhanced in vivo accessibility to foreign DNA methylases: a novel in vivo probe for chromatin structure of yeast. *Genes Dev* **6**: 186–196. http://dx.doi.org/10.1101/gad.6.2.186.

Smith ER, Allis CD, Lucchesi JC. 2001. Linking global histone acetylation to the transcription enhancement of X-chromosomal genes in Drosophila males. *J Biol Chem* **276**: 31483–31486. http://dx.doi.org/10.1074/jbc.C100351200.

Smith JS, Brachmann CB, Celic I, Kenna MA, Muhammad S, Starai VJ, Avalos JL, Escalante-Semerena JC, Grubmeyer C, Wolberger C, et al. 2000. A phylogenetically conserved NAD+-dependent protein deacetylase activity in the Sir2 protein family. *Proc Natl Acad Sci U S A* **97**: 6658–6663. http://dx.doi.org/10.1073/pnas.97.12.6658.

Smith JS, Brachmann CB, Pillus L, Boeke JD. 1998. Distribution of a limited Sir2 protein pool regulates the strength of yeast rDNA silencing and is modulated by Sir4p. *Genetics* **149**: 1205–1219. https://www.ncbi.nlm.nih.gov/pubmed/9649515.

Smith S, Stillman B. 1989. Purification and characterization of CAF-I, a human cell factor required for chromatin assembly during DNA replication in vitro. *Cell* **58**: 15–25. http://dx.doi.org/10.1016/0092-8674(89)90398-x.

Sneppen K, Dodd IB. 2015. Cooperative stabilization of the SIR complex provides robust epigenetic memory in a model of SIR silencing in Saccharomyces cerevisiae. *Epigenetics* **10**: 293–302. http://dx.doi.org/10.1080/15592294.2015.1017200.

Sorida M, Hirauchi T, Ishizaki H, Kaito W, Shimada A, Mori C, Chikashige Y, Hiraoka Y, Suzuki Y, Ohkawa Y, et al. 2019. Regulation of ectopic heterochromatin-mediated epigenetic diversification by the JmjC family protein Epe1. *PLoS Genet* **15**: e1008129. http://dx.doi.org/10.1371/journal.pgen.1008129.

Soruco MML, Chery J, Bishop EP, Siggers T, Tolstorukov MY, Leydon AR, Sugden AU, Goebel K, Feng J, Xia P, et al. 2013. The CLAMP protein links the MSL complex to the X chromosome during Drosophila dosage compensation. *Genes Dev* **27**: 1551–1556. http://dx.doi.org/10.1101/gad.214585.113.

Spierer A, Begeot F, Spierer P, Delattre M. 2008. SU(VAR)3-7 links heterochromatin and dosage compensation in Drosophila. *PLoS Genet* **4**: e1000066. http://dx.doi.org/10.1371/journal.pgen.1000066.

Stavenhagen JB, Zakian VA. 1994. Internal tracts of telomeric DNA act as silencers in Saccharomyces cerevisiae. *Genes Dev* **8**: 1411–1422. http://dx.doi.org/10.1101/gad.8.12.1411.

Steakley DL, Rine J. 2015. On the Mechanism of Gene Silencing in Saccharomyces cerevisiae. *G3: Genes, Genomes, Genetics* **5**: 1751–1763. https://www.g3journal.org/content/5/8/1751 (Accessed May 14, 2020).

Stergachis AB, Debo BM, Haugen E, Churchman LS, Stamatoyannopoulos JA. 2020. Single-molecule regulatory architectures captured by chromatin fiber sequencing. *Science* **368**: 1449–1454. http://dx.doi.org/10.1126/science.aaz1646.

Stone EM, Reifsnyder C, McVey M, Gazo B, Pillus L. 2000. Two classes of sir3 mutants enhance the sir1 mutant mating defect and abolish telomeric silencing in Saccharomyces cerevisiae. *Genetics* **155**: 509–522. https://www.ncbi.nlm.nih.gov/pubmed/10835377.

Storchová Z, Breneman A, Cande J, Dunn J, Burbank K, O'Toole E, Pellman D. 2006. Genome-wide genetic analysis of polyploidy in yeast. *Nature* **443**: 541–547. http://dx.doi.org/10.1038/nature05178.

Strahl-Bolsinger S, Hecht A, Luo K, Grunstein M. 1997. SIR2 and SIR4 interactions differ in core and extended telomeric heterochromatin in yeast. *Genes Dev* **11**: 83–93. http://dx.doi.org/10.1101/gad.11.1.83.

Straub T, Grimaud C, Gilfillan GD, Mitterweger A, Becker PB. 2008. The chromosomal high-affinity binding sites for the Drosophila dosage compensation complex. *PLoS Genet* **4**: e1000302. http://dx.doi.org/10.1371/journal.pgen.1000302.

Straub T, Zabel A, Gilfillan GD, Feller C, Becker PB. 2013. Different chromatin interfaces of the Drosophila dosage compensation complex revealed by high-shear ChIP-seq. *Genome Res* **23**: 473–485. http://dx.doi.org/10.1101/gr.146407.112.

Strom AR, Emelyanov AV, Mir M, Fyodorov DV, Darzacq X, Karpen GH. 2017. Phase separation drives heterochromatin domain formation. *Nature* **547**: 241–245. http://dx.doi.org/10.1038/nature22989.

Strome S, Kelly WG, Ercan S, Lieb JD. 2014. Regulation of the X chromosomes in Caenorhabditis elegans. *Cold Spring Harb Perspect Biol* **6**. http://dx.doi.org/10.1101/cshperspect.a018366.

Struhl K, Segal E. 2013. Determinants of nucleosome positioning. *Nat Struct Mol Biol* **20**: 267–273. http://dx.doi.org/10.1038/nsmb.2506.

Stulemeijer IJ, Pike BL, Faber AW, Verzijlbergen KF, van Welsem T, Frederiks F, Lenstra TL, Holstege FC, Gasser SM, van Leeuwen F. 2011. Dot1 binding induces chromatin rearrangements by histone methylation-dependent and -independent mechanisms. *Epigenetics Chromatin* **4**: 2. http://dx.doi.org/10.1186/1756-8935-4-2.

Stunnenberg R, Kulasegaran-Shylini R, Keller C, Kirschmann MA, Gelman L, Bühler M. 2015. H3K9 methylation extends across natural boundaries of heterochromatin in the absence of an HP1 protein. *EMBO J* **34**: 2789–2803. http://dx.doi.org/10.15252/embj.201591320.

Suka N, Luo K, Grunstein M. 2002. Sir2p and Sas2p opposingly regulate acetylation of yeast histone H4 lysine16 and spreading of heterochromatin. *Nat Genet* **32**: 378–383. http://dx.doi.org/10.1038/ng1017.

Suka N, Suka Y, Carmen AA, Wu J, Grunstein M. 2001. Highly Specific Antibodies Determine Histone Acetylation Site Usage in Yeast Heterochromatin and Euchromatin. *Mol Cell* **8**: 473–479.

Sunwoo H, Colognori D, Froberg JE, Jeon Y, Lee JT. 2017. Repeat E anchors Xist RNA to the inactive X chromosomal compartment through CDKN1A-interacting protein (CIZ1). *Proc Natl Acad Sci U S A* **114**: 10654–10659. http://dx.doi.org/10.1073/pnas.1711206114.

Sural TH, Peng S, Li B, Workman JL, Park PJ, Kuroda MI. 2008. The MSL3 chromodomain directs a key targeting step for dosage compensation of the Drosophila melanogaster X chromosome. *Nat Struct Mol Biol* **15**: 1318–1325. http://dx.doi.org/10.1038/nsmb.1520.

Sussel L, Vannier D, Shore D. 1993. Epigenetic switching of transcriptional states: cis- and trans- acting factors affecting establishment of silencing at the HMR locus in Saccharomyces cereivisae. *Molecular and Cellular Biology* **13**: 3919–3928.

Swygert SG, Senapati S, Bolukbasi MF, Wolfe SA, Lindsay S, Peterson CL. 2018. SIR proteins create compact heterochromatin fibers. *Proc Natl Acad Sci U S A* **115**: 12447–12452. http://dx.doi.org/10.1073/pnas.1810647115.

Syrett CM, Sindhava V, Hodawadekar S, Myles A, Liang G, Zhang Y, Nandi S, Cancro M, Atchison M, Anguera MC. 2017. Loss of Xist RNA from the inactive X during B cell development is restored in a dynamic YY1-dependent two-step process in activated B cells. *PLoS Genet* **13**: e1007050. http://dx.doi.org/10.1371/journal.pgen.1007050.

Taddei A, Hediger F, Neumann FR, Bauer C, Gasser SM. 2004. Separation of silencing from perinuclear anchoring functions in yeast Ku80, Sir4 and Esc1 proteins. *EMBO J* **23**: 1301–1312. http://dx.doi.org/10.1038/sj.emboj.7600144.

Taddei A, Van Houwe G, Nagai S, Erb I, van Nimwegen E, Gasser SM. 2009. The functional importance of telomere clustering: global changes in gene expression result from SIR factor dispersion. *Genome Res* **19**: 611–625. http://dx.doi.org/10.1101/gr.083881.108.

Takahashi Y-H, Schulze JM, Jackson J, Hentrich T, Seidel C, Jaspersen SL, Kobor MS, Shilatifard A. 2011. Dot1 and histone H3K79 methylation in natural telomeric and HM silencing. *Mol Cell* **42**: 118–126. http://dx.doi.org/10.1016/j.molcel.2011.03.006.

Tanny JC, Kirkpatrick DS, Gerber SA, Gygi SP, Moazed D. 2004. Budding yeast silencing complexes and regulation of Sir2 activity by protein-protein interactions. *Mol Cell Biol* **24**: 6931–6946. http://dx.doi.org/10.1128/MCB.24.16.6931-6946.2004.

Teytelman L, Thurtle DM, Rine J, van Oudenaarden A. 2013. Highly expressed loci are vulnerable to misleading ChIP localization of multiple unrelated proteins. *Proc Natl Acad Sci U S A* **110**: 18602–18607. http://dx.doi.org/10.1073/pnas.1316064110.

Thon G, Bjerling KP, Nielsen IS. 1999. Localization and properties of a silencing element near the mat3-M mating-type cassette of Schizosaccharomyces pombe. *Genetics* **151**: 945–963. http://dx.doi.org/10.1093/genetics/151.3.945.

Thon G, Bjerling P, Bünner CM, Verhein-Hansen J. 2002. Expression-state boundaries in the mating-type region of fission yeast. *Genetics* **161**: 611–622. https://www.ncbi.nlm.nih.gov/pubmed/12072458.

Thorvaldsdóttir H, Robinson JT, Mesirov JP. 2013. Integrative Genomics Viewer (IGV): high-performance genomics data visualization and exploration. *Brief Bioinform* **14**: 178–192. http://dx.doi.org/10.1093/bib/bbs017.

Thurtle DM, Rine J. 2014. The molecular topography of silenced chromatin in Saccharomyces cerevisiae. *Genes Dev* **28**: 245–258. http://dx.doi.org/10.1101/gad.230532.113.

Thurtle-Schmidt DM, Dodson AE, Rine J. 2016. Histone Deacetylases with Antagonistic Roles in Saccharomyces cerevisiae Heterochromatin Formation. *Genetics* **204**: 177–190. http://dx.doi.org/10.1534/genetics.116.190835.

Tikhonova E, Fedotova A, Bonchuk A, Mogila V, Larschan EN, Georgiev P, Maksimenko O. 2019. The simultaneous interaction of MSL2 with CLAMP and DNA provides redundancy in the initiation of dosage compensation in Drosophila males. *Development* **146**. http://dx.doi.org/10.1242/dev.179663.

Trewick SC, Minc E, Antonelli R, Urano T, Allshire RC. 2007. The JmjC domain protein Epe1 prevents unregulated assembly and disassembly of heterochromatin. *EMBO J* **26**: 4670–4682. http://emboj.embopress.org/cgi/doi/10.1038/sj.emboj.7601892.

Triolo T, Sternglanz R. 1996. Role of interactions between the origin recognition complex and SIR1 in transcriptional silencing. *Nature* **381**: 251–253.

Tudor M, Mitchelson A, O'hare K. 1996. A 1·5 kb direct repeat sequence flanks the suppressor of forked gene at the euchromatin–heterochromatin boundary of the Drosophila melanogaster X chromosome. *Genet Res* **68**: 191–202. https://www.cambridge.org/core/services/aop-cambridge-core/content/view/D46D586FB7B001590F4DD0BD5DA9F62D/S0016672300034169a.pdf/div-class-title-a-1-5-kb-direct-repeat-sequence-flanks-the-span-class-italic-suppressor-of-forked-span-gene-at-the-euchromatin-heterochromatin-boundary-of-the-span-class-italic-drosophila-melanogaster-span-x-chromosome-div.pdf (Accessed May 31, 2020).

Valencia M, Bentele M, Vaze MB, Herrmann G, Kraus E, Lee SE, Schär P, Haber JE. 2001. NEJ1 controls non-homologous end joining in Saccharomyces cerevisiae. *Nature* **414**: 666–669. http://dx.doi.org/10.1038/414666a.

Valenzuela L, Dhillon N, Dubey RN, Gartenberg MR, Kamakaka RT. 2008. Long-range communication between the silencers of HMR. *Mol Cell Biol* **28**: 1924–1935. http://dx.doi.org/10.1128/MCB.01647-07.

Valenzuela L, Dhillon N, Kamakaka RT. 2009. Transcription independent insulation at TFIIIC-dependent insulators. *Genetics* **183**: 131–148. http://dx.doi.org/10.1534/genetics.109.106203.

van Leeuwen F, Gafken PR, Gottschling DE. 2002. Dot1p modulates silencing in yeast by methylation of the nucleosome core. *Cell* **109**: 745–756. http://dx.doi.org/10.1016/s0092-8674(02)00759-6.

Venkatasubrahmanyam S, Hwang WW, Meneghini MD, Tong AHY, Madhani HD. 2007. Genome-wide, as opposed to local, antisilencing is mediated redundantly by the euchromatic factors Set1 and H2A.Z. *Proc Natl Acad Sci U S A* **104**: 16609–16614. http://dx.doi.org/10.1073/pnas.0700914104.

Verdel A, Jia S, Gerber S, Sugiyama T, Gygi S, Grewal SIS, Moazed D. 2004. RNAi-mediated targeting of heterochromatin by the RITS complex. *Science* **303**: 672–676. http://dx.doi.org/10.1126/science.1093686.

Verrier L, Taglini F, Barrales RR, Webb S, Urano T, Braun S, Bayne EH. 2015. Global regulation of heterochromatin spreading by Leo1. *Open Biol* **5**. http://dx.doi.org/10.1098/rsob.150045.

Villa R, Schauer T, Smialowski P, Straub T, Becker PB. 2016. PionX sites mark the X chromosome for dosage compensation. *Nature* **537**: 244–248. http://dx.doi.org/10.1038/nature19338.

Volpe TA, Kidner C, Hall IM, Teng G, Grewal SIS, Martienssen RA. 2002. Regulation of heterochromatic silencing and histone H3 lysine-9 methylation by RNAi. *Science* **297**: 1833–1837. http://dx.doi.org/10.1126/science.1074973.

Wang J, Reddy BD, Jia S. 2015. Rapid epigenetic adaptation to uncontrolled heterochromatin spreading. *Elife* **4**. http://dx.doi.org/10.7554/eLife.06179.

Wang J, Tadeo X, Hou H, Tu PG, Thompson J, Yates JR 3rd, Jia S. 2013. Epe1 recruits BET family bromodomain protein Bdf2 to establish heterochromatin boundaries. *Genes Dev* **27**: 1886–1902. http://dx.doi.org/10.1101/gad.221010.113.

Wang X, Hayes JJ. 2008. Acetylation Mimics within Individual Core Histone Tail Domains Indicate Distinct Roles in Regulating the Stability of Higher-Order Chromatin Structure. *Mech Chem Biosyst* **28**: 227–236. https://mcb.asm.org/content/28/1/227.

Weiss K, Simpson RT. 1998. High-Resolution Structural Analysis of Chromatin at Specific Loci: Saccharomyces cerevisiae Silent Mating Type Locus HML. *Molecular and Cellular Biology* **18**: 2522–2537.

Woodcock CB, Horton JR, Zhang X, Blumenthal RM, Cheng X. 2020. Beta class amino methyltransferases from bacteria to humans: evolution and structural consequences. *Nucleic Acids Res*. http://dx.doi.org/10.1093/nar/gkaa446.

Wurtele H, Kaiser GS, Bacal J, St-Hilaire E, Lee E-H, Tsao S, Dorn J, Maddox P, Lisby M, Pasero P, et al. 2012. Histone H3 lysine 56 acetylation and the response to DNA replication fork damage. *Mol Cell Biol* **32**: 154–172. http://dx.doi.org/10.1128/MCB.05415-11.

Xu EY, Bi X, Holland MJ, Gottschling DE, Broach JR. 2005. Mutations in the nucleosome core enhance transcriptional silencing. *Mol Cell Biol* **25**: 1846–1859. http://dx.doi.org/10.1128/MCB.25.5.1846-1859.2005.

Xu L, Seki M. 2020. Recent advances in the detection of base modifications using the Nanopore sequencer. *J Hum Genet* **65**: 25–33. https://www.nature.com/articles/s10038-019-0679-0.

Yamada T, Fischle W, Sugiyama T, Allis CD, Grewal SIS. 2005. The nucleation and maintenance of heterochromatin by a histone deacetylase in fission yeast. *Mol Cell* **20**: 173–185. http://dx.doi.org/10.1016/j.molcel.2005.10.002.

Yuan G-C, Liu Y-J, Dion MF, Slack MD, Wu LF, Altschuler SJ, Rando OJ. 2005. Genome-scale identification of nucleosome positions in S. cerevisiae. *Science* **309**: 626–630. http://dx.doi.org/10.1126/science.1112178.

Zhang H, Roberts DN, Cairns BR. 2005. Genome-wide dynamics of Htz1, a histone H2A variant that poises repressed/basal promoters for activation through histone loss. *Cell* **123**: 219–231. http://dx.doi.org/10.1016/j.cell.2005.08.036.

Zhang K, Mosch K, Fischle W, Grewal SIS. 2008. Roles of the Clr4 methyltransferase complex in nucleation, spreading and maintenance of heterochromatin. *Nat Struct Mol Biol* **15**: 381–388. http://dx.doi.org/10.1038/nsmb.1406.

Zhang T, Zhang W, Jiang J. 2015. Genome-Wide Nucleosome Occupancy and Positioning and Their Impact on Gene Expression and Evolution in Plants. *Plant Physiol* **168**: 1406–1416. http://dx.doi.org/10.1104/pp.15.00125.

Zhang Z, Shibahara K, Stillman B. 2000. PCNA connects DNA replication to epigenetic inheritance in yeast. *Nature* **408**: 221–225. http://dx.doi.org/10.1038/35041601.

Zofall M, Fischer T, Zhang K, Zhou M, Cui B, Veenstra TD, Grewal SIS. 2009. Histone H2A.Z cooperates with RNAi and heterochromatin factors to suppress antisense RNAs. *Nature* **461**: 419–422. http://dx.doi.org/10.1038/nature08321.

Zofall M, Grewal SIS. 2006. Swi6/HP1 recruits a JmjC domain protein to facilitate transcription of heterochromatic repeats. *Mol Cell* **22**: 681–692. http://dx.doi.org/10.1016/j.molcel.2006.05.010.

Zofall M, Yamanaka S, Reyes-Turcu FE, Zhang K, Rubin C, Grewal SIS. 2012. RNA elimination machinery targeting meiotic mRNAs promotes facultative heterochromatin formation. *Science* **335**: 96–100. http://dx.doi.org/10.1126/science.1211651.